



Cite this: *Chem. Soc. Rev.*, 2024, 53, 3134

Computational approach inspired advancements of solid-state electrolytes for lithium secondary batteries: from first-principles to machine learning

Zhuoyuan Zheng, * Jie Zhou and Yusong Zhu*

The increasing demand for high-security, high-performance, and low-cost energy storage systems (EESs) driven by the adoption of renewable energy is gradually surpassing the capabilities of commercial lithium-ion batteries (LIBs). Solid-state electrolytes (SSEs), including inorganics, polymers, and composites, have emerged as promising candidates for next-generation all-solid-state batteries (ASSBs). ASSBs offer higher theoretical energy densities, improved safety, and extended cyclic stability, making them increasingly popular in academia and industry. However, the commercialization of ASSBs still faces significant challenges, such as unsatisfactory interfacial resistance and rapid dendrite growth. To overcome these problems, a thorough understanding of the complex chemical–electrochemical–mechanical interactions of SSE materials is essential. Recently, computational methods have played a vital role in revealing the fundamental mechanisms associated with SSEs and accelerating their development, ranging from atomistic first-principles calculations, molecular dynamic simulations, multiphysics modeling, to machine learning approaches. These methods enable the prediction of intrinsic properties and interfacial stability, investigation of material degradation, and exploration of topological design, among other factors. In this comprehensive review, we provide an overview of different numerical methods used in SSE research. We discuss the current state of knowledge in numerical auxiliary approaches, with a particular focus on machine learning-enabled methods, for the understanding of multiphysics-couplings of SSEs at various spatial and time scales. Additionally, we highlight insights and prospects for SSE advancements. This review serves as a valuable resource for researchers and industry professionals working with energy storage systems and computational modeling and offers perspectives on the future directions of SSE development.

Received 13th October 2023

DOI: 10.1039/d3cs00572k

rsc.li/chem-soc-rev

School of Energy Science and Engineering, Nanjing Tech University, Nanjing, Jiangsu Province 211816, China. E-mail: zhuoyuan@njtech.edu.cn, zhuyys@njtech.edu.cn



Zhuoyuan Zheng

Dr Zheng Zhuoyuan is an Associate Professor at Nanjing Tech University. He earned his bachelor's and master's degrees from Tongji University and obtained his doctoral degree in Mechanical Engineering from Wichita State University in May 2018. From 2018 to 2021, he worked as a postdoctoral researcher at the University of Illinois at Urbana-Champaign. In March 2022, he joined the School of Energy Science and Engineering at Nanjing Tech University. His research mainly focuses on the study of safe, low-cost, high-performance electrochemical energy storage and conversion materials and devices.



Jie Zhou

Jie Zhou received her PhD degree under the supervision of Prof. Yitai Qian at the University of Science and Technology of China in 2019. Then she continued her postdoctoral research at USTC. She is currently an associate professor at Nanjing Tech University. Her research focuses on the investigation of high-capacity electrode materials for energy storage and electrochemical performance.

1. Introduction

The growing adoption of renewable energy sources has created a substantial need for efficient energy storage systems.^{1–3} Lithium-ion batteries (LIBs) have conventionally served as secondary batteries for storing and utilizing renewable energy.⁴ Nonetheless, the increasing demand for energy storage systems that offer high-security, high-performance, and low-cost options has highlighted the limitations of commercial LIBs.^{5,6} One of the primary concerns is safety, as LIBs are susceptible to thermal runaway and fire hazards. Moreover, the energy density of LIBs is approaching its theoretical limit, impeding further advancements and limiting their integration into diverse applications.

To overcome these limitations, solid-state electrolytes (SSEs) have emerged as highly promising candidates for next-generation all-solid-state batteries (ASSBs).^{7–9} SSEs offer superior theoretical energy densities, improved safety, and extended cyclic stability.¹⁰ By replacing traditional liquid electrolytes with SSEs, lithium secondary batteries, both LIBs and more advanced setups such as lithium metal, lithium–sulfur and lithium–oxygen batteries, can surpass the limitations of conventional batteries and provide a more efficient and secure energy storage solution.^{11,12} SSEs can be classified based on their material types, including inorganic SSEs, polymer SSEs, garnet-type SSEs, hybrid composite SSEs, and nanostructured SSEs, each exhibiting distinct strengths and weaknesses.^{13–15} For instance, inorganic SSEs demonstrate high ionic conductivity, a wide electrochemical stability window, excellent thermal stability, and compatibility with lithium metal; however, they possess limited flexibility and mechanical properties, high interfacial resistance, restricted processability, and the potential for dendrite growth.^{16,17} Conversely, ultrathin and super-tough gel polymer electrolytes (GPEs) offer good flexibility and mechanical properties, easy processability, but they have limited uniformity and continuity, uneven distribution

of Li⁺ flux, a narrow electrochemical stability window, lower ionic conductivity, and the potential for solvent evaporation and electrolyte leakage.¹⁸ Furthermore, despite the attractive properties of SSEs, their industrialization faces challenges due to the absence of cost-effective and large-scale manufacturing technologies capable of producing high-quality SSEs with comparable thickness to polymer separators in conventional LIBs.¹⁹ Presently, there is no practical solid alternative to standard liquid LIBs that surpasses them in terms of key performance indicators such as energy and power density, cycling lifetime, and cost.²⁰

To address the aforementioned issues and expedite the advancement of SSEs, researchers have turned to computational methods.²¹ Numerical approaches have been proven to be highly effective tools in the materials science field, especially to study various aspects related to SSEs at different scales.²² Atomistic first-principles calculations provide a fundamental understanding of SSE materials by simulating their atomic structure and electronic properties.²³ By employing principles of quantum mechanics, these calculations accurately predict intrinsic properties such as the ionic migration barrier, diffusion coefficient, and thermodynamic stability. Molecular dynamics (MD) simulations enable the study of SSEs' dynamic behavior at the atomic level.²⁴ By simulating the movement of atoms and ions over time, researchers can investigate ion diffusion, analyze transport mechanisms, explore factors influencing interfacial stability at different temperatures, pressures, and compositions, and mitigate issues like dendrite growth. Multiphysics modeling in the continuum domain extends the understanding of SSEs to larger length scales.²⁵ By considering the macroscopic behavior of SSEs, researchers can study phenomena like charge transport through electrodes and electrolytes, electrochemical reactions, and the impact of external conditions on SSE performance under realistic operating conditions. More importantly, machine learning techniques have revolutionized SSE research by leveraging large datasets and complex algorithms to uncover the complicated patterns, relationships, and trends.^{26–28} These methods play a vital role in the discovery of new SSE materials and in optimizing synthesis and manufacturing processes by accurately predicting properties, expediting the screening process, and reducing the need for costly and time-consuming experimental trials. Overall, computational methods offer numerous advantages in SSE research, and ultimately accelerate the development of SSEs and pave the way for the realization of high-performance ASSBs.

Given the significant advancements achieved through computational approaches in the field of SSEs, there is an urgent need for a comprehensive review that consolidates the current state of knowledge. Although previous reviews have summarized experimental results^{29–31} and molecular-level simulation studies²¹ of SSEs for lithium secondary batteries, a noticeable gap remains in the literature regarding extensive coverage of multi-scale computational research on SSEs, particularly in tandem with machine learning methods. Bridging this knowledge gap is crucial to expedite the development process. Therefore, this review aims to provide an in-depth overview of the various numerical methods employed in SSE research and their applications across different scales. A particular



Dr Yusong Zhu is a professor at School of Energy Science and Engineering, Nanjing Tech University (NJTech). He received his PhD degree in 2013 from Fudan University (FUDU), and then he did research work on polymer materials for energy storage at the Chemical Resources Laboratory in the Tokyo Institute of Technology (TITech). His current research interests focus on the advanced materials for solid-state lithium/

sodium/zinc batteries, aqueous rechargeable batteries, supercapacitors and fuel cells. Dr Zhu has filed over 15 patents and patent applications, and co-authored more than 120 relevant peer-reviewed publications.

Yusong Zhu

emphasis will be placed on the role of machine learning-assisted approaches and their significant contributions in understanding the fundamental mechanisms and guiding the design optimization of SSEs.

In this comprehensive review, we will present and discuss the recent advancements in the development of SSEs for lithium secondary batteries using computational approaches. The review will be structured as follows to provide a systematic exploration of the topic. Section 2 will provide a brief overview of different numerical techniques utilized at various scales. Section 3 will focus on the estimation of intrinsic properties of SSEs, such as crystal structure prediction and ion migration mechanisms, using computational methods. Section 4 will analyze the electrochemical and chemical compatibility of various electrode-SSE pairs, elucidating the computational understanding of the interactions and interfaces between SSEs and electrode materials. Section 5 will investigate the dynamics and failure mechanisms of SSEs during operation, shedding light on the understanding of SSE behavior under different conditions. Section 6 will highlight the role of machine learning methods in material design for SSEs, showcasing their potential to predict material properties, optimize synthesis processes, and guide the discovery of new SSE materials. Finally, we will summarize the current state of numerical-inspired research on SSEs and provide valuable insights into future directions and potential advancements. In this review, we aim to offer a valuable resource for researchers, graduate students, and professionals in academia and the industrial sector to stay updated on recent advancements in the field of SSEs. We believe that this review will ultimately expedite the development of all-solid-state batteries by providing an insightful overview of the role of computational approaches.

2. Numerical approaches at various scales

In recent years, computational methods have become increasingly important in advancing the research and development of

SSEs for lithium secondary batteries. These methods have been applied with Multiphysics couplings at various scales,³² including atomistic, molecular, and mesoscopic levels, as depicted in Fig. 1. In particular, by simulating and analyzing SSE behaviors at different spatial and time scales with the assistance of machine learning techniques, computational approaches have provided valuable insights into the fundamental properties and failure mechanisms of SSEs. They have not only facilitated the exploration of new materials but also optimized battery performance and enhanced our understanding of SSE behavior under different operating conditions. Table 1 summarizes the functions, pros, and cons of various numerical methods. In the following sections, we will explore the specific numerical techniques used in SSE research, explaining their functions and mechanisms in detail.

2.1. First-principles calculations

First-principles calculations serve as the foundational computational method for studying SSEs. These calculations leverage the principles of quantum mechanics to precisely predict intrinsic properties like ionic conductivity, diffusion coefficients, and thermodynamic stability.

2.1.1. Density functional theory (DFT) method. The DFT method is extensively employed to simulate the electronic structure and thermodynamic properties of SSEs based on a variety of computational packages, such as VASP,³³ CASTEP,³⁴ PAW,³⁵ etc. By solving the Kohn-Sham equation (1) for the system's electrons, DFT provides insights into the energy levels, band structure, and electronic density distribution of SSE materials,³⁶

$$[-(\hbar^2/2m)\nabla^2 + V(\mathbf{r}) + V_H(\mathbf{r}) + V_{XC}(\mathbf{r})]\psi_i(\mathbf{r}) = \varepsilon_i\psi_i(\mathbf{r}) \quad (1)$$

where \hbar is Planck's constant divided by 2π , m is the mass of the electron, ∇^2 is the Laplace operator representing the kinetic energy, $V(\mathbf{r})$ is the external potential acting on the electron, $V_H(\mathbf{r})$ is the Hartree potential arising from the electron-electron

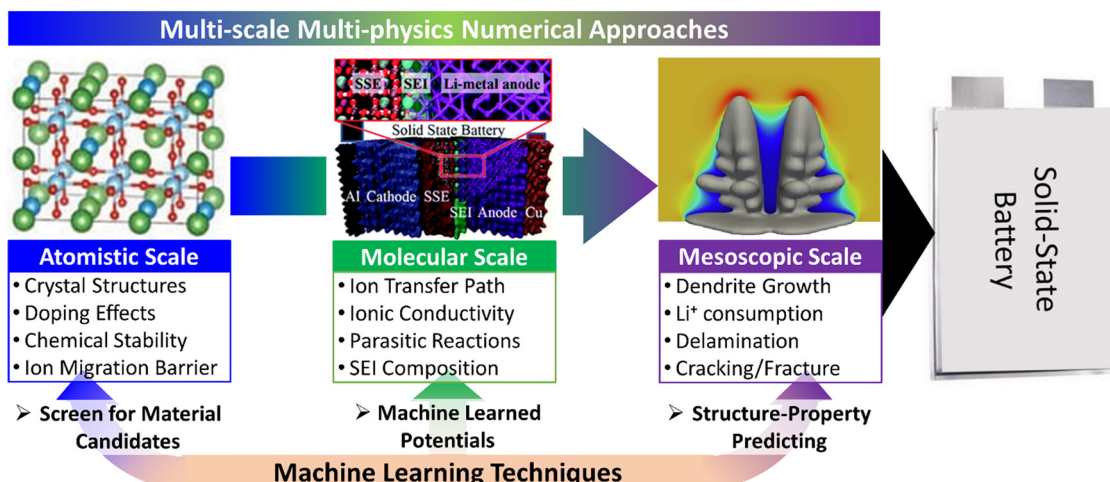


Fig. 1 Schematic diagram of multi-scale computational methods for the research and development of SSEs.

Table 1 Functions, pros, and cons of various numerical methods

Numerical methods	Functions	Pros	Cons
First-principle calculation	<ul style="list-style-type: none"> Predicts the electronic structure and properties of materials Analyzes chemical reactions and bonding 	<ul style="list-style-type: none"> Provides an accurate electronic structure and properties High level of precision 	<ul style="list-style-type: none"> Computationally intensive and time-consuming Limited to small system sizes and time scales Limited to short time scales
Molecular dynamics simulation	<ul style="list-style-type: none"> Studies the dynamic behavior of atoms/molecules Analyzes phase transitions and diffusion 	<ul style="list-style-type: none"> Captures atomic motion and intermolecular interactions Suitable for studying equilibrium and dynamic properties Captures stochastic and time-dependent processes Efficient for rare event simulations 	<ul style="list-style-type: none"> Computational cost increases with system size Simplified model assumptions may lead to inaccuracies Computationally expensive for large system sizes Requires accurate input data
Kinetic Monte Carlo simulations	<ul style="list-style-type: none"> Analyzes kinetic processes and reaction rates Studies diffusion and growth mechanisms 		
Thermodynamic phase equilibrium analysis	<ul style="list-style-type: none"> Predicts phase behavior and equilibrium Determines phase diagrams 	<ul style="list-style-type: none"> Analyzes phase transitions and equilibrium properties Can provide insights into thermodynamic stability Suitable for complex geometries 	<ul style="list-style-type: none"> Sensitive to system size and assumptions Requires discretization and meshing of the domain Higher computational cost compared to analytical methods Requires large amounts of training data Interpretability and transferability may be challenging
Finite element modeling	<ul style="list-style-type: none"> Analyzes multiphysics (mechanical, thermal, and electrochemical) couplings Predicts structural responses, performance, and failure modes Predicts material properties and behavior 	<ul style="list-style-type: none"> Captures distributed mechanical and electrochemical phenomena Enables data-driven modeling 	
Machine learning approaches	<ul style="list-style-type: none"> Accelerates materials discovery and design 	<ul style="list-style-type: none"> Can handle complex and high-dimensional data 	

interactions, and $V_{XC}(\mathbf{r})$ is the exchange–correlation potential representing the effects of electron–electron interactions beyond the classical Coulomb interaction. The wavefunction $\psi_i(\mathbf{r})$ and its corresponding eigenvalue ϵ_i represent the electronic wavefunction and energy level, respectively. This information plays a crucial role in understanding ion migration mechanisms and electronic transport properties within SSEs. DFT calculations also enable the prediction of phase stability and investigation of phase transitions in SSE materials under diverse temperature and pressure conditions. However, it is important to note that DFT calculations can be computationally intensive and might underestimate or overlook the impact of dynamic and electrochemical effects, which are essential for accurately capturing the behavior of SSEs under realistic operating conditions.

2.1.2. Nudged elastic band (NEB) method. The NEB method is highly advantageous for investigating ion diffusion mechanisms in SSEs. It entails the creation of a sequence of intermediate states, determining their energies using electronic structure methods, and arranging them along a reaction coordinate.³⁷ Forces acting on each state are computed using eqn (2), where a force correction step is applied to push the images and minimize forces perpendicular to the reaction coordinate,

$$\mathbf{F}_i = -\nabla E_{i,\text{perp}} \quad (2)$$

where \mathbf{F}_i is the force acting on the i th image and $E_{i,\text{perp}}$ is the energy of the image projected onto the reaction coordinate. The NEB method involves an iterative optimization process that minimizes the forces and identifies the lowest energy configuration, thereby representing the optimal diffusion pathway.³⁸ By calculating the energy barriers between the images along the pathway, the NEB method provides a quantitative measure of

the energy landscape.³⁹ This information is crucial for understanding the mechanisms of ion migration and determining diffusion coefficients within SSE materials. Nevertheless, the NEB method can be computationally demanding. Additionally, it relies on the assumption of a single minimum energy pathway, which may not fully capture the complex diffusion behavior observed in SSE systems.

2.2. Molecular dynamics (MD) simulation

MD simulation is a highly effective computational technique utilized for studying the behaviors and properties of SSEs at the atomistic level to provide valuable insights into the structural dynamics, thermal properties, and diffusion mechanisms of ions.⁴⁰ MD simulations usually incorporate the Lennard-Jones (LJ) potential (3), which describes the interatomic interactions in the system, including the combined effect of attractive van der Waals forces and repulsive forces arising from electron repulsion at close distances,

$$V(r) = 4\epsilon[(\sigma/r)^{12} - (\sigma/r)^6] \quad (3)$$

where $V(r)$ is the potential energy between two atoms at a distance r . The parameters ϵ and σ determine the depth of the potential well and the distance at which the potential is zero, respectively.

MD simulations play a multifaceted role in the study of SSEs by accurately capturing the complex dynamics and interactions between ions and the SSE matrix.⁴¹ First, MD simulations enable the exploration of the structural stability and phase transitions of SSE materials. By simulating the system at different temperatures and pressures, researchers can identify phase boundaries and observe the structural changes that occur within SSEs. This knowledge is essential for designing SSEs that are stable and efficient. Second, MD simulations

provide crucial insights into ion diffusion mechanisms. By tracking the trajectories and velocities of individual ions, researchers can quantify diffusion coefficients and gain a deeper understanding of the factors influencing ion transport.⁴² Besides, MD simulations can explore the impact of external factors such as temperature, pressure, and electric fields on SSE properties. However, MD simulations have limitations, such as computational constraints and reliance on force fields for accuracy.

Ab initio molecular dynamics (AIMD). One widely used variant of MD simulations for SSEs is the AIMD method. AIMD simulations involve setting up the initial system configuration and performing electronic structure calculations, such as DFT, to determine forces and energies.⁴³ The equations of motion are then numerically integrated to track atomic positions and velocities over time. Sampling techniques are employed to allow the system to evolve, and thermostats and barostats can be included for temperature and pressure control.^{44,45} AIMD simulations provide valuable insights into the dynamic behavior of SSEs at the quantum mechanical level, facilitating the study of chemical reactions, phase transitions, and material properties. The diffusivity of ion species, D , can be obtained using the Einstein relation (4),⁴⁶

$$D = \frac{1}{2d\Delta t N} \sum_{i=1}^N |\mathbf{r}_i(t + \Delta t) - \mathbf{r}_i(t)|^2 \quad (4)$$

where d is the dimension of the system, N is the number of mobile ions, $\mathbf{r}_i(t)$ is the position of ion i at time t and Δt is the time interval. The angle brackets represent averaging over Δt . The ionic conductivity σ is thus calculated using the Nernst-Einstein relation (5),

$$\sigma = \frac{Nq^2}{VkT} D \quad (5)$$

where V is the total volume, q is the charge of the ion, and k is the Boltzmann constant. Despite these merits, AIMD simulations can be computationally intensive because they require solving quantum-mechanical equations for all atoms at each time step. As a result, the size and time scale of systems that can be studied are limited. Furthermore, AIMD simulations are sensitive to the choice of exchange-correlation functionals and the level of theory used, which may introduce errors.

2.3. Kinetic Monte Carlo (KMC) simulations

KMC simulations offer a detailed understanding of the microscopic processes involved in the dynamics of SSEs. Through a stochastic approach, KMC simulations track the individual movement of atoms or particles, enabling the study of long-time scale phenomena that are challenging to observe experimentally.⁴⁷ These simulations provide insights into ion diffusion mechanisms, kinetics of defect formation and annihilation, and overall ionic conductivity of SSE materials. KMC simulations involve constructing a potential energy landscape and transition rates for atomic or particle movements. By randomly selecting events based on their rates, the simulation

progresses, allowing for the exploration of diffusion pathways and calculation of observable quantities using the rate eqn (6),⁴⁸

$$\frac{dP_i(t)}{dt} = \sum_{j \neq i} R_{j \rightarrow i} P_j(t) - \sum_{j \neq i} R_{i \rightarrow j} P_i(t) \quad (6)$$

where $P_i(t)$ represents the probability of being in state i at time t and $R_{j \rightarrow i}$ is the transition rate from state j to state i . KMC simulations can provide insights into the mechanisms of ionic transport, considering materials and structural parameters. They can identify dominant diffusion pathways and assess the effects of factors like temperature, concentration, and defects.⁴⁹ Moreover, KMC simulations can be conducted on large system sizes, allowing for the study of realistic SSE configurations.⁵⁰ However, accurate results depend on the precise determination of transition rates, which can be challenging to obtain experimentally or theoretically.

2.4. Thermodynamic phase equilibrium analysis

Thermodynamic phase equilibrium analysis enables the determination of phase diagrams, which illustrate the stable phases and their compositions under varying temperature and pressure conditions.⁵¹ This analysis assists in identifying phase transitions and predicting the behavior of SSE materials under diverse operating conditions.⁵² Furthermore, it aids in the selection and design of SSE materials with optimal properties for specific applications by minimizing the Gibbs free energy of the system, according to eqn (7),⁵³

$$\Delta G = x_1 x_2 (A_{12}x_1 + A_{21}x_2) \quad (7)$$

where ΔG represents the excess Gibbs free energy, x_1 and x_2 are the mole fractions of two components, respectively; and A_{12} and A_{21} are the interaction parameters. Thermodynamic models can be used to describe the stability and phase transitions of SSEs with various electrode active materials by considering the chemical potentials and activities of different components.⁵⁴ But these models assume equilibrium conditions and may not fully capture the kinetics and non-equilibrium behavior exhibited by SSE materials, including defects, grain boundaries, and surface effects.

2.5. Finite element modeling (FEM)

FEM plays a crucial role in the study of SSEs, serving multiple functions. It allows for accurate prediction and analysis of SSE materials' behavior under various operational conditions, including temperature, pressure, and electric fields. FEM also provides valuable insights into the structural integrity, thermal management and electrochemical performance of SSEs, and greatly aids in the design and optimization of SSE architectures and geometries to enhance their efficiency and performance.⁵⁵ FEM offers a comprehensive understanding of the multi-physics behaviors, *i.e.*, electrochemical, thermal and mechanical, exhibited by SSE systems.⁵⁶ It can handle complex geometries, heterogeneities, and boundary conditions, enabling the analysis of localized phenomena like interfacial effects,

concentration gradients, and stress distributions. This capability allows researchers to investigate and address crucial challenges related to SSE performance.

Multi-physics simulation. Multi-physics simulation, particularly through the use of FEM, has become an essential tool in the study of SSEs. SSEs are complex systems that involve a combination of electrochemical, thermal, and mechanical processes. A comprehensive understanding and predicting the behavior of these multi-physics phenomena in a single simulation framework is crucial for the failure analysis and optimal design of SSEs under various operational conditions, such as temperature, pressure, and electric fields.⁵⁷

The electrochemical behavior in SSEs is governed by the Nernst–Planck equation (8) and the Poisson equation (9), which describe the transport of ions through the solid electrolyte:

$$J_i = -D_i \nabla c_i - \frac{z_i F}{RT} D_i c_i \nabla \varphi \quad (8)$$

$$\nabla^2 \varphi = -\rho_i / \epsilon \quad (9)$$

where J_i is the flux of the ionic species, D_i is the diffusion coefficient, ∇c_i is the concentration gradient, z_i is the valence of the ionic species, and F and R are Faraday's constant and gas constant, respectively. T is the temperature, and $\nabla \varphi$ is the gradient of the electric potential. ∇^2 is the Laplacian operator and ρ_i and ϵ are the charge density and permittivity, respectively.

The thermal behavior in SSEs is described by the heat transfer eqn (10), which accounts for heat conduction and any heat generation or absorption within the material:

$$\rho C \partial T / \partial t = \nabla (k \nabla T) + Q \quad (10)$$

where ρ and C are the density and specific heat capacity of the material, respectively, t is time, k is thermal conductivity, and Q represents any heat sources or sinks.

The mechanical behavior in SSEs is governed by the equations of linear elasticity, which describe the deformation and stress distribution within the material.

By coupling the above governing equations and specifying the boundary conditions and material properties, FEM can provide valuable insights into the structural integrity, thermal management, and electrochemical performance of SSEs, addressing critical challenges, such as improving ionic conductivity and enhancing interfacial stability.⁵⁸

Phase field (PF) method. The PF Method is a computational tool used to simulate complex phase transitions and microstructural evolution in materials.^{59,60} It uses a PF function to represent different phases or microstructures within a material, making it particularly powerful for the study of SSEs. By solving partial differential equations derived from the free energy functional (11), the PFM allows for the evolution of the PF over time and space.⁶¹

$$\partial \varphi_p / \partial t = D \nabla^2 (\partial F_p / \partial \varphi_p) \quad (11)$$

where φ_p is the PF variable and F_p is the free energy functional.

The PFM has advantages over traditional methods as it captures complex microstructural features without explicit interface tracking.⁶² It smoothly transitions between phases, enabling efficient simulation of diverse morphologies and topologies. It finds applications in solidification, grain growth, phase separation, and microstructure evolution in various materials. The PFM can also be coupled with other governing equations to study multi-physics phenomena, such as heat transfer or fluid flow. This allows for the investigation of complex interactions and the prediction of material behavior under realistic conditions.

Above all, FEM does have limitations that need to be considered. It relies heavily on accurate input parameters, such as material properties and boundary conditions, which can be challenging to determine experimentally or theoretically. Therefore, validation of FEM results often requires the use of experimental data or comparison with other computational methods. Despite these limitations, FEM remains an indispensable tool in the study of SSEs, contributing significantly to our understanding, optimization, and advancement of these materials for various applications.

2.6. Machine learning (ML) approaches

ML approaches contribute significantly to the prediction of SSE properties by leveraging experimental or computational data. ML techniques have seen increasing application in various aspects,⁶³ including the discovery of advanced active materials through efficient screening of vast databases or high-throughput calculations, predicting the microstructures of SSEs and estimating their intrinsic structure–property relationships, uncovering new reaction and ion diffusion mechanisms, diagnosing and prognosing material degradation and failure, and optimizing SSE compositions and architectures for enhanced performance,⁶⁴ etc.

The operation of ML techniques involves training computational models on labeled datasets, which can be acquired from online material databases such as materials project (MP),⁶⁵ automatic flow (AFLOW),⁶⁶ and open quantum materials database (OQMD).⁶⁷ The input variables (features) capture relevant parameters of the SSE system, e.g., stable crystal structures, free energy, highest occupied molecular orbital (HOMO) and lowest unoccupied molecular orbital (LUMO) energy, etc., while the output variable represents the targeted electrochemical or mechanical properties.

By employing various ML algorithms like neural networks, support vector machines, or random forests, these models learn intricate patterns and relationships within the data, enabling accurate predictions or classifications. Rigorous testing and validation using independent datasets assess the performance and generalizability of these models.

High-throughput screening (HTS). HTS is an effective technique employed in materials science to swiftly assess numerous materials or compounds for specific properties or characteristics, adhering to predefined criteria or constraints.⁶⁸ HTS frequently utilizes computational models that rely on fundamental equations, such as those based on DFT, to predict

material properties.⁶⁹ It involves the utilization of computational methods and algorithms to efficiently investigate and analyze extensive databases or combinatorial libraries of materials. This enables the identification of correlations between structural features and desired material properties, unveiling valuable patterns and relationships that can guide subsequent material design and screening endeavors.

Neural networks (NNs). NNs function through feedforward propagation, activation functions, and backpropagation.^{70–72} In feedforward propagation, input data are passed through layers of interconnected neurons, which perform computations using weighted sums and activation functions. Activation functions introduce non-linearity, enabling the network to learn complex patterns. Backpropagation is a vital process where the network adjusts its weights and biases by propagating the error backward through the layers, facilitating learning and optimization. Key equations in neural networks include the feedforward eqn (12), error calculation equations such as mean squared error, and backpropagation equations for gradient computation,

$$a = f(Wx + b) \quad (12)$$

where a represents the activation of the neuron, f is the activation function applied to the weighted sum of inputs, W denotes the weight matrix, x is the input vector, and b represents the bias vector. These equations facilitate the training and optimization of neural networks, enabling them to learn from data and make predictions or classifications while capturing complex relationships in the data.

Support vector machines (SVMs). SVMs are widely utilized for classification and regression tasks.⁷³ The underlying mechanisms of SVMs entail the pursuit of an optimal hyperplane that effectively separates distinct classes or approximates a regression function. SVMs employ the kernel trick to transform data into higher-dimensional spaces, wherein linear separation becomes feasible by maximizing the margin between the hyperplane and the nearest data points, commonly referred to as support vectors, $m = 2/w$, where w denotes the Euclidean norm of the weight vector. These equations enable SVMs to determine the optimal decision boundary or regression function, facilitating precise classification or regression tasks.

Overall, the integration of ML techniques brings notable benefits to SSE studies.^{74–76} ML approaches enable efficient utilization of vast data resources, leading to valuable insights and facilitating the design of highly efficient and customized SSE systems with high-dimensional compositional spaces, which may be beyond the capability of traditional analytical methods.⁷⁷ However, it is important to note the limitations of ML approaches in SSE research. The accuracy and reliability of ML predictions heavily rely on the quality and representativeness of the training data. Insufficient or biased datasets can result in unreliable models and erroneous predictions. Moreover, ML models may struggle with generalization, performing well on training data but poorly on new, unseen data. The interpretability of ML models can be challenging, as they often

function as black boxes, making it difficult to understand the underlying physical or chemical mechanisms driving the predictions. Additionally, computational resources and time can be limiting factors, especially for complex models or extensive datasets.

3. Prediction of intrinsic properties of SSEs

In the quest to advance high-performance ASSBs, the identification of suitable SSEs with enhanced properties is of utmost importance. One cost-effective and accurate approach for discovering promising SSE materials is through the employment of numerical methods to estimate their inherent properties. This includes utilizing techniques like DFT and MD simulations to predict stable crystal structures and understand ion migration mechanisms, which are vital factors in the search for appealing SSEs.⁷⁸ In this section, we will discuss the application of various numerical approaches for exploring SSEs with desirable stability and ionic conductivity properties, and their impact on the development of high-performance ASSBs.

3.1. Prediction of stable phases

The development of high-performance ASSBs hinges on the discovery of SSEs with appropriate structures and improved properties. By utilizing numerical methods, researchers can predict stable crystal structures of inorganic electrolytes, as well as the morphologies of composite or polymer electrolytes.^{79–81}

In the case of halide SSEs, their ionic conductivities have historically lagged behind sulfide or oxide counterparts.⁸² However, recent decades have witnessed significant efforts to identify promising halide materials.^{83–85} For example, Park *et al.* employed first-principles calculations to systematically identify 12 stable Li_3MCl_6 SSEs with wide electrochemical stability windows and excellent chemical stabilities against cathode materials and moisture.⁸⁶ To gain a deeper understanding of structure stability and its impact on Li^+ migration, a lithium ytterbium-based halide (Li_3YbCl_6) was investigated.^{87,88} The trigonal and orthorhombic crystal structures of Li_3YbCl_6 (Fig. 2(a) and (b)) exhibited metastable properties and wide electrochemical windows. Notably, the orthorhombic material displayed greater chemical stability and higher ionic conductivity. In addition to halide SSEs, compositionally complex materials have also been explored. One such material, $(\text{Li},\text{Sr})(\text{Ta},\text{Nb},\text{Zr},\text{Hf})\text{O}_{3-\delta}$ (LSTNZH), exhibited high ionic conductivity attributed to the control of grain boundaries.⁸⁹ This discovery highlights the significance of compositionally complex SSEs in achieving desirable transport properties.

Element doping has emerged as a widely utilized strategy for enhancing the properties of SSEs. Numerical studies have revealed the effectiveness of fluorination in improving ionic conductivity^{90,91} and optimizing interfacial stability.^{92,93} By employing DFT and AIMD, researchers have investigated the mechanisms of fluorination in $\text{Li}_2\text{OHCl}_{0.9}\text{F}_{0.1}$ SSEs.⁹⁴ The study examined the impact of fluorination on crystal structures and

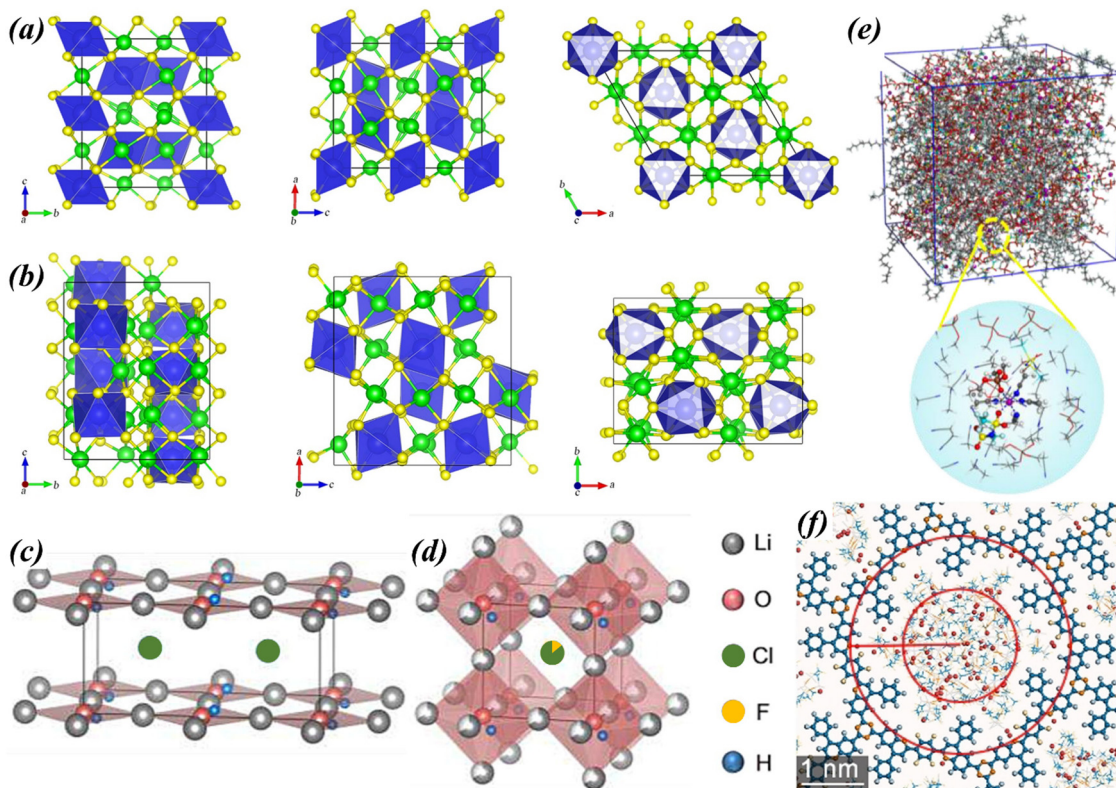


Fig. 2 Crystal structures of $1 \times 1 \times 2$ supercells of (a) trigonal and (b) orthorhombic Li_3YbCl_6 . Reprinted from ref. 88, with permission from Elsevier. The crystal structure of (c) orthorhombic antiperovskite Li_2OHCl and (d) cubic antiperovskite $\text{Li}_2\text{OHCl}_{0.9}\text{F}_{0.1}$ (Li in grey, O in red, Cl in green, F in yellow, and H in blue); the partially fluorinated Cl^- ions are located at the A-site of the antiperovskite structure. Reprinted from ref. 94, with permission from Elsevier. (e) Snapshot of SSE-TMP electrolyte based on MD results. Reprinted from ref. 100, with permission from Elsevier. (f) Optimized structures of LiTFSI in the channels of Q-COF; the distance between the outer red circle and the inner red circle is about 0.85 nm. Reprinted from ref. 103, © 2021 Wiley-VCH GmbH.

the migration of Li-ions. Fig. 2(c) and (d) illustrate the crystal structures of Li_2OHCl and fluorine-doped $\text{Li}_2\text{OHCl}_{0.9}\text{F}_{0.1}$, respectively, where the F-doping is represented by a partially fluorinated Cl^- at the A-site of the antiperovskite structure.

Fluorination induced lattice defects and disorder between F^- and Cl^- ions, resulting in a transition from the original orthorhombic phase to a stable cubic phase. This structural change facilitated ion transport by creating close ion transport sites and reducing energy barriers for ion migration. Furthermore, in conventional SSEs like lithium garnet-based solid electrolytes (LGPS), element doping with Ge, Sn, ZnO, and other elements has been shown to improve moisture stability without compromising ionic conductivity.^{95–97} DFT and AIMD studies have been conducted to investigate the effects of dopants on moisture interaction with LGPS and the formation mechanism of H_2S .⁹⁸ These investigations revealed that surface Se substitution in LGPS weakened moisture adsorption and suppressed H_2S evolution.

Further research is also needed to understand the relationship between internal structure optimization and the micro-dynamics of Li^+ transport at the electrode–electrolyte interfaces of polymer/composite electrolytes.⁹⁹ MD simulations have been utilized to study the stable structure of trimethyl phosphate (TMP) molecular anchored polymers, as depicted in Fig. 2(e).¹⁰⁰

The simulations revealed that TMP molecules actively contribute to the Li^+ solvation shell formation, while the polymer molecules encapsulate the Li^+ solvation shell, creating a polymer framework. This arrangement enhances the Li^+ diffusion coefficient and regulates the Li^+ solvation structure, indicating the reversibility and stability of batteries. Porous materials, such as covalent organic frameworks (COFs), have gained significant attention for their potential to provide fast ionic conducting pathways, offering new possibilities for designing efficient SSEs.^{101,102} DFT and MD calculations have been employed to investigate the stable hopping paths of Li^+ along the one-dimensional pore walls of COFs, as depicted in Fig. 2(f).¹⁰³ The calculations revealed that Li^+ ions are distributed around the nitrogen and fluorine atoms of the COF frameworks at a distance of approximately 0.85 nm, indicating an affinity between Li^+ and COF materials.

In summary, these studies provide valuable insights for evaluating the performances of newly discovered active SSEs, contributing to the ongoing efforts in designing SSEs with improved stability and properties.

3.2. Exploration on the ion migration mechanisms

Different solid electrolyte materials exhibit unique ion transport mechanisms, resulting in diverse material properties and

avenues for modification. In this section, we will discuss numerical studies that have investigated the ion migration behaviors of various materials, including solid inorganic electrolytes, polymer electrolytes, nanostructured materials, and composite electrolytes.

Solid inorganic electrolytes (SIEs). Solid inorganic electrolytes have emerged as promising candidates for advanced lithium rechargeable batteries.¹⁰⁴ These electrolytes, composed of oxide materials such as Li-La-Zr-O,¹⁰⁵ Li-La-Ti-O,¹⁰⁶ Li-Ta-P-O,¹⁰⁷ and lithium-bearing sodium superionic conductors (NASICON),¹⁰⁸ sulfide materials like Li-P-S,¹⁰⁹ Li-Ge-P-S,¹¹⁰ Li-P-S-Cl,¹¹¹ Li-Si-P-S-Cl¹¹² and Li-Si-As-S-I¹¹³ or halide materials like Li-Y-F,¹¹⁴ Li-In-Cl,¹¹⁵ and Li-Zn-I,¹¹⁶ offer several advantages over conventional liquid electrolytes. Notably, they exhibit high ionic conductivity, enabling efficient ion transport and faster charging and discharging rates.¹¹⁷ Recent research by Mo's group has challenged the conventional understanding of ion hopping in superionic conductor materials,

introducing a novel conceptual framework.¹¹⁸ Using AIMD, they proposed a mechanism where multiple ions move in a highly coordinated manner along the garnet channel, as depicted in Fig. 3(a) and (b). This concerted ion migration approach significantly enhances ionic conductivity and reduces energy barriers. Doping high-energy sites with Li ions to activate this concerted ion migration has been proven to be an effective strategy in the design of SIEs. Another advantage of SIEs is their wide electrochemical and thermal stability window.³⁶ They can tolerate high-voltage and high-temperature applications without significant chemical decomposition, enhancing the safety of batteries.

While SIEs offer numerous advantages, they still face challenges related to structural and chemical instability in sulfide SEs,¹¹⁹ low compatibility with electrodes in oxide SEs,¹²⁰ and rapid interfacial degradation in halide/sulfide SEs.¹²¹ Additionally, there is often an inverse correlation between ionic conductivity and electrochemical stability.¹²² To overcome these

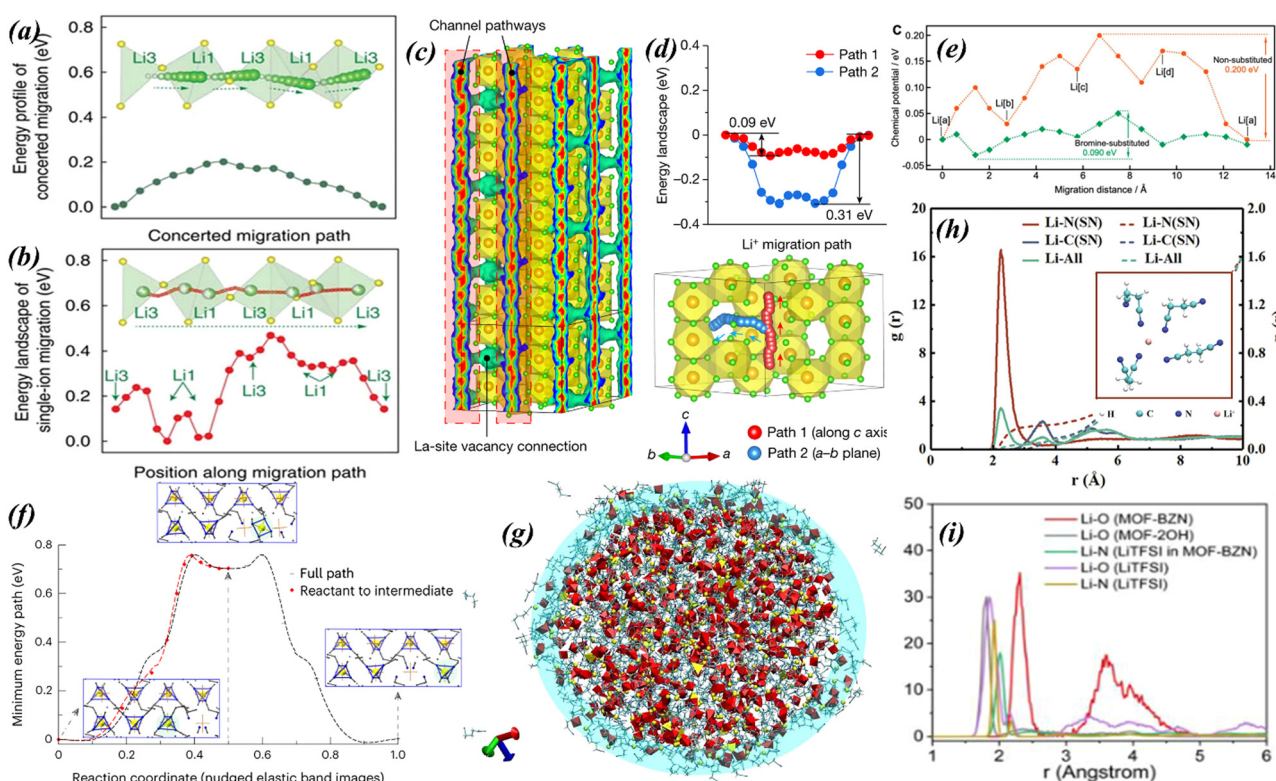


Fig. 3 (a) Migration energy barrier in LGPS for concerted migration of multiple Li ions hopping into the next sites along the diffusion channel; insets show the Li⁺ path (green spheres) and O/S ions (yellow spheres). (b) The energy landscape of single Li⁺ along the migration channel (shown in insets) across multiple Li sites (partially filled green spheres) and Li⁺ pathway (red spheres). Reprinted with permission from ref. 118. (c) Li⁺ probability density in the vacancy-containing LaCl₃ lattice. (d) Li⁺ migration paths in the vacancy-containing LaCl₃ lattice and corresponding energy barriers. The red path represents Li⁺ migration in channels (along the *c* axis) and the blue path represents exchange migration between adjacent channels through La-vacancy sites (*a*–*b* plane). Reprinted from ref. 129, with permission from Springer Nature. (e) Potential energy as a function of migration distance along the Li[a]–Li[b]–Li[c]–Li[d]–Li[a] pathway. Reprinted from ref. 135, with permission from AAAS. (f) DFT calculation for the analysis of the minimum energy path for Li⁺ migration in the bulk, in the *b* crystallographic direction; the geometries of the initial, intermediate and final structures, as well as the location for a migrating Li⁺, are shown as insets. (g) Snapshots of (Adpn)₂-LiPF₆ cocrystals after an equilibration of 10 ns at room temperature; the liquid-like surface-layer is shown in a cyan ring. Reprinted from ref. 150, with permission from Springer Nature. (h) Calculated radial distribution functions (*g*(*r*), solid lines) and coordination numbers (*n*(*r*), dashed lines) for Li–N (red), Li–C (blue), and Li–all (green); the inset illustrates the snapshots of SN and Li⁺ obtained by MD simulation at 25 °C. Reprinted from ref. 154, © 2023 Wiley-VCH GmbH. (i) Calculated RDFs of MOF-BZN, MOF-OH-V and LiTFSI. Reprinted from ref. 173, © 2023 Wiley-VCH GmbH.

challenges, researchers have proposed various modification strategies. One promising approach is the synthesis of a novel phosphorus-free sulfide SE, $\text{Li}_{6.8}\text{Si}_{0.8}\text{As}_{0.2}\text{S}_5\text{I}$.¹¹³ This material exhibits improved air stability and reduced cost while maintaining an impressive ionic conductivity of 10.4 mS cm^{-1} at 25°C . The enhanced performance of this material is attributed to silicon doping, as confirmed by MD analysis using advanced deep-learning potential techniques. Another innovative idea is to identify high-ionic-conductivity materials that undergo multiple phase transitions and transform into ionically conducting but electronically insulating products at electrode-electrolyte interfaces. One example is the lithium thioborate (Li–B–S) material system, which includes compounds like $\text{Li}_5\text{B}_7\text{S}_{13}$, Li_3BS_3 , $\text{Li}_2\text{B}_2\text{S}_5$, $\text{Li}_{10}\text{B}_{10}\text{S}_{20}$ and $\text{Li}_9\text{B}_{19}\text{S}_{33}$. These materials have been studied using DFT and MD simulations, demonstrating ultrahigh single-crystal ionic conductivities and wide electrochemical stability windows.^{123–125} In fact, their performance rivals or even surpasses that of well-known oxide SES.

Meanwhile, while sulfides generally possess a flexible sulfur sublattice,¹²⁶ oxides are known for their rigid structural framework. As a result, oxide SESs often exhibit lower ionic conductivity and higher activation energy compared to sulfides. However, oxides offer superior chemical and mechanical stability.¹²⁷ To understand the ion migration mechanisms in oxide SESs, Jian-Fang *et al.* conducted an extensive investigation focused on the transport of lithium ions in LiTa_2PO_8 and its derivatives using DFT calculations and AIMD simulations.¹²⁸ Their study revealed a remarkable finding of one-dimensional liquid-like lithium-ion conduction in LiTa_2PO_8 . This conduction mechanism was characterized by a disordered distribution of lithium ions and remarkably low energy barriers of only 0.2 eV. These findings provide valuable insights into the mechanisms responsible for the high ionic conductivity observed in oxide SESs. By understanding the underlying ion migration mechanisms, researchers can pave the way for the future discovery and design of advanced solid-state electrolytes.

To enhance Li-ion diffusion in halide solid electrolytes, a Ta^{5+} -doped $\text{Li}_x\text{Ta}_y\text{La}_z\text{Cl}_3$ material was proposed. This material introduces vacancies that form a three-dimensional lattice, facilitating Li-ion diffusion.¹²⁹ The presence of La vacancies in the LaCl_3 lattice enables the migration of Li^+ ions, as illustrated in Fig. 3(c) through AIMD analysis. Energy landscape analysis revealed low barriers of 0.09 eV along the *c*-axis channel (red path in Fig. 3(d)) and 0.31 eV along the *a*–*b* plane (blue path in Fig. 3(d)), emphasizing the crucial role of La vacancies in enabling rapid Li^+ conduction. The influences and functions of vacant sites on the ion-migration behaviors have further been confirmed by DFT calculations, highlighting that the balance between Li-ion and vacant-site content is a more critical aspect than the aliovalent substitution-induced structural changes.¹³⁰ Besides, lithium nitride halides (LNCl) have drawn attention due to their thermodynamic stability against lithium metal.¹³¹ Victor *et al.* conducted an extensive investigation into the fundamental lithium diffusion mechanism in fully-reduced Li_5NCl_2 SE using AIMD simulations.¹³² They discovered that the mechanochemical synthesis procedure

introduces local structural disorder, creating lower-energy percolation paths within the SE. This study not only provides valuable insights for optimizing the conductivity of LNCl, but it also suggests the potential use of highly-disordered electrolytes as artificial protection layers between SEs and lithium-metal anodes. This approach could enhance the safety and performance of lithium-based energy storage systems.

Multi-element doping is a promising strategy to enhance the ionic conductivity of SIEs by reducing the potential barrier for Li-ion migration.^{133,134} Prof. Kanno's research group has made significant advancements in this area by establishing a rule for producing advanced SIEs and designing a series of crystals, such as $\text{Li}_{9.54}[\text{Si}_{1-\delta}\text{M}_\delta]_{1.74}\text{P}_{1.44}\text{S}_{11.1}\text{Br}_{0.3}\text{O}_{0.6}$ ($\text{M} = \text{Ge}, \text{Sn}; 0 \leq \delta \leq 1$), through a multi-substitution approach to create high-entropy lithium superionic conductors.¹³⁵ Theoretical calculations (shown in Fig. 3(e)) indicated that the energy barrier for Li-ion migration in the material without element substitution was 0.20 eV. However, through bromine substitution, the energy barrier could be significantly reduced to 0.09 eV, thereby promoting ion conduction. This study opens up new avenues for exploring novel superionic conductors in commercial applications, including those with millimeter-thick electrode packages. By leveraging the potential of multi-element doping, researchers can further enhance the performance and efficiency of solid-state batteries. The development of high-entropy lithium superionic conductors through multi-element doping showcases the potential to engineer solid electrolytes with improved conductivity. By carefully selecting and substituting elements in the crystal lattice, researchers can reduce energy barriers and enhance ion conduction. This approach not only contributes to the fundamental understanding of ion migration mechanisms but also offers practical solutions for the design of advanced solid-state batteries with enhanced performance and reliability.

Table 2 compares the ionic conductivity, electrochemical stable window, and cycling performance of various SIEs.

Polymer electrolytes (PEs). Compared to liquid and ceramic electrolytes, PEs, including solid polymer electrolytes (SPEs) and gel polymer electrolytes (GPEs), offer several advantages such as ease of processing, availability, and operational safety.^{136,137} However, their widespread adoption is hindered by their relatively low ionic conductivity (around $10^{-4} \text{ S cm}^{-1}$ at 25°C) and low Li^+ transference number (around 0.3).¹³⁸ Overcoming these limitations is crucial to match the performance of state-of-the-art electrolytes, and it requires a deep understanding of the Li-ion conduction mechanisms in polymer electrolytes. Considerable efforts have been devoted to studying polymers such as poly(ethylene oxide) (PEO),^{139,140} polyacrylonitrile (PAN),¹⁴¹ poly(methyl methacrylate) (PMMA),¹⁴² poly(vinylidene fluoride) (PVDF),¹⁴³ and poly(vinylidene fluoride-co-hexafluoropropylene) (PVDF-HFP),¹⁴⁴ among others. Effective approaches to enhance the Li^+ transference number and ion conductivity involve regulating the solvation structure of Li^+ within the polymer matrix, increasing the connectivity between solvation sites on the polymer chains, and modifying the microstructure and functional groups of the polymer

Table 2 Comparison of electrochemical properties of SIEs

Solid inorganic electrolyte type	Ionic conductivity (mS cm ⁻¹) at room temp.	Electrochemical stable window (V) vs. Li ⁺ /Li	Cycling performance	Ref.
Li _{6+x} Si _x As _{1-x} S ₅ I ($x = 0.8$)	10.4	~2.227	62 500 cycles at 2.44 mA cm ⁻²	113
Li ₃ InCl ₆	1.49	2.5–4.2	100 cycles at 14 mA g ⁻¹	119
Li ₃ B ₇ S ₁₃	62	1.59–2.19	—	123
Li ₉ B ₁₉ S ₃₃	80	1.59–2.19	—	123
Li ₃ BS ₃	0.36	—	—	124
Li _{6+2x} [B ₁₀ S ₁₈]S _x ($x \approx 1$)	0.13	1.3–2.5	140 h at 0.3 mA cm ⁻²	125
LiTa ₂ PO ₈	1.2	—	700 h at 0.2 mA cm ⁻²	128
Li _{0.388} Ta _{0.238} La _{0.475} Cl ₃	3.02	~4.35	5000 h at 1 mA h cm ⁻²	129
Li _{3-x} Lu _{1-x} Zr _x Cl ₆	1.5	1.44–4.25	1000 cycles at 36 mA g ⁻¹	131
Li ₃ NCl ₂	1	0.6–2.7	—	132
Li _{9.54} Si _{1.74} P _{1.44} S _{11.7-z} Cl _{0.3} O _z ($0 < z \leq 0.6$)	28	0.5–5	20 cycles at 0.122 mA cm ⁻²	133
Li _{9.54} [Si _{0.6} Ge _{0.4}] _{1.74} P _{1.44} S _{11.1} Br _{0.3} O _{0.6}	32	~4.25	30 cycles at 0.587 mA cm ⁻²	135

matrix. Numerical studies have confirmed that implementing these solutions can lead to stable lithium/electrolyte interfaces with low resistance.^{145,146}

The use of SPEs with “soft” or polarizable ligand groups has emerged as an attractive option due to their weaker binding with Li-ions, potentially promoting higher conductivity.^{147–149} Prabhat *et al.* successfully synthesized an adiponitrile-LiPF₆ co-crystal that exhibited significantly high ion conductivity (around 10⁻⁴ S cm⁻¹) and a Li⁺ transference number of 0.54.¹⁵⁰ Interestingly, DFT calculations (Fig. 3(f)) indicated that the Li⁺ conduction in the bulk of the co-crystal had a large energy barrier, contradicting the experimental measurements. This discrepancy suggested an unforeseen mechanism of ion conduction in these soft-solid electrolytes. The MD models further revealed the formation of a liquid-like layer on the surface of the co-crystal (Fig. 3(g)). This layer facilitated preferential ion diffusion through fluid grain boundaries, thereby promoting low-resistance ion conduction. The presence of this liquid-like layer on the co-crystal's surface explained the high ion conductivity observed experimentally, despite the large energy barriers within the bulk of the co-crystal.

Propylene carbonate (PC), succinonitrile (SN), PEO oligomers, and inorganic fillers have been recognized as valuable plasticizers in SPEs for modifying the solvation of Li ions and enhancing their migration.^{151–153} Recent advancements in MD and DFT simulations have provided insights into the working principles of SN as a plasticizer.^{154,155} The calculated radial distribution functions ($g(r)$) and coordination numbers ($n(r)$) (Fig. 3(h)) revealed that the interaction between SN and lithium salt was primarily dominated by Li⁺ and the N atom of SN, while the Li⁺···C and Li⁺···polymer interactions were comparatively insignificant. The formation of a solvated sheath-like structure [SN···Li⁺] between SN and Li⁺ (inset of Fig. 3(h)) was identified as the key mechanism for the rapid transport of Li⁺ through the polymer segments. This solvated sheath-like structure, uniformly distributed throughout the SPE, plays a crucial role in enhancing Li⁺ transport. The interaction between SN and Li⁺ led to the formation of a protective layer around Li⁺ ions, facilitating their easy movement through the polymer matrix. This mechanism of enhanced Li⁺ transport through the solvated sheath structure suggests promising applications

for ambient-temperature, high-voltage lithium–metal batteries (LMBs).

GPE is a type of polymer electrolyte that consists of a polymer matrix that is infused with the liquid electrolyte. The polymer matrix provides mechanical stability, while the liquid electrolyte facilitates ion conduction.^{156,157} However, a deeper understanding of the ion transport pathway within GPEs is still necessary. Qifang *et al.* conducted a study to investigate the ion conduction mechanism in GPEs by preparing *in situ* polymerized GPEs with a fluoroethylene carbonate (FEC) solvent.¹⁵⁸ Through MD simulations, they revealed that these GPEs exhibited a high binding energy with Li ions, resulting in the formation of an electron-rich “Milky Way” interface layer between the liquid electrolyte and the polymer matrix. This interface layer facilitated the formation of abundant transfer pathways for Li ions, enhancing ion conductivity within the GPEs. The presence of the Milky Way interface layer created a favorable environment for ion migration, enabling efficient ion transport through the gel electrolyte.

In addition to the strategies mentioned earlier, another approach to enhance ion conductivity involves the use of macromolecule-based polyelectrolytes. Polyelectrolytes have ionizable groups along their backbones, allowing for the covalent attachment of anions and facilitating the mobilization of Li ions with high transference numbers ranging from 0.8 to 0.98, making them effective single-ion-conductors (SICs).^{159,160} By leveraging these interactions, researchers aim to improve ion transport and stability, advancing the development of efficient and reliable electrochemical energy storage systems.^{161,162} One novel method to improve ion conductivity in SPEs is the incorporation of 1,4-diiodotetrafluorobenzene (1,4-DITFB), a typical halogen-bond donor, into the polymer matrix.¹⁶³ This approach takes advantage of the halogen-bonding interaction between the electron-deficient iodine atom and the electron-rich oxygen atoms of the polymers. This interaction weakens the solvation ability of the polymer towards Li ions, enabling the formation of a thin and uniform solid electrolyte interface (SEI) layer. The SEI layer promotes the mobility of Li⁺ and reduces interfacial resistance on the lithium metal anode, improving overall performance. Similarly, SIC electrolytes synthesized *via* a one-pot polycondensation

reaction method have been developed, incorporating ionizable monomers, cross-linkers, and an oligomeric polymer matrix.^{27,164} These electrolytes demonstrate abundant active sites for Li⁺, accelerated chain relaxation, and reduced energy for ion conduction, resulting in high ionic conductivity, remarkable ion transference numbers, and stable Li plating–stripping behaviors, as observed in experimental measurements.

The design and synthesis methods used for molecular and supramolecular organo-ionic electrolytes have inspired the development of robust and tough PEs without compromising on ionic conductivity.^{165,166} Supramolecular electrolytes often incorporate dynamic bonds to improve electrode–electrolyte contact and mitigate stress concentration, strong cross-linking bonds to enhance mechanical strength, and weak bonds to contribute to high conductivity.^{167–169} The use of supramolecular structures in polyelectrolytes also enables efficient recycling of cathode materials, promoting the sustainability of battery technologies.¹⁷⁰ Supramolecular materials hold great potential for enhancing the performance and reliability of batteries.

Table 3 compares the ionic conductivity, electrochemical stable window, and cycling performance of various PEs.

Nanostructured electrolytes. Nanostructured materials, such as metal–organic frameworks (MOFs) and covalent organic frameworks (COFs), present distinct advantages as artificial channels for ionic conduction due to their tunable pore structure and chemical environment.¹⁷¹ One promising approach for developing quasi-solid electrolytes involves confining small amounts of liquid electrolyte inside a nanoporous host matrix. This method allows for good electrode contact, low volatility, stability, and safe operation at high temperatures.¹⁷²

A recent advancement in this field was made by Shaoming Huang's group, who developed a high-performance SSE based on MOFs by chemically grafting soft multicationic oligomers onto the pore walls.¹⁷³ This modification enabled highly selective superionic conduction through bilayer zwitterionic nanochannels (BZNs). MD simulations revealed that the peak of radial distribution functions (RDFs(*r*)) for Li–O in MOF-BZNs was larger than that in LiTFSI (Fig. 3(i)), indicating a lower binding energy for Li⁺ in MOF-BZNs and easier release of Li⁺ in

the nanochannels. These MOF-derived mixed ionic/electronic conductors not only served as solid-state electrolytes but also as cathodes for solid-state Li–O₂ batteries, demonstrating their versatility and potential for use in multiple applications.¹⁷⁴ The development of MOF-based SSEs opens up new possibilities for the design of high-performance and safe solid-state batteries.

The design and synthesis of polymers of intrinsic micro-porosity (PIMs) have been inspired by MOFs and COFs, offering promising potential as SSEs.¹⁷⁵ MD analysis confirms that, through careful material selection and structure design, PIMs possess sub-nanometer interconnected pathways that enable efficient ion transport. These interconnected pathways in PIMs act as “sieves for size selectivity of ions” or “solvation cages for Li⁺,” allowing for the selective transport of Li⁺ while blocking larger unwanted species. This unique property of PIMs results in high Li⁺ mobility (1.06×10^{-3} S cm⁻¹ at 25 °C), demonstrating excellent electrochemical and mechanical stabilities.¹⁷⁶ The development of PIMs as a new class of SSEs with enhanced ion transport properties holds great promise for advancing the field of solid-state batteries. Further research and optimization of PIMs, along with a deeper understanding of their ion transport mechanisms through advanced simulation techniques, will contribute to the development of next-generation solid-state electrolytes.

In summary, the utilization of nanostructured electrolytes has a broad impact on accelerating the development of safe and high-performance solid-state batteries. These materials offer unique properties that enable improved ionic conduction, providing opportunities for enhanced energy storage systems.

Composite electrolytes (CEs). Both SIEs and PEs offer practical solutions to address safety concerns and enhance energy density in LIBs due to their lightweight, flexibility, and flame retardancy. However, they each face their own challenges, such as low ionic conductivity for PEs and poor interfacial properties for SIEs. To overcome these limitations, CEs have emerged as a promising family of SSEs that combine the advantages of both SIEs and PEs.^{177,178}

CEs consist of a polymer electrolyte as the skeleton and inorganic fillers.¹⁷⁹ By incorporating inorganic materials, either inert fillers (e.g., TiO₂,¹⁸⁰ Al₂O₃,¹⁸¹ etc.) or active fillers (e.g., Li-La-Ti-O,¹⁸² Li-La-Zr-O,¹⁸³ etc.), into the polymer matrix, CEs

Table 3 Comparison of electrochemical properties of PEs

Solid inorganic electrolyte type	Ionic conductivity (mS cm ⁻¹) at room temp.	Electrochemical stable window (V) vs. Li ⁺ /Li	Cycling performance	Ref.
PEGMEA/LiTFSI	0.1	~5.2	1500 h at 0.1 mA cm ⁻²	142
PVDF/LiTFSI	0.77	~5.2	2600 h at 11.5 mg cm ⁻²	143
Polythiourea/LiClO ₄	0.1	~4.8	650 h at 0.1 mA cm ⁻²	145
Li[N(SO ₂ F) ₂][NCCH ₂ CH ₂ CN] ₂	0.1	~4.0	100 cycles at 1 μA cm ⁻²	147
(Adpn) ₂ LiPF ₆	~0.1	~5.0	120 cycles at 0.01 mA cm ⁻²	150
LiTFSI/LiDFOB/succinonitrile (SN)	2.86	~5.0	10 000 h at 2.5 mA cm ⁻²	151
Crosslinked LiTFSI/LiDFOB/SN	1.08	~5.4	>4800 h at 1 mA cm ⁻²	152
Poly(propylene carbonate)/SN	0.53	~5.6	1000 h at 0.05 mA cm ⁻²	154
Poly(ethyl acrylate)/SN/LiTFSI	1.2	~4.9	600 h at 0.5 mA cm ⁻²	155
[Li(DMF) ₃][TFSI]/PVDF-HFP	1.55	~4.97	3000 h at 0.1 mA cm ⁻²	157
Crosslinked FEC-MMA-TEGDMA-ETPTA	0.25	~5.65	8000 h at 1 mA cm ⁻²	158
PEO/LiTFSI/1,4-DITFB	0.12	—	700 h at 0.1 mA cm ⁻²	163

enhance the overall ionic conductivity while retaining the desirable properties of polymers. This approach has gained significant attention and is considered one of the most promising SSE families nearing commercial application due to several advantages.^{184–186} First, the incorporation of inorganic fillers increases the number of available pathways for ion conduction, leading to improved overall ionic conductivity. This enhancement in ion transport enables faster and more efficient charging and discharging of the battery. Second, the inorganic fillers can act as physical barriers, hindering the growth of lithium dendrites during cycling and improving the safety of the battery. Dendrites are finger-like lithium metal structures that can penetrate the separator and cause short circuits, leading to thermal runaway. The presence of inorganic fillers helps to suppress dendrite formation, improving the stability and safety of the battery. Finally, the combination of polymer and inorganic materials allows for fine-tuning of properties, such as mechanical strength, thermal stability, and interfacial stability between electrodes and electrolyte,¹⁸⁷ to meet the specific requirements of different battery applications. This versatility enables the design of CEs with tailored properties suitable for various battery systems.

Recent advancements have made significant strides in understanding the ion migration mechanisms of CEs, leading to improvements in their performance, particularly in terms of ionic conductivity, interfacial compatibility, mechanical strength, and electrochemical stability. These advancements in CE research have brought us closer to practical implementation in commercial energy storage devices.

In a study conducted by Mogurampelly *et al.*, atomistic MD and KMC simulations were used to investigate the effect of $\beta\text{-Al}_2\text{O}_3$ nanoparticles on the ion transport properties in a PEO melt with lithium bis(trifluoromethanesulfonyl)imide (LiBF_4) salt.¹⁸⁸ The researchers observed that the introduction of nanoparticles resulted in a decrease in the mobility of Li^+ and the overall conductivity of the electrolyte. This decrease in ion mobility and conductivity was attributed to several factors. First, the presence of nanoparticles induced conformational and dynamic changes in the polymer matrix, hindering the segmental motion of the polymer chains (Fig. 4(a)). This restricted motion of the polymer chains led to a decrease in the mobility of Li^+ . Additionally, the interactions between the nanoparticles and the ions created additional energy barriers

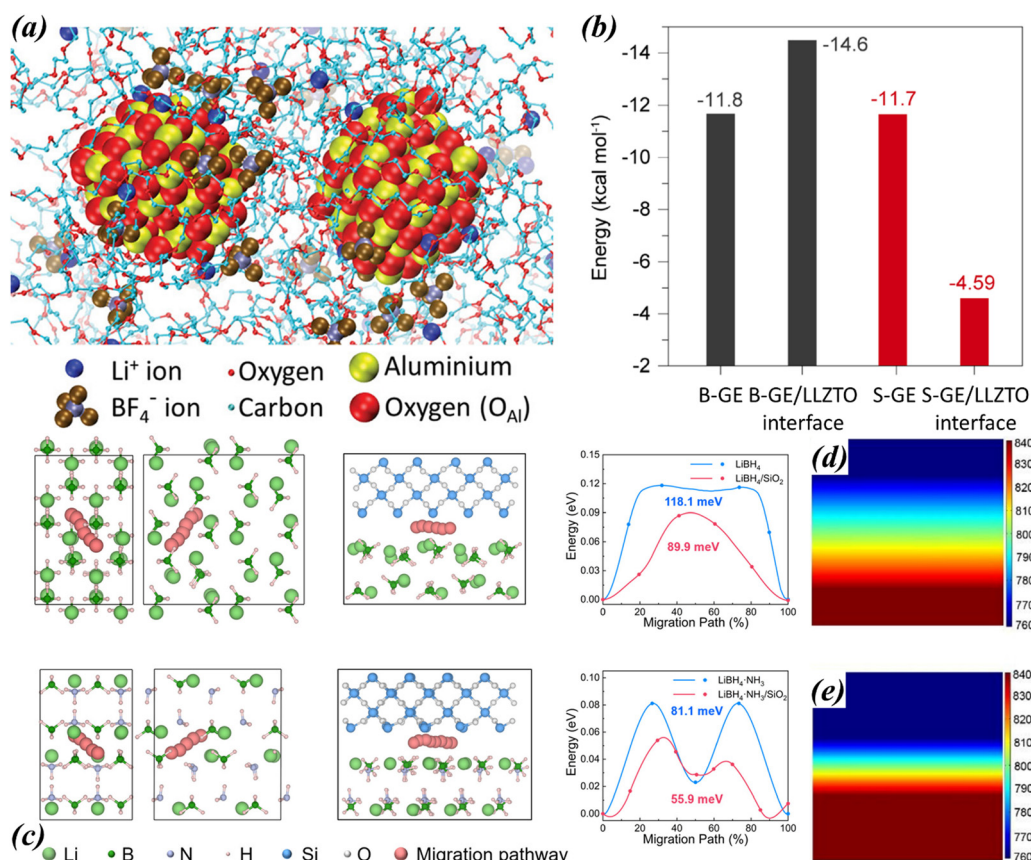


Fig. 4 (a) Close view of poly(ethylene oxide)- LiBF_4 - Al_2O_3 nanocomposites via all atom MD simulations. Reprinted with permission from ref. 188. Copyright © 2015 American Chemical Society. (b) Comparison of Li^+ solvation free energy calculated from MD simulation among the B-GE, B-GE/LLZTO interface, LLZTO, and S-GE/LLZTO interface. Reprinted from ref. 189, with permission from Springer Nature. (c) Simulated migration pathway of interstitial Li in (upper left) LiBH_4 , (upper middle) $\text{LiBH}_4\text{-SiO}_2$, (bottom left) $\text{LiBH}_4\text{-NH}_3$, (bottom middle) $\text{LiBH}_4\text{-NH}_3\text{-SiO}_2$, and (upper right, bottom right) the corresponding energy curves from DFT calculations. Reprinted (adapted) with permission from ref. 196. Copyright © 2022 American Chemical Society. Distributions of Li^+ at the electrode–electrolyte interfaces in the (d) ionogel electrolyte and (e) liquid electrolyte-based batteries from FE simulations. Reprinted from ref. 206, with permission from Elsevier.

that impeded the migration of Li^+ . These interactions between the nanoparticles and ions introduced further restrictions on ion movement, contributing to the decrease in ion conductivity. The findings from this study highlight the complex interplay between nanoparticles and ion transport in composite electrolytes. Understanding the effects of nanoparticles on the ion transport mechanisms is crucial for the design and optimization of composite electrolytes for high-performance solid-state lithium-ion batteries.

To further improve the ionic conductivity and cycling stability of composite electrolytes, researchers have explored various strategies. One approach is the incorporation of SICs into the electrolyte matrix. For example, a single-ion-conductor (SIC)-based composite layer composed of $\text{Li}_{6.4}\text{La}_3\text{Zr}_{1.4}\text{Ta}_{0.6}\text{O}_{12}$ (LLZTO) fillers and a (P(STFSI)Li)-co-PEGDA matrix was designed on the lithium metal electrode.¹⁸⁹ The cross-linked polymer matrix presents the single-ion-conducting characteristic, with a Li^+ transference number of $t_{\text{Li}^+} = 0.96$ (denoted as S-GE). Compared to the bi-ion-conducting matrix (B-GE), this composite layer effectively weakened the coordination of Li^+ with the polymer chain and increased ion diffusivity. As explained through MD analysis (Fig. 4(b)), Li^+ solvation free energy of the S-GE/LLZTO interface was significantly lower than that of B-GE and B-GE/LLZTO. Another approach involves the design of composite electrolytes with lithophilic backbones and multifunctional coatings. Sheng *et al.* proposed a composite electrolyte composed of flower-like Co_3O_4 microspheres as a lithophilic backbone and polydopamine (PDA) as a multifunctional coating. The dissociation of lithium salt was enhanced due to the high binding energy of anions on the PDA surface, which served as a versatile mediator, finely tuning ionic distribution and transport behavior through multiple Lewis acid-base interactions. This design, supported by DFT calculations, showed improved performance.¹⁹⁰ In another recent development, β -cyclodextrin (CD) with self-assembled LiTFSI salt (CD-TFSI) was used as an interface modifier to coat SIE nanoparticles. This approach aimed to bridge the ion diffusion gap between the polymer matrix and the SIE, while optimizing their interfacial contacts. The use of CD-TFSI as an interface modifier improved the overall performance of the composite electrolyte, as reported in experimental studies.¹⁹¹ These advancements in CE design demonstrate the potential for enhancing the ionic conductivity and stability of SSEs.

LiBH_4 is a thermodynamically stable solid electrolyte against Li metal; however, its narrow electrochemical stable window (<2 V vs. Li^+/Li) limits its practical application.¹⁹² To address this limitation, a CE based on PMMA/ LiBH_4 was developed.¹⁹³ Through a combination of DFT calculations and experimental observations, it was determined that the BH_4^- anions of LiBH_4 and $-\text{OCH}_3$ groups of PMMA formed covalent bonds. This bonding strategy aimed to prevent electronic leakage, extend the oxidative stability of the anions, and kinetically block electron percolation. As a result, the proposed CE demonstrated unprecedented electrochemical and cycling stability. Confinement of materials within nanopores has shown

significant potential for inducing improvements in functionality.¹⁹⁴ This concept has also been applied to LiBH_4 , leading to enhanced properties. In recent studies, the impact of nanoconfinement of LiBH_4 within ordered mesoporous SiO_2 scaffolds has been extensively investigated.^{195,196} DFT calculations have provided valuable insights into the behavior of ions within the confined space of the composite electrolytes. As illustrated in Fig. 4(c), the migration of interstitial Li in the crystals of LiBH_4 and ammoniated LiBH_4 was hindered by the large diffusion barrier, whereas the ion diffusion at the interfaces between SiO_2 and LiBH_4 were greatly decreased. These calculations have shown that nanoconfinement reduces the diffusion barrier for ions, enabling fast and efficient migration pathways. The interfacial space between LiBH_4 and the mesoporous SiO_2 scaffold plays a crucial role in facilitating ion transport, resulting in superior conductivity compared to bulk LiBH_4 electrolytes.

Ionogel-based CEs have emerged as advanced options for lithium batteries due to their unique combination of ionic conductivity and mechanical stability.^{197,198} These electrolytes consist of a polymer gel matrix infused with ionic liquids (ILs), creating a highly conductive pathway for Li^+ . The ILs are salts composed of organic cations and inorganic (e.g., Cl^- , Br^- , and PF_6^-) or organic anions (TFSI^-) with a melting point lower than 100 °C.¹⁹⁹ They offer advantages such as high ionic conductivity, improving charge/discharge rates and overall performance.²⁰⁰ The polymer gel matrix enhances stability and durability, reducing the risk of electrode deformation and leakage.²⁰¹ These electrolytes also have a wide electrochemical stability window, enabling higher voltage operation and utilization of high-capacity electrode materials.²⁰² Furthermore, they show promise in enhancing the safety of lithium batteries, making them suitable for extreme temperature conditions.²⁰³ Both the “ceramic-in-ionogel” and “ionogel-in-ceramic” approaches have recently been developed as CEs for lithium batteries. These approaches utilize either active ceramics like $\text{Li}_{6.5}\text{La}_3\text{Zr}_{1.5}\text{Ta}_{0.5}\text{O}_{12}$ ²⁰⁴ or inert ceramics like Al_2O_3 .²⁰⁵ Through AIMD simulations, it has been demonstrated that the concentration gradient of ceramics within the electrolyte effectively decouples the interfacial reaction and ion diffusion processes, facilitating enhanced ion transport kinetics and interfacial stability.²⁰⁵ Moreover, the designed organic/inorganic hybrid quaternary ionogel electrolyte has been found to greatly enhance the dissociation of Li salt.²⁰⁶ Li^+ concentration gradient at the electrode-ionogel electrolyte interface was found to be insignificant when compared to the liquid electrolyte system *via* FE simulations, indicating the increased free Li^+ in the ionogel electrolyte, reduced Li^+ clusters, and uniform Li^+ flux (Fig. 4(d) and (e)). In another study, Xianhong *et al.*²⁰⁷ introduced a hybrid cross-linked poly(ionic liquid)s ionogel (POSS-C PIL-*n*) that combines polyhedral oligomeric silsesquioxanes (POSS) and poly(ethylene glycol)diacrylate (PEGDA). This ionogel exhibited high mechanical flexibility, good ionic conductivity, and excellent thermal and electrochemical stability, and holds promise for practical applications in flexible electronic devices.

In addition to the previously discussed advancements, CEs have also been explored to promote the air/water stability of lithium metal in LMBs.²⁰⁸ For example, a composite based on polyvinylidene chloride (PVDC) was developed to simultaneously protect the Li metal anode from air/water corrosion and act as a SSE.²⁰⁹ The MD results revealed that the Li^+ ions in the composite electrolyte coordinate with the oxygen atoms of bis(trifluoromethanesulfonyl)imide (TFSI^-) anions within or between LiTFSI aggregates. This coordination generates Li^+ hopping pathways with a distance of approximately 2.0 Å, which is a small value close to that of an inorganic electrolyte. These pathways are formed through the salt clusters along the PVDC chains. The use of PVDC in the composite electrolyte not only serves as a protective barrier against air and water, but also facilitates the transport of Li^+ . The coordinated Li^+ ions within the CE are able to hop along the PVDC chains, enabling efficient ion transport. This combination of air/water stability and favorable Li^+ transport pathways contribute to the improved performance and safety of lithium metal batteries.

Table 4 compares the ionic conductivity, electrochemical stable window, and cycling performance of various CEs.

4. Electrochemical and chemical compatibility of electrode–SSE pairs

Despite the numerous advantages of SSEs over conventional liquid counterparts, their interfacial compatibility with electrode active materials remains a key challenge that hinders the commercialization of ASSBs.²¹⁰ The compatibility between the electrode and SSE pair encompasses several critical aspects.

First, poor contact at solid–solid or particle–particle interfaces can result in relatively high interfacial impedance, limiting the rate performance and cyclic stability of SSBs, particularly those with electrodes experiencing a high volume change and high-voltage electrodes.^{211,212} To enable wide-scale

application in SSBs, significant improvements are needed to reduce the loss of contact and enhance ion transport pathways at the SSE/electrode interface.²¹³ Second, certain SSEs, such as sulfide electrolytes, are susceptible to hydrolysis in humid air.²¹⁴ Addressing this vulnerability requires a fundamental understanding of the electrode–electrolyte interfaces and the development of modification approaches as prerequisites for resolving the issue.²¹⁵ Finally, the chemical reactions that occur at the interface between the electrodes and SSEs during electrochemical cycling are a primary cause of capacity fade and cell failure in ASSBs, making it an important focus of this section.²¹⁶ The intrinsic thermodynamic instability between the electrodes and SSEs, including interfacial reactions and the formation of interphase byproducts, significantly impacts the ability to realize the full potential of SSBs. Numerical methods have been vastly employed to investigate this instability due to its tedious and costly experimental determination.^{217,218}

Recent studies have systematically explored the evolution of interfacial reactions between sulfide SSEs and commonly used cathode active materials in the presence of moisture air using first principles computation databases dependent on thermodynamic phase equilibrium analyses.^{219,220} The chemical and electrochemical reaction energies at cathode/SSE interfaces were analyzed, as illustrated in Fig. 5(a) and (b), revealing that the electrochemical reaction was significantly stronger than the chemical reaction, thereby dominating the interfacial reaction. This can be attributed to the large difference in the chemical potential of sulfur in SSEs and oxygen in the cathode, leading to ion mutual diffusion and the formation of byproducts. Furthermore, it was found that the hydrolysis reactions of sulfide SSEs can be inhibited by substituting P^{5+} with metalloid ions in period IV, V, and VI elements (such as Ga^{3+} , Ge^{4+} , Sb^{5+} , etc.) and late-transition-metal ions (such as Zn^{2+} , Cu^{2+} , and Ag^+). In addition, research conducted by Mo's group explored the electrochemical deposition behaviors of lithium at the

Table 4 Comparison of electrochemical properties of CEs

Solid inorganic electrolyte type	Ionic conductivity (mS cm^{-1}) at room temp.	Electrochemical stable window (V) vs. Li^+/Li	Cycling performance	Ref.
PEO/garnet electrolytes containing LiTFSI	>0.1	2.5–5.0	680 h at 0.5 mA cm^{-2}	139
PEO/ $\text{Li}_{0.25}\text{Ga}_{0.25}\text{La}_3\text{Zr}_2\text{O}_{12}$	0.072	~4.6	500 h at 0.8 mA cm^{-2}	140
Ca-doped CeO_2 /LiTFSI/PEO	0.13	~4.5	1000 h at 0.1 mA cm^{-2}	153
Sub-1 nm inorganic cluster/PEO	0.52	~5.1	1000 cycles at 0.5C	184
$\text{La}_2\text{Zr}_2\text{O}_7$ /PEO	0.02	~49.2	1500 cycles at 0.1C	185
PAN/ LiClO_4 :LLZTO	1.18	—	5000 h at 1 mA cm^{-2}	186
PVDF-Li _{1.4} A _{0.4} Ti _{1.6} (PO ₄) ₃ /DMF	0.6	~4.5	1500 cycles at 2C	187
Li _{6.4} La ₃ Zr _{1.4} Ta _{0.6} O ₁₂ /P(STFSI)Li- <i>co</i> -PEGDA	0.1	~3.0	400 h at 3 mA h cm^{-2}	189
Co ₃ O ₄ /PDA/PEO	0.71	~4.8	500 cycles at 1C	190
β -CD/PEO/LLZTO	0.87	~5.1	200 cycles at 0.2C	191
LiBH_4 /PMMA	0.5	~10	6000 h at 2.15 mA cm^{-2}	193
Li(NH ₃) _x BH ₄ @SiO ₂	39.5	~2.09	100 h at 0.1 mA cm^{-2}	196
Hierarchically architected ionogel	0.38	~5.0	1800 at 0.05 mA cm^{-2}	201
Poly(ethylene glycol)diamine-BTA	4.79	~4.5	1000 h at 0.5 mA cm^{-2}	202
PBDT/LiTFSI/Pyr _{1.4} TFSI	0.56	—	900 h at 0.1 mA cm^{-2}	203
LLZO/3 M LiTFSI-EmimFSI-PMMA	1.33	~5.5	600 h at 0.5 mA cm^{-2}	204
P(VDF-HFP)/EMIMTFSI/Al ₂ O ₃	0.25	~4.5	1000 h at 0.1 mA h cm^{-2}	205
PEO/SiO ₂ /LiTFSI	1.5	~5.0	100 cycles at 0.2C	206
POSS-PEGDA/BMIm [TFSI]	2.5	~5.1	350 h at 0.1 mA cm^{-2}	207

SSE-anode interface during the lithiation process using large-scale MD simulations.²²¹ This study revealed the atomistic pathways and energy barriers of lithium crystallization at solid interfaces, which followed multi-step pathways mediated by interfacial lithium atoms with disordered and random-closed-packed configurations as intermediate steps, leading to energy barriers for crystallization. Collectively, these studies provide a comprehensive understanding of the electrochemical and chemical stability trends in SSEs. They have also proposed distinct engineering strategies to facilitate better interfacial compatibility and contact, including surface modification of SSEs and material rational design, which can advance the commercialization of ASSBs.

4.1. Surface modification

Surface modification is an effective approach for improving the interfacial properties between SSEs and electrodes. Various methods have been explored, including mechanical polishing and calcination,²²² chemical composition alteration,²²³ introducing additives,²²⁴ coating protective layers,²²⁵ etc. One of the initial attempts involved polishing the SIE particles to improve Li wetting, but it is not likely to solve the dendrite growth problem.²²⁶

Artificially adjusting the local composition of SSEs, such as introducing ion-deficient or defect-rich layers on their surfaces, has been shown to improve their contact with metallic anodes,

prevent their reduction phenomenon by the metal anode, and greatly decrease the ultralow interfacial resistance.²²⁷ DFT calculations have revealed the adhesion energies of metal anodes with pristine and modified SSEs (Fig. 5(c) and (d)). By removing Na atoms from the SSE's (001) surface, the exposed O layer becomes more reactive due to the presence of dangling bonds, leading to higher adhesion energy and stronger interfacial strength between the anode and ion-deficient SSEs.

In addition, the introduction of thin protective buffer layers, e.g., metals, alloys, organics, oxides, etc., is another popular method to improve the wetting of the electrode/SSE interface and prevent parasitic reactions.^{228–231} Numerical approaches have been employed to study the interfacial stability and kinetics of SSEs and metal anodes, as well as the underlying mechanisms, offering guidance on effective material selection strategies for electrode-SSE pairs and buffer layers.²³² The evolution of the SSE/anode interface without a buffer layer and with buffer layer/anode and buffer layer/SSE interfaces has been comprehensively assessed using atomistic simulations, offering guidance on material selection strategies for electrode-SSE pairs and buffer layers.²³³ Fig. 5(e)–(g) illustrate the evolution of the SSE/anode ($\text{Na}_3\text{PS}_4/\text{Na}$) interface without a buffer layer, as well as the buffer layer/anode and buffer layer/SSE interfaces over time in the simulations. By comparing these with the references, the calculated P-P radial distribution function (RDF) shown in the bottom heat map of Fig. 5(e)

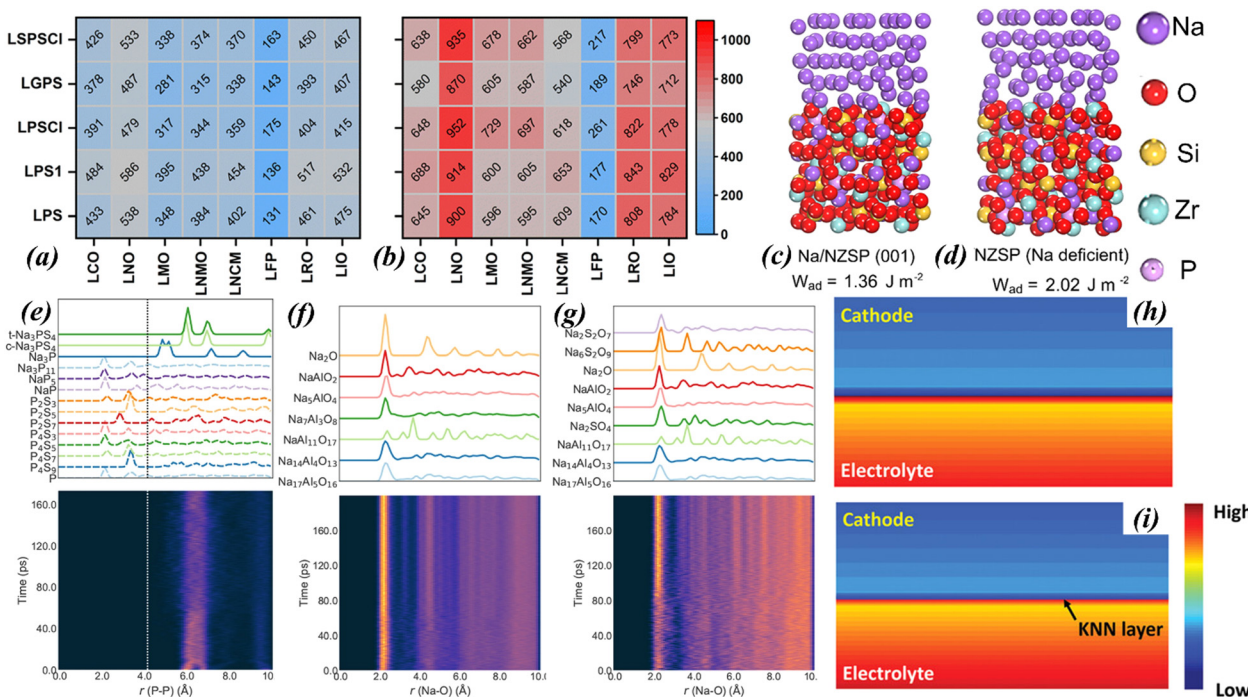


Fig. 5 (a) Chemical and (b) electrochemical compatibility between common cathodes and SSEs in meV per atom. Reproduced from ref. 219 with permission from the Royal Society of Chemistry. Calculated adhesion strengths (W_{ad}) for metal/SSE interfaces (c) with and (d) without the introduction of an ion-deficient layer. Reprinted with permission from ref. 227. Copyright 2020 American Chemical Society. Evolution of the (e) P-P RDF at the SSE/anode interface, Na–O bonds at (f) the anode/buffer and (g) buffer/cathode interfaces, with respect to simulation time plotted as a heat map, with a higher brightness indicating a higher value of $g(r)$; the RDFs of reference materials are provided above the heat map. Reprinted with permission from ref. 233. Copyright 2018 American Chemical Society. Simulated ion concentration at cathode–CE interfaces (h) with and (i) without the KNN layer (the arrow indicates the position of buffer layers). Reproduced with permission from ref. 245.

indicates the absence of P , P_xS_y , NaP , NaP_5 , and Na_3P_{11} phases. This suggests that the dominant reaction products at the SSE/anode interface are Na_2S and Na_3P , which is in agreement with experimental results. Importantly, the introduction of Al_2O_3 buffer layers at the SSE/anode interfaces was found to have little impact on the RDFs of most bonds. This indicates a relatively low to zero driving force for reactions between Al_2O_3 and the metal anode/SSE, resulting in the stabilization of the electrode–SSE pair. Recently, the adoption of electronic blocking layers like LiH , LiF , Li_3N and organic lithium salts on the surfaces of SIE particles has been observed to increase the critical electrical bias for dendrite growth, enhance ionic conductivity and oxidation stability, and has gained popularity as a promising direction for modifying electrode–SSE pairs.^{234–236} Surface coating techniques, such as liquid-phase deposition of nanosized SIEs,²³⁷ lithiophilic metallic²³⁸ or electron-blocking interlayers,²³⁹ electrodeposition,²⁴⁰ and removal of impurities,²⁴¹ have also been explored to address various issues encountered by lithium metal batteries and facilitate intimate contact with SSEs, forming nanoscale electronic/ionic transportation networks for high reversibility capacity and superior rate capability. However, achieving the desired rate performances for fast-charging targets of electric vehicles still poses challenges.

As for PEs and CEs, despite their flexibility, they still face challenges in terms of compatibility with electrodes, leading to interfacial reactions, space-charge layers, and high interfacial resistance, which negatively impact cyclic performances of batteries.^{242–244} To address these issues, a ferroelectric buffer layer ($K_{0.5}Na_{0.5}NbO_3$, KNN) has been introduced between the CE and electrode.²⁴⁵ This buffer layer could be polarized under the interfacial potential drop, attenuating charge accumulation and improving compatibility and ion migration. Finite element modeling (Fig. 5(h) and (i)) demonstrates that ion distribution at CE–electrode interfaces was effectively controlled through ferroelectric engineering. Without the buffer layer, thick ion-accumulated and ion-deficient layers were generated, hindering interfacial ion conduction and causing chemical degradation. Conversely, the oriented ferroelectric polarizations of the KNN layer significantly weaken the sharp potential drop and suppress the growth of the solid–electrolyte interphase (SEI). Similarly, a sandwich-structured ceramic-gel CE,²⁴⁶ and a composite interface composed of the mechanically robust Li_ySn alloy and the ion-conducting Li_3N ,²⁴⁷ were proposed for use in Li batteries. In this configuration, a GPE modification layer was coated on both sides of the SIE. The modification layer optimized Li^+ conduction, reduced interfacial polarization and parasitic reactions, and enhanced interfacial compatibility.

4.2. Rational design of material composition

Element doping is a widely adopted method to address the incompatibility issues of electrode–SIE pairs.^{248,249} For instance, first-principles calculations proved that silicon doping in LiPON could greatly promote its interfacial stability with silicon-based electrodes due to the strong electron hybridization between doped silicon and SSE; meanwhile, the doped

silicon could also provide channels for Li diffusion due to mutual electrostatic interaction.¹¹

As for PEs, the poor interfacial compatibility and the behavior of heterogeneous lithium deposits in PEs are closely linked to membrane phase separation.²⁵⁰ Recent studies have focused on the preparation of PEs through *in situ* solidification of various liquid precursors, enabling the formation of hyperconformal cross-linked networks that exhibit improved properties such as ionic conductivity, oxidation stability, and mechanical flexibility.^{251–253} The enhanced performance of these cross-linked PEs has been elucidated through DFT calculations, revealing two key factors.²⁵⁴ First, the cross-linked PE exhibits a higher binding energy with Li^+ and cathode active materials, promoting the dissociation of the Li salt and enhancing the ion transference number and the interfacial stability between the electrolyte and electrodes. Fig. 6(a) compares the calculated probabilities of electron cloud density distribution for *in situ* ring-opening polymerization of 1,3-dioxolane (PDOL) and cross-linked PDOL with polyhedral silsesquioxane (PS) as the cross-linking agent. The larger binding energy between Li^+ and cross-linked PDOL demonstrated their strong interaction and the promoted solvation behavior. Second, the interconnected network of the cross-linked polymer facilitates efficient transport of Li^+ throughout the electrolyte. By employing *in situ* solidification techniques to create cross-linked polymer networks, researchers have successfully enhanced the crucial properties of solid polymer electrolytes.^{255,256}

It is important to note that MD simulation results indicate that the morphology of deposited lithium is strongly influenced by the homogeneity of the polymer membrane. The structural compatibility between the primary and secondary segments of the polymer chain plays a significant role.²⁵⁷ Dissimilarity in molecular electrostatic fields among segments can lead to localized lithium deposition, unstable growth of SEIs and unexpected cell failures during electrochemical operation.²⁵⁸ Fig. 6(b) illustrates the DFT calculated electrostatic potentials of the modified poly(trimethylene carbonate) (PTMC) with different secondary segment species, including triethylene glycol diacrylate (TEGDA), 2-(2-ethoxyethoxy)ethyl acrylate (EOEOEA), and 1,6-hexanediol diacrylate (HDDA). The distinct polarizations of the secondary monomers offer varying levels of compatibility with PTMC, influencing the structural heterogeneities of the polymer. Therefore, membrane homogeneity should also be considered when rationally selecting plasticizers, cross-linkers and precursors.

The use of CEs comprising a polymer matrix and one or more fillers has experienced significant growth. The selection and proportion of different fillers in CEs are critical challenges in achieving optimized material design, leading to increased attention in this area.^{259–261} An innovative design involving a new nanocomposite filler, positively charged nanosheets (lamellated C_3N_4 and CeO_2), has been introduced.²⁶² DFT calculations have revealed that these lamellated fillers possessed a high specific area, allowing for better contact with electrodes. They also exhibited a strong binding energy with the anions of the salts, attributed to electrostatic forces, which

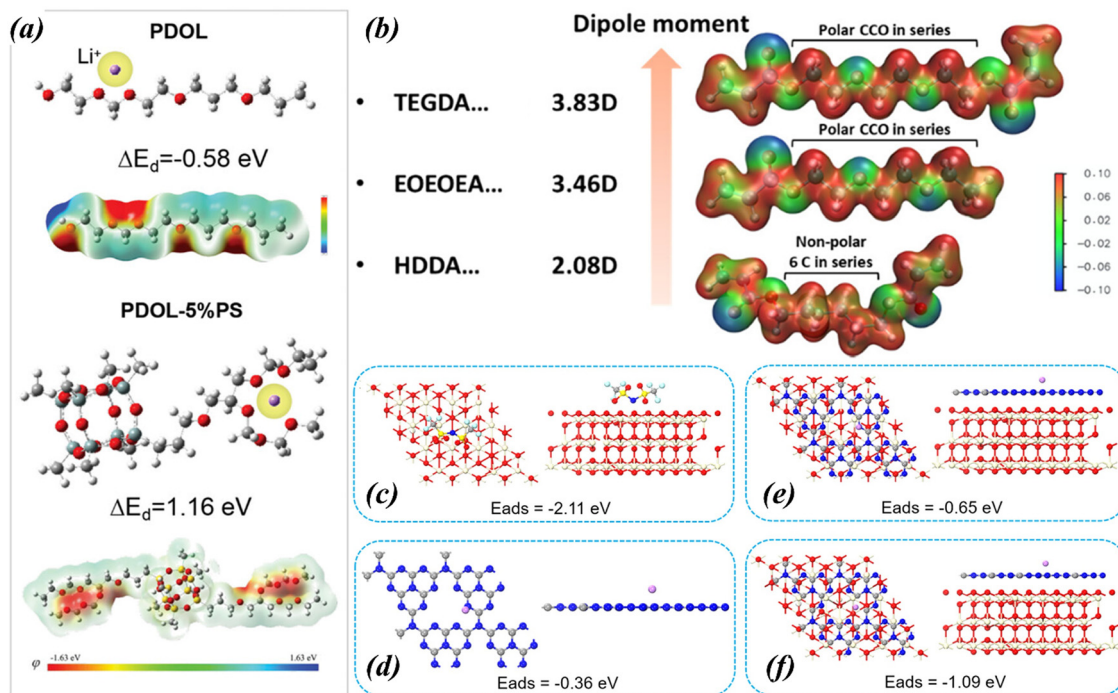


Fig. 6 (a) DFT calculations to assess the probabilities of electron cloud density distribution of PDOL and PS-cross-linked PDOL, and their binding energy with Li⁺ under the coordination of each group and free Li⁺. Reprinted from ref. 254, © 2023 Wiley-VCH GmbH. (b) Calculated electrostatic potentials and dipole moments of various secondary segments with the PTMC primary chain. Reprinted with permission from ref. 257. The calculated adsorption energy comparison of (c) the CeO₂ and anion (TFSI⁻), (d) C₃N₄ and Li⁺, (e) CeO₂-C₃N₄ composite and Li⁺, and (f) CeO₂-C₃N₄ composite containing oxygen/nitrogen defects and Li⁺. The pink, blue, gray, red, pale yellow, deep yellow, and Cambridge blue balls represent lithium, nitrogen, carbon, oxygen, cerium, sulfur, and fluorine atoms, respectively. Reprinted from ref. 262, with permission from Elsevier.

improved the dissociation of lithium salt and allowed the free cation (Li⁺) movement through the polymer and C₃N₄ network (Fig. 6(c)). Additionally, they contained abundant oxygen and nitrogen defects, acting as coordination sites for Li⁺ and benefiting its transport (Fig. 6(d)–(f)). To fully exploit the synergistic effects of different components, a complex ternary CE has been developed, consisting of a PVDF-HFP host matrix, clinoptilolite (CPT) as a passive filler, and ionic liquids and lithium salts as active fillers.²⁶³ This development highlights the significant influence of the rational selection of the matrix and fillers on the cyclic behavior of batteries due to their interactions. By carefully considering the composition and interaction of the matrix and fillers, researchers aim to optimize the performance and cyclic behavior of battery systems.

5. Dynamics and failure mechanisms of SSEs

Despite the increasing computational efforts to understand the intrinsic properties of SSEs and investigate their electrochemical and chemical compatibility, there is still a need for a comprehensive evaluation at the mesoscale level. This evaluation specifically focuses on the multiphysics-based dynamics and failure mechanisms of electrode-electrolyte composites, which consist of active materials (AMs), SSEs, and additives/binders. Such a mechanical-electrochemical coupled

assessment is crucial for determining the performance, safety, and longevity of SSBs.²⁶⁴ In this section, we delve into mesoscale studies to examine two key aspects: mesoscale ion diffusion and the corresponding multiphysics-based responses of SSEs, as well as the initiation and propagation of dendrites. By exploring these phenomena, our aim is to uncover the underlying mechanisms that govern the behavior and failure modes of SSEs. These findings will provide valuable insights for developing targeted strategies to overcome challenges and improve the reliability and efficiency of SSB technologies.

5.1. Ion diffusion induced multiphysics evolution

SSBs at the cell level typically utilize composite electrodes to minimize interfacial resistance and optimize electronic and ionic pathways. This necessitates a comprehensive evaluation that takes into account various factors, such as the shape, composition, and particle size of the materials, as well as their lithiation-induced volume changes,^{265–267} among others. A fundamental understanding of ion behavior within SSEs is crucial for enhancing their transport properties and overall performance. To this end, mesoscale studies have been conducted to investigate the dynamic migration of ions through the SSE lattice and the resulting mechanical changes in the materials. By harnessing the knowledge gained from the mesoscale studies, we can enhance the design and performance of SSBs, bringing us closer to realizing the full potential of these next-generation energy storage devices.

One of the primary requirements for SIE-based SSBs is achieving sufficient effective ionic conductivity to enable high power capability and fast charging. To analyze the ionic and electronic percolation, as well as the utilization of active materials (AMs) and the microstructure layout in composite cathodes, microstructural FEM methods were employed (Fig. 7(a)).^{268,269} The composition and particle size of the electrode materials played a significant role in determining the effective ionic conductivity. It was observed that increasing the fraction of AMs can lead to higher energy density, but it also reduces the ionic conductivity. Similarly, smaller particle sizes resulted in lower conductivity due to the increased total number of particles acting as obstacles for ion transport. This leads to a narrower ionic pathway and a higher tortuosity factor (Fig. 7(b)). Moreover, Fig. 7(c) demonstrates the resulting utilization levels of AMs and SIEs, representing the fractions

of materials that remain electrochemically active. It was observed that electronic conduction became limited with SIE contents above 31 vol%, whereas ionic conduction was limited when SIEs were below 21 vol%. This indicates that the range of well-performing composites is relatively narrow, as the SE does not provide sufficient connectivity for ionic conduction in highly AM-dominated microstructures.

Furthermore, in comparison to liquid electrolyte systems, SIEs exhibit unique characteristics due to their rigidity and exclusive migration mechanisms, which eliminate concentration gradients for ion transport through the SIEs. Nonetheless, at high charge/discharge rates, the behavior of solid-state composite electrodes, particularly the spatial inhomogeneity in the local state-of-charge, requires investigation to assess the influence of electrode microstructures on rate capability.^{270,271} Simulations have revealed Li concentration

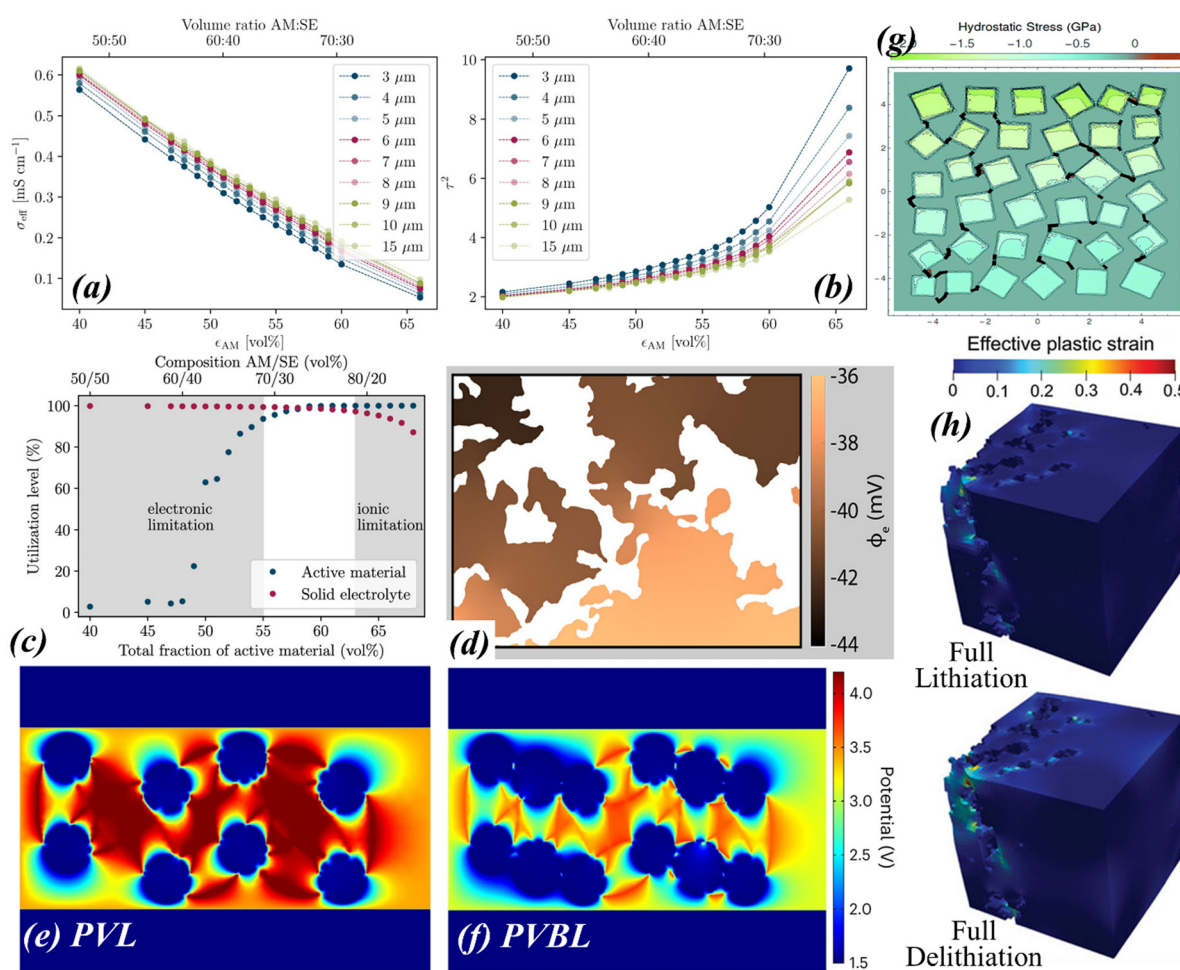


Fig. 7 (a) Effective ionic conductivity and (b) ionic tortuosity factor of composite microstructures versus composition for uniformly distributed AM; electrode void space held constant at $\phi = 15\%$. Reprinted with permission from ref. 268. Copyright 2020 American Chemical Society. (c) Utilization level of AM and SE for composite cathode arrangements at a constant porosity of 20% and AM particle size $d = 5 \mu\text{m}$. Reprinted with permission from ref. 269. Copyright 2019 American Chemical Society. (d) Local SE potential in the electrode. Reprinted with permission from ref. 270. Copyright 2021 American Chemical Society. Simulations of the potential distribution in (e) PVDF-LLTO and (f) PVDF-BTO-LLTO composite electrolytes. Reprinted with permission from ref. 273, Springer Nature. (g) Evolution of damage in the solid electrolyte material; cracks (marked with black lines) propagate from corner to corner, cutting off diffusion paths for Li within the electrolyte. Reprinted from ref. 279, with permission from the Royal Society of Chemistry. (h) Effective plastic strain evolution investigation of Si-SE-C anode materials using a chemo-elasto-plastic modeling framework for large deformation at the end of lithiation (top) and delithiation (bottom) stages. Reprinted from ref. 294, © 2023 Wiley-VCH GmbH.

gradients within the active material, which arise from the depth of the electrode. The lithiation process occurs at a faster rate in certain regions of the electrode due to ionic conduction within the SE phase and the gradient in the electrostatic potential of the SE (Fig. 7(d)). Consequently, while single-ion-conducting SIEs do not exhibit Li^+ concentration gradients, concentrated current still exists in the composite electrode regions near the interface with the bulk SIEs. This phenomenon is influenced by the cell design and manufacturing processes.

As for the polymer-based CEs, the low conductivity and the presence of a space charge layer (SCL) between the polymer matrix and inorganic fillers significantly impede the transport of Li-ions.²⁷² To understand the interactions between the polymer matrix and fillers, the evolution of the potential field through the CE was estimated using Multiphysics simulations.²⁷³ Fig. 7(e) and (f) illustrate the comparison between PVDF-BTO-LTTO (PVBL) and PVDF-LTTO (PVL) composite electrolytes. It was observed that the PVBL composite electrolytes exhibit a more homogeneous potential distribution and negligible Li^+ concentration polarization. This suggests that the introduction of ceramic dielectrics (BaTiO_3 , BTO) weakens the SCL by promoting the dissociation of the Li salt. The coupling of BTO and LTTO in the PVBL composite electrolytes is beneficial for achieving a homogeneous interfacial potential and electric field. Based upon a similar principle, a unique relaxor ferroelectric polymer of poly(vinylidene fluoride-*co*-trifluoroethylene-*co*-chlorotrifluoroethylene) [P(VDF-TrFE-CTFE)] with an ultrahigh dielectric constant,²⁷⁴ and a CE consisting of PVDF and ferroelectric LiTaO_3 ,²⁷⁵ were fabricated. By mitigating the SCL and promoting a more favorable interfacial environment, these composite electrolytes offer enhanced performance and reduced risk of safety issues associated with Li dendrite formation and related problems.²⁷⁶

It should not be overlooked that the volume expansion of electrodes can damage the integrity of solid-solid interfaces with SSEs and hinder ion/electron transport, resulting in the mechanical degradation of SSEs such as micro-cracks, fractures, and delamination, ultimately resulting in short circuits in solid-state batteries.^{277,278} This is one of the core scientific issues affecting the performance of solid-state lithium batteries.²⁶⁴ To accelerate the research and development process, it is necessary to conduct a comprehensive systemic analysis of the multi-physics coupling behavior at the electrode-SSE interface, including (1) the evolution mechanism of the connectivity of the solid-solid interface under extreme and potential non-uniform volume changes and various constraint conditions, (2) the influence of stacking pressure on the morphological evolution and electrochemical behavior of the silicon anode and electrolyte materials, and (3) the potential non-uniform lithium deposition behavior on the surface and inside of the solid electrolyte. Establishing more comprehensive and accurate theoretical models, quantifying the mechanical-chemical-electrochemical coupled constitutive relationship at the interface, is an important approach to address these issues.

To quantitatively assess the mechanical reliability of composite electrodes, Carter's group pioneered the use of a coupled

electro-chemo-mechanical FEM combined with cohesive zone modeling.²⁷⁹ Fig. 7(g) depicts the simulated distribution of hydrostatic stress and crack propagation in a composite electrode, where the SSE is represented by the continuous phase, and the AM particles are represented by the rectangular phase. Observations reveal that cracks initiate and propagate due to the intercalation-induced expansion of the electrode particles. However, this phenomenon can be mitigated by using tougher SSEs or by incorporating smooth AM particles, which helps to delay the initiation and propagation of cracks. By addressing the mechanical degradation in SSEs and optimizing the design of composite electrodes, it is possible to minimize the occurrence of mechanical failures and extend the lifespan of SSBs.

Advanced fabrication techniques, such as templating,²⁸⁰ photopatterning,²⁸¹ sputtering,²⁸² and 3D printing,²⁸³ have enabled the development of 3D patterned composite electrodes with low tortuosity. These 3D architectures, which encompass lattice,²⁸⁴ interdigitated²⁸⁵ and patterned structures,²⁸⁶ have demonstrated significantly improved mass transfer and interfacial charge transfer, leading to enhanced performance in solid-state batteries. The implementation of 3D architectures in composite electrodes provides several advantages. First, it promotes more homogeneous distribution of the local state-of-charge throughout the electrode thickness, resulting in improved overall performance.²⁸⁷ Besides, the utilization of 3D architectures allows for increased areal energy density, enabling greater energy storage capacity within the same electrode footprint.^{288–290} The insights gained from studying these 3D electrode architectures provide the foundation for developing new strategies to address the power/energy trade-offs in SSBs. However, it is important to note that the introduction of 3D patterns can introduce complex electrochemical-mechanical couplings, which require further investigation and understanding. As such, additional research is needed to fully develop the design strategies for composite electrodes based on 3D architectures.

In contrast to traditional graphite-based composite electrodes, metal negative electrodes, such as Li, Si and Sn, have high theoretical charge storage capacity and are promising candidates for high-energy ASSBs.^{291,292} However, these alloy-anodes undergo substantial volumetric and structural changes during the reaction with lithium.²⁹³ Therefore, it is crucial to understand the impact of introducing SSEs on the electrochemical performance and cyclic stability of these alloy-negative electrodes. A chemo-elasto-plastic modeling approach has been employed to gain deeper insights into the mechanical behavior of these electrodes (Fig. 7(h)).²⁹⁴ In the absence of a SSE in the composite anode, silicon experienced significant effective plastic strain and high von Mises stresses during the lithiation-delithiation process. However, by incorporating SSE and carbon additives, the plastic deformation of silicon was significantly reduced. This can be attributed to the mechanical cushioning effect of the SSE, which compensates for stress concentration in silicon, along with the limited volume expansion and contraction due to the presence of SSE. Other metal candidates, such as aluminum, have also been explored.^{295,296} Despite volume

changes during cycling, Al-based electrodes maintain their mechanical integrity without significant formation of internal porosity. This behavior can be attributed to the mechanical confinement provided by the all-solid stack and the relatively stable and planar interfacial contact between the negative electrode and the SSE. These findings highlight the distinct advantages of solid-state architectures and microstructure engineering of the alloy anode in enabling stable ASSBs by mitigating the mechanical stresses and strains experienced by the alloy-electrodes.

In summary, the optimization of the composition and microstructure in composite cathodes has the potential to enhance the effective ionic conductivity and overall performance of SSBs. Valuable guidance for designing high-performance composite cathodes can be derived from insights gained through microstructural FEM analyses, leading to improved efficiency and reliability of SSBs. However, further research is necessary to deepen our understanding of the electrochemical-mechanical interactions within these complex structures and develop mature design strategies.

5.2. Failure of SSEs and dendrite propagation

Failure mechanisms in SSEs vary depending on the type of material, including inorganics, polymers, and composites. Understanding these failure mechanisms is crucial for improving the stability and performance of SSEs in lithium batteries.

Inorganic SSEs, such as oxide- or sulfide-based materials, commonly face failure due to interfacial reactions with electrodes, leading to the formation of insulating layers or the dissolution of the SSE, causing increased interfacial resistance and decreased overall performance.²⁹⁷ Mechanical stress and strain can also result in the cracking or delamination of inorganic SSEs, reducing their ionic conductivity and compromising the integrity of the solid-state electrolyte.²⁹⁸ On the other hand, PEs may exhibit failure mechanisms related to their low mechanical strength, forming cracks or voids under stress and deformation, and compromising their structural integrity and overall performance.²⁹⁹ Additionally, PEs may suffer from degradation or decomposition at high temperatures, resulting in a loss of conductivity and stability.³⁰⁰ Composites, which combine inorganics and polymers to leverage their individual advantages, can exhibit failure mechanisms associated with the interfaces between the components.³⁰¹ Poor interfacial adhesion or chemical incompatibility between the constituents can lead to delamination or debonding of the composite layers, reducing their effectiveness as a solid-state electrolyte.

Dendrite growth is one of the most critical failure modes of SSEs and poses significant challenges for the development of safe and reliable SSBs. These dendrites can result in short circuits, reduced battery lifespan, and safety hazards.³⁰² The factors that affect the propagation of dendrites include ion diffusion, concentration gradients, the mechanical response of SSEs during lithium plating–stripping, microstructural defects, grain boundaries (GBs), and electronic conductivity facilitating Li electrodeposition inside SSEs.^{303–305} A recent study found

that the SEI at the GBs of $\text{Li}_7\text{La}_3\text{Zr}_2\text{O}_{12}$ sheets could be reduced to LiC_x through electrochemical cycling, exacerbating lithium penetration.³⁰⁶ In this section, we will explore the current understanding of dendrite initiation and propagation mechanisms, drawing insights from numerical studies. The key factors influencing dendrite formation will be highlighted, and various approaches proposed to inhibit or suppress dendritic growth will be discussed.

A numerical model developed by Markus, based on the extended Butler–Volmer equation, has been used to investigate crack propagation in SSEs induced by non-uniform Li plating in their defects, which leads to dendrite formation.³⁰⁷ On one hand, the pressure in SSEs continuously increases during the Li plating process, surpassing their fracture strengths, and resulting in crack extension, dendrite growth, and ultimately internal short circuits. The electrodeposition of Li is a plastic flow process, influenced by the critical current density and defect size.³⁰⁸ On the other hand, the built-up high pressure can inhibit the Li-plating-related redox reaction. Consequently, appropriate pressure should be applied in ASSBs based on the existing surface defects and permissible current density, in agreement with experimental observations.³⁰⁴

Recently, a theory has emerged regarding the separation of dendrite initiation and propagation in SSEs, as depicted in Fig. 8(a).³⁰⁹ The process of dendrite initiation is primarily influenced by the local fracture toughness of SSE materials. Initially, lithium is plated into the pores or defects of SSEs through microcracks caused by electric leakage.³¹⁰ As these pores become filled, further deposition can generate hydrostatic stress on the pore surfaces, exceeding their mechanical fracture strength. This lithiation-induced cracking is affected by factors such as current density, fracture strength near grain boundaries, and pore size (Fig. 8(b)). In contrast, crack propagation occurs due to the wedge opening of SSE materials from the interfaces with Li metal anodes. This propagation is accelerated by the lower fracture toughness of the material and high stack pressures, as well as influenced by the geometry and aspect ratio of the defects.³¹¹ Fig. 8(c)–(f) illustrate simulations of the fracture process in a NASICON-type SSE with modified defect morphologies, including semi-sphere, semi-ellipsoid, pyramid, and cube, using an electro-chemo-mechanical model. Notably, the semi-spherical defect exhibited catastrophic asymmetric cracking near the surface of the SSE, indicating the transmission of local stress concentration and accumulated damage from the defect tip to the bulk material. This finding emphasizes the importance of addressing the potential issues arising from such stress concentration and damage propagation during the surface treatment of SSEs. The abovementioned studies provide valuable insights and inspiration for potential solutions to tackle the dendrite problem by implementing appropriate surface treatments for SSEs.

Dendrite suppression strategies. Significant efforts have been dedicated to controlling the dendrite growth in SSBs, leading to considerable progress in this area. The influence of the mechanical properties of electrodes and SSEs on dendrite suppression and cycling stability in ASSBs has been

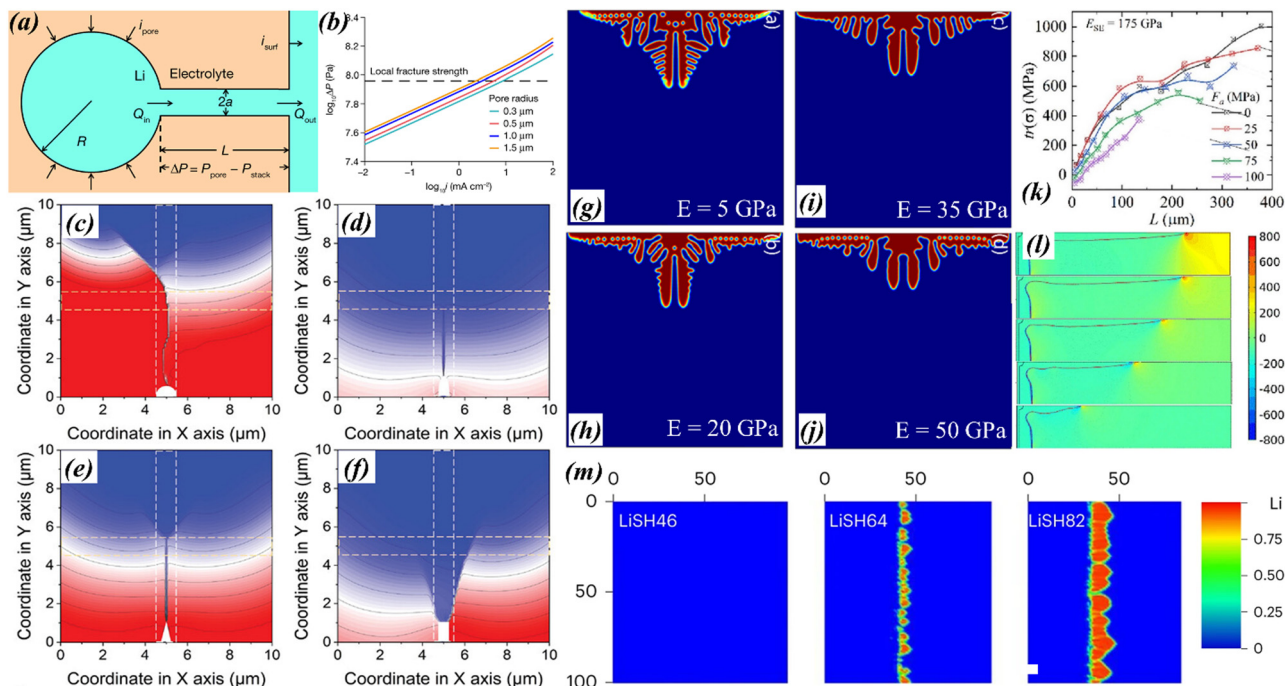


Fig. 8 (a) Schematic of the infiltrated Li in the pore–crack system near the surface of SSE. (b) The Li-plating induced pressure in the pore as a function of current density with the pore radii ranging from 1.5 to 0.3 μm ; dashed lines show the local fracture strength σ_c of the electrolyte. Reprinted from ref. 309, with permission from Springer Nature. Local displacement of SSE under Li-plating induced stress with different geometries of the interfacial defects: (c) semi-sphere, (d) semi-ellipsoid, (e) pyramid, and (f) cube. Reprinted with permission from ref. 311. Dendrite morphologies from the phase-field simulation in SSEs with various elastic moduli: (g) 5 GPa, (h) 20 GPa, (i) 35 GPa, and (j) 50 GPa; the yield strength of the electrolyte is fixed to be 7.7 MPa. Reprinted with permission from ref. 312. Copyright 2022 American Chemical Society. (k) Effect of the applied compressive pressure on the stress concentration during dendrite growth, and (l) the corresponding simulated morphology. Reprinted from ref. 262, with permission from Elsevier. (m) The phase field simulation of lithium dendrites on LiSH anodes in ASSBs cycled at 1C; the thickness of the electrode and SE is along the horizontal direction. Reprinted from ref. 318, with permission from Springer Nature.

investigated using an elastoplastic strain coupled phase-field model.³¹² Phase field (PF) simulation results have revealed that an increased Young's modulus or yield strength can enhance the ability of SSEs to withstand higher stresses, thereby inhibiting vertical dendrite growth and promoting uniform lithium deposition (as shown in Fig. 8(g)–(j)). Importantly, studies have indicated that the fracture toughness of SSEs may have a more prominent influence on the dendrite penetration behavior compared to the modulus. This is due to the infiltration of viscoelastic Li filaments within defects or cracks in SSEs, resulting in significant stress concentrations at the tips of these filaments, ultimately leading to local failure (Fig. 8(b)).²⁶²

Furthermore, an effective and straightforward solution to address dendrite-related issues in SSBs is to apply a reasonable compressive traction on the surface of the SSE during battery fabrication. This approach has shown promising results, as it can shift the interfacial overpotential, slow down parasitic reaction kinetics, and ensure intimate contact with the electrodes, as suggested by mechano-chemical simulation results.²⁶² In Fig. 8(k) and (l), it can be observed that increasing the stack pressure from 0 to 100 MPa reduced the stress concentration at the tip of the Li filament from 1000 to 400 MPa. Experimental measurements have also confirmed the effectiveness of this approach, as the interfacial resistance reached an

unprecedented value of 0 $\Omega\cdot\text{cm}^2$ when high external pressures of 400 MPa were applied.³¹³ This notable reduction in interfacial resistance can be attributed to the suppression of both dendrite formation during cathodic polarization and void formation under anodic load.

However, it is important to consider that applying excessive stack pressure on Li metal can lead to mechanical failures such as plastic deformation, creeping, and fatigue.³¹⁴ To address this issue, an effective approach is to replace Li metal with rigid Li intermetallic alloys, such as Li–indium (Li–In),³¹⁵ Li–aluminum (Li–Al),³¹⁶ and Li–magnesium (Li–Mg),³¹⁷ as anodes. The use of these alloys can significantly enhance the electro-chemical stability of the anode. Unlike Li metal, which follows the Voce hardening law and allows unconstrained deformation, the presence of solute atoms in Li alloys increases the energy barriers for dislocation movement. Consequently, Li alloys conform to the Swift hardening law, enabling them to withstand higher stack pressure while preventing stress transfer towards the SSEs.

Moreover, the incorporation of low-modulus, ion-conductive soft additives, such as hard carbon (HC), as buffer layers has been employed to alleviate stress concentration during lithiation and prevent cracking.^{318,319} A simulated dendrite growth in a Li₆PS₅Cl electrolyte with varying HC contents, as shown in

Fig. 8(m) using the phase-field technique, demonstrated the impact of HC on the electrode performance. Notably, an electrode containing 60 wt% HC (LiSH46) exhibited optimized lithium diffusion, a well-maintained composite anode morphology, minimal dendrite formation, and improved stability. In contrast, an electrode with 20 wt% HC (LiSH82) demonstrated severe dendrite propagation, higher lithium consumption, and rapid capacity degradation. These findings highlight the significance of applying “soft” buffer materials in enhancing the stability of the batteries.

The design of 3D architectures for SSEs has always been a crucial technique to advance LIBs. This design approach offers several benefits, including reducing ion and electron diffusion pathways, minimizing interfacial resistance, and enhancing areal capacity, energy density, and power density.^{320–322} Recently, bi-/tri-layer architectures have been proposed, consisting of dense layers and porous ion-/electron-conducting layers. In this design, the thick porous layer serves as a mechanical support, ion diffusion pathway, and Li⁰ storage space, while the thin dense layer prevents Li penetration and internal short-circuits.^{323,324} Drawing inspiration from this design principle, 3D structures using MOFs have been developed for both the Li anode host^{325,326} and composite electrolytes.³²⁷ These structures facilitate delocalized Li⁺ flux and enable compact Li deposition with robust inorganic-rich SEI layers, as suggested by numerical simulations. This advancement in SSE frameworks holds the potential to open up new research directions for next-generation high-energy-density Li rechargeable batteries.

Last but not the least, similar to one of the strategies mentioned earlier to improve the compatibility of the electrode-SSE pairs, computational methods have indicated that adding a protective coating on the electrode–electrolyte interface, as well as choosing electrochemically compatible components of the electrolyte, can effectively address issues related to current heterogeneity and dendrite growth. This approach facilitates good solid contact, enhances Li wettability, and reduces interfacial resistance, particularly for CEs composed of various components.³²⁸ The introduction of a protective layer has demonstrated a significant increase in critical current density and battery stability.³²⁹ By implementing these measures, the overall performance and reliability of the battery system can be greatly improved.

6. Machine learning assisted design of SSEs

The development and optimization of SSEs for advanced LIBs require fast and accurate modeling techniques to predict material properties under realistic operating conditions. The application of ML approaches in material design has revolutionized the exploration and development of SSEs with tailored properties.

ML algorithms can be trained on known compositions and properties to predict the performance of new compositions for inverse design, providing valuable insights into material

behavior and aiding in the design and optimization process.³³⁰ Hamad *et al.* used a random forest-based model to predict the ionic conductivity of SSEs for LIBs and sodium-ion batteries, with experimental validation (Fig. 9(a)).^{331,332} They collected training data from experimental reports of 160 samples and selected 50 material features to avoid overfitting and ensure training accuracy. The ML model achieved high accuracy during cross-validation, with a coefficient of determination (R^2) of 0.97, a root mean squared error (RMSE) of 0.005, and a mean absolute error (MAE) of 0.007. Additionally, by screening around 30 000 compositions from the inorganic crystal structure database (ICSD), LiYS₂ was suggested as a promising candidate with comprehensive properties. To efficiently screen a large number of compositions, Mukhopadhyay *et al.* compared the precision of eight different algorithms for estimating the ionic conductivities of SSEs.³³³ They incorporated various features, including activation energy, operating temperature, lattice parameters, and unit cell volume, for model training. The resulting artificial neural network (ANN) model showed excellent prediction accuracy, with a RMSE of 0 and an MAE of 0.002 (Fig. 9(b)). By leveraging ML models and training them on diverse datasets, researchers can identify promising SSE candidates and accurately predict their properties, which contributes to the optimization of SSEs.

Machine-learned potentials (MLPs) represent another application of ML in material design, addressing computational challenges faced by DFT, classical force fields, and AIMD simulations,³³⁴ and offering an attractive and reliable tool to extend numerical simulations to longer timescales and larger systems while maintaining accuracy at the first-principles level.³³⁵ The quality of MLPs in the field of SSEs depends on factors such as high-quality and diverse training sets and the intrinsic defects in the materials.³³⁶ By evaluating these factors, researchers have revealed the Li diffusion behaviors in different lithium ionic conductors, including Li₇P₃S₁₁, Li₁₀GeP₂S₁₂, Li₃ErCl₆, and Li₃YBr₆.³³⁷ MLPs have shown the ability to reasonably reproduce DFT energies and forces, lattice parameters, and local structures of materials. They have also captured non-linear Arrhenius behavior in Li⁺ diffusion in Li₃ErCl₆ and the polyanion rotation phenomenon of [PS₄]³⁻ tetrahedra in Li₇P₃S₁₁ at room temperature. Fig. 9(c) shows the final structures of the rotated [PS₄]³⁻ after a 1 μs simulation at 300 K. The rotation of [PS₄]³⁻ was discovered to be associated with a part of the longer-chain [P₂S₇]⁴⁻ group, leading to the mismatch between the motion of Li⁺ diffusion and the direction of polyanion rotation. In other words, there was no paddle-wheel effect in crystalline Li₇P₃S₁₁ at room temperature according to the simulation results,³³⁸ and the rotational [PS₄]³⁻ polyanion groups had a slightly negative impact on the overall Li⁺ diffusion in crystalline Li₇P₃S₁₁, which was also discovered in the BH₄-substituted Li argyrodite structure.³³⁹ These findings highlight the capabilities of MLPs in accurately simulating complex systems and providing insights into the behavior of SSEs.

Furthermore, ML techniques applied at the atomistic and molecular levels can analyze large datasets of materials properties, enabling the screening of compositions and identification

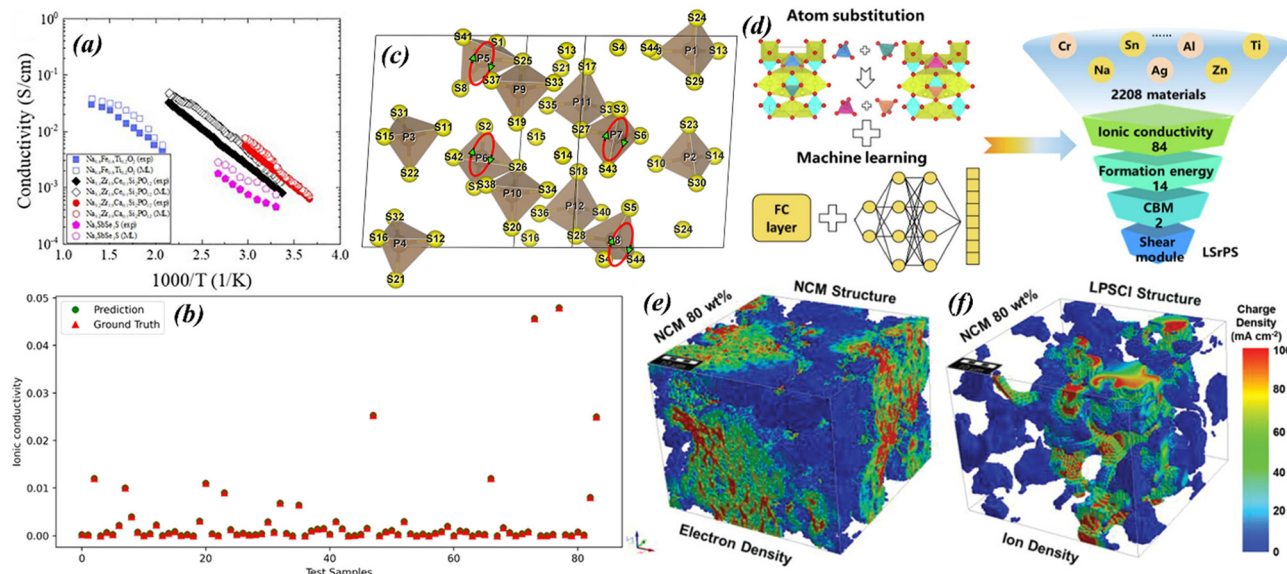


Fig. 9 (a) Comparison of the experiments and predicted ionic conductivities of 4 SSEs as a function of temperature *via* RF model. Reprinted from ref. 331, with permission from Elsevier. (b) Comparison of the experimentally measured and predicted ionic conductivity by ANN. Reprinted with permission from ref. 333. (c) Final structures with PS_4 polyanion rotations in crystalline $\text{Li}_7\text{P}_3\text{S}_{11}$ after 1 μs MLMD simulations at 300 K. Reprinted with permission from ref. 337. (d) ML-enabled fast screening framework to identify the best design of LGPS through element substitution. Reprinted from ref. 342, with permission from Elsevier. (e) The electron density in the electrode and (f) Li^+ density in the LPSCl structure with 80 wt% NCM electrodes. Reprinted from ref. 347, © 2020 Wiley-VCH Verlag GmbH & Co. KGaA, Weinheim.

of promising candidates with stable crystal structures and desired characteristics.³⁴⁰ High-throughput screening (HTS) techniques have been adopted to explore the correlation between material properties such as ionic conductivity and electrochemical stability with phonon band centers.³⁴¹ By training algorithms with a dataset of 53 compounds, HTS was conducted on 14 000 Li-containing compounds in the Materials Project database, resulting in the identification of 18 SSE candidates spanning various compounds like oxides, fluorides, chlorides, bromides, and nitrides. ML-enabled HTS methods have also been developed for element substitution in SSEs, which can be tedious to explore extensively *via* experiments or theoretical calculations. A case study on LGPS showcased the identification of the best substitution scheme, $\text{Li}_{10}\text{SrP}_2\text{S}_{12}$, which exhibited a high ionic conductivity of 12.58 mS cm⁻¹, a high modulus of 10 GPa, and excellent electronic insulation (Fig. 9(d)).³⁴² A similar approach was applied to the doped LLZO system, utilizing a training dataset of 208 samples and employing molecular, structural, and electronic descriptors as key features.³⁴³ The relative density of LLZO was found to be the most critical factor influencing the ionic conductivity, followed by electronegativity. The HTS approach can also be combined with other numerical methods to create a multiscale platform for predicting SSE behaviors. For example, Ren *et al.*³¹² conducted a phase-field simulation to investigate the impacts of the yield strengths of the Li anode and SSE, as well as the SSEs' elastic modulus on dendrite growth (Fig. 8(g)–(j)). A training dataset was then generated using the PF model, and ML algorithms were utilized to establish fundamental relationships between macroscale mechanical properties and microscale dendrite morphologies. This approach offers a novel

direction for combining data-driven approaches with physics-based modeling, which can guide the selection and design of electrode and electrolyte materials with increased accuracy and efficiency.

Besides, ML model-assisted digital twin techniques have the capability to surpass the limitations of physics-based numerical methods. Through the exploration of large datasets of structural features and corresponding material properties, these models enable the estimation of structure–property relationships in real objects with complex and nonuniform microstructures, as well as localized electrochemical phenomena.^{344–346} The knowledge obtained from digital twin modeling can guide the optimal design of batteries with specific topologies and optimize their functionalities. For instance, a digital twin model for an ASSB based on a solid sulfide electrolyte was proposed.³⁴⁷ This model scrutinized mass transport and interfacial electrochemical kinetics on a voxel-based complex microstructure, capturing micro-timescale phenomena. Fig. 9(e) and (f) show the Li^+ concentration in the solid sulfide electrolyte structure with different contents of cathode active materials. It can be observed that with a low content of solid sulfide electrolyte (20 wt%) and limited ionic pathways, the ion density becomes concentrated and heterogeneous. This suggests the critical role of blending ratios between electrodes and electrolytes in achieving favorable electronic and ionic conductivities.

7. Summary and outlook

The growing interest and research focus on SSBs are fueled by the global shift towards green energy and the increasing

demand for high-performance and affordable energy storage systems. As the world embraces renewable energy sources, the need for efficient and sustainable energy storage solutions becomes critical. SSBs offer significant advantages over conventional lithium-ion batteries, including enhanced safety, higher energy density, and longer lifespan. These factors have sparked intense interest among researchers, industry experts, and policymakers, all working towards the development of advanced SSB technologies that can meet the rising demand for clean and reliable energy storage.

The academic community has made substantial progress in the development of SSBs. Researchers have been actively exploring novel materials, advanced characterization techniques, and innovative design strategies to create SSEs with exceptional properties such as high ionic conductivity ($\geq 1 \text{ S cm}^{-1}$), excellent mechanical characteristics, good electrochemical stability, and minimal interfacial resistance. By harnessing computational methods and revolutionary materials, the development of SSBs holds tremendous potential in transforming the way we store and utilize energy, making it more sustainable and efficient.

This review provides a systematic and comprehensive analysis of computational methods employed in the development of SSEs for next-generation ASSBs. Various numerical approaches, including first-principles calculations, molecular dynamics simulations, kinetic Monte Carlo simulations, thermodynamic phase equilibrium analysis, finite element modeling, and machine learning techniques, have been extensively utilized in SSE research. These computational methods serve multiple purposes, including the prediction of intrinsic properties of SSEs (such as stable phases and ion migration mechanisms), evaluation of the electrochemical and chemical compatibility of electrode-SSE combinations, and exploration of the multiphysics-based dynamic responses and primary failure modes of SSEs. Furthermore, the significant potential of machine learning-assisted design of SSEs is highlighted, emphasizing its integral role in accelerating SSE development, and providing valuable insights and prospects for future advancements.

To further expedite the development of SSEs, we propose to address the following issues in future research:

(1) Design and optimization of SSE materials: continued research into the design and optimization of SSE materials is crucial for achieving improved electrochemical performance, enhanced stability, and reduced interfacial resistance. This can be accomplished by exploring strategies such as reducing the lithium content, modifying the bonding and polarizability of the anion framework, or tailoring processing conditions within a multi-compositional space approach.

(2) Expanding the application of machine learning approaches: machine learning techniques can be further extended to optimize fabrication procedures and parameters, diagnose performance degradation, analyze failure mechanisms, and optimize the design of SSEs, including composite electrolytes. This broader application of machine learning can accelerate the development of SSEs and improve their overall performance.

(3) Multiscale modeling and simulations: developing multiscale models capable of capturing microscale and macroscale phenomena is essential for accurately predicting and understanding the behavior of SSEs. Integrating different numerical methods, such as atomistic simulations and continuum modeling, can provide comprehensive insights into the complex behavior of SSEs and enable more accurate predictions.

(4) Advanced characterization techniques: advancements in characterization techniques, including *in situ* and operando methods, can offer real-time information on the electrochemical processes within SSEs. By combining these techniques with computational modeling, deeper and more reliable insights into the structure–property relationships can be obtained, guiding SSE design and optimization.

(5) Exploring beyond lithium-ion batteries: while the focus of this review is on SSEs for lithium secondary batteries, the principles and approaches discussed can be extended to other battery types and energy storage systems. Investigating SSEs for alkali metal and multivalent ion batteries opens up new opportunities for energy storage technology and can contribute to the development of more diverse, low-cost, and efficient energy storage solutions.

Addressing these issues will significantly contribute to the ongoing development of SSEs and accelerate the commercialization of advanced all-solid-state batteries with improved performance, safety, and energy density.

Conflicts of interest

The authors declare that they have no known competing financial interests or personal relationships that could have appeared to influence the work reported in this paper.

Acknowledgements

This work was supported by the National Natural Science Foundation of China (51873086 and 22201275), the Anhui Provincial Natural Science Foundation (no. 2208085QB32) and the Special Fund for Carbon Peak and Carbon Neutralization Scientific and Technological Innovation Project of Jiangsu Province (BE2022042).

References

- N. Nitta, F. Wu, J. T. Lee and G. Yushin, *Mater. Today*, 2015, **18**, 252–264.
- J. M. Tarascon and M. Armand, *Nature*, 2001, **414**, 359–367.
- T. Perveen, M. Siddiq, N. Shahzad, R. Ihsan, A. Ahmad and M. I. Shahzad, *Renewable Sustainable Energy Rev.*, 2020, **119**, 109549.
- J. Speirs, M. Contestabile, Y. Houari and R. Gross, *Renewable Sustainable Energy Rev.*, 2014, **35**, 183–193.
- J. W. Choi and D. Aurbach, *Nat. Rev. Mater.*, 2016, **1**, 16013.
- C. P. Grey and D. S. Hall, *Nat. Commun.*, 2020, **11**, 6279.

- 7 Z.-Y. Wang, C.-Z. Zhao, S. Sun, Y.-K. Liu, Z.-X. Wang, S. Li, R. Zhang, H. Yuan and J.-Q. Huang, *Matter*, 2023, **6**, 1096–1124.
- 8 J. Janek and W. G. Zeier, *Nat. Energy*, 2023, **8**, 230–240.
- 9 J. Janek and W. G. Zeier, *Nat. Energy*, 2016, **1**, 16141.
- 10 D. Cao, X. Sun, Y. Wang and H. Zhu, *Energy Storage Mater.*, 2022, **48**, 458–465.
- 11 X. Zheng, M. Yuan, Y. Zhao, Z. Li, K. Shi, H. Li and G. Sun, *Adv. Energy Mater.*, 2023, **13**, 2204019.
- 12 Z. Pan, D. J. L. Brett, G. He and I. P. Parkin, *Adv. Energy Mater.*, 2022, **12**, 2103483.
- 13 M. Pasta, D. Armstrong, Z. L. Brown, J. Bu, M. R. Castell, P. Chen, A. Cocks, S. A. Corr, E. J. Cussen, E. Darnbrough, V. Deshpande, C. Doerrer, M. S. Dyer, H. El-Shinawi, N. Fleck, P. Grant, G. L. Gregory, C. Grovenor, L. J. Hardwick, J. T. S. Irvine, H. J. Lee, G. Li, E. Liberti, I. McClelland, C. Monroe, P. D. Nellist, P. R. Shearing, E. Shoko, W. Song, D. S. Jolly, C. I. Thomas, S. J. Turrell, M. Vestli, C. K. Williams, Y. Zhou and P. G. Bruce, *J. Phys.: Energy*, 2020, **2**, 032008.
- 14 Y. Ren, T. Danner, A. Moy, M. Finsterbusch, T. Hamann, J. Dippell, T. Fuchs, M. Müller, R. Hoft, A. Weber, L. A. Curtiss, P. Zapol, M. Klenk, A. T. Ngo, P. Barai, B. C. Wood, R. Shi, L. F. Wan, T. W. Heo, M. Engels, J. Nanda, F. H. Richter, A. Latz, V. Srinivasan, J. Janek, J. Sakamoto, E. D. Wachsman and D. Fattakhova-Rohlfing, *Adv. Energy Mater.*, 2023, **13**, 2201939.
- 15 H.-L. Yang, B.-W. Zhang, K. Konstantinov, Y.-X. Wang, H.-K. Liu and S.-X. Dou, *Adv. Energy Sustainability Res.*, 2021, **2**, 2000057.
- 16 T. Krauskopf, F. H. Richter, W. G. Zeier and J. Janek, *Chem. Rev.*, 2020, **120**, 7745–7794.
- 17 R. Koerver, W. Zhang, L. de Biasi, S. Schweidler, A. O. Kondrakov, S. Kolling, T. Brezesinski, P. Hartmann, W. G. Zeier and J. Janek, *Energy Environ. Sci.*, 2018, **11**, 2142–2158.
- 18 Q. Kang, Z. Zhuang, Y. Liu, Z. Liu, Y. Li, B. Sun, F. Pei, H. Zhu, H. Li, P. Li, Y. Lin, K. Shi, Y. Zhu, J. Chen, C. Shi, Y. Zhao, P. Jiang, Y. Xia, D. Wang and X. Huang, *Adv. Mater.*, 2023, 2303460.
- 19 Y. Wu, K. Wang, K. Liu, Y. Long, C. Yang, H. Zhang, W. Pan, W. Si and H. Wu, *Adv. Energy Mater.*, 2023, 2300809.
- 20 R. Pacios, A. Villaverde, M. Martínez, M. Casas-Cabañas, F. Aguesse and A. Kvasha, *Adv. Energy Mater.*, 2023, 2301018.
- 21 A. M. Nolan, Y. Zhu, X. He, Q. Bai and Y. Mo, *Joule*, 2018, **2**, 2016–2046.
- 22 K. Yang, D. Liu, Z. Qian, D. Jiang and R. Wang, *ACS Nano*, 2021, **15**, 17232–17246.
- 23 Q. He, B. Yu, Z. Li and Y. Zhao, *Energy Environ. Mater.*, 2019, **2**, 264–279.
- 24 Y. Zhang, Y. Zhao and C. Chen, *Phys. Rev. B: Condens. Matter Mater. Phys.*, 2013, **87**, 134303.
- 25 S. Shi, J. Gao, Y. Liu, Y. Zhao, Q. Wu, W. Ju, C. Ouyang and R. Xiao, *Chin. Phys. B*, 2016, **25**, 018212.
- 26 C. Uebing and R. Gomer, *J. Chem. Phys.*, 1994, **100**, 7759–7766.
- 27 Y. He, C. Wang, P. Zou, R. Lin, E. Hu and H. L. Xin, *Angew. Chem., Int. Ed.*, 2023, e202308309.
- 28 S. Curtarolo, G. L. W. Hart, M. B. Nardelli, N. Mingo, S. Sanvito and O. Levy, *Nat. Mater.*, 2013, **12**, 191–201.
- 29 J. Liu, H. Yuan, H. Liu, C.-Z. Zhao, Y. Lu, X.-B. Cheng, J.-Q. Huang and Q. Zhang, *Adv. Energy Mater.*, 2022, **12**, 2100748.
- 30 Y. Zheng, Y. Yao, J. Ou, M. Li, D. Luo, H. Dou, Z. Li, K. Amine, A. Yu and Z. Chen, *Chem. Soc. Rev.*, 2020, **49**, 8790–8839.
- 31 H. Aziam, B. Larhrib, C. Hakim, N. Sabi, H. Ben Youcef and I. Saadoune, *Renewable Sustainable Energy Rev.*, 2022, **167**, 112694.
- 32 A. A. Franco, A. Rucci, D. Brandell, C. Frayret, M. Gaberscek, P. Jankowski and P. Johansson, *Chem. Rev.*, 2019, **119**, 4569–4627.
- 33 G. Kresse and J. Furthmüller, *Phys. Rev. B: Condens. Matter Mater. Phys.*, 1996, **54**, 11169–11186.
- 34 M. D. Segall, J. D. L. Philip, M. J. Probert, C. J. Pickard, P. J. Hasnip, S. J. Clark and M. C. Payne, *J. Phys.: Condens. Matter*, 2002, **14**, 2717.
- 35 G. Kresse and D. Joubert, *Phys. Rev. B: Condens. Matter Mater. Phys.*, 1999, **59**, 1758–1775.
- 36 Y. Wang, W. D. Richards, S. P. Ong, L. J. Miara, J. C. Kim, Y. Mo and G. Ceder, *Nat. Mater.*, 2015, **14**, 1026–1031.
- 37 G. Henkelman and H. Jónsson, *J. Chem. Phys.*, 2000, **113**, 9978–9985.
- 38 D. Sheppard, R. Terrell and G. Henkelman, *J. Chem. Phys.*, 2008, **128**, 134106.
- 39 G. Henkelman, B. P. Uberuaga and H. Jónsson, *J. Chem. Phys.*, 2000, **113**, 9901–9904.
- 40 D. Frenkel and B. Smit, in *Understanding Molecular Simulation*, ed. D. Frenkel and B. Smit, Academic Press, San Diego, 2nd edn, 2002, pp. 1–6.
- 41 H. Hua, X. Yang, P. Zhang and J. Zhao, *J. Phys. Chem. C*, 2023, **127**, 17324–17334.
- 42 M. Lemaalem and P. Carbonniere, *Solid State Ionics*, 2023, **399**, 116304.
- 43 D. G. Truhlar, *Phys. Today*, 2010, **63**, 54–56.
- 44 S. Nosé, *J. Chem. Phys.*, 1984, **81**, 511–519.
- 45 W. G. Hoover, *Phys. Rev. A: At., Mol., Opt. Phys.*, 1985, **31**, 1695–1697.
- 46 A. Van der Ven, G. Ceder, M. Asta and P. D. Tepesch, *Phys. Rev. B: Condens. Matter Mater. Phys.*, 2001, **64**, 184307.
- 47 A. F. Voter, Introduction to the Kinetic Monte Carlo Method, in *Radiation Effects in Solids*, ed. K. E. Sickafus, E. A. Kotomin and B. P. Uberuaga, Springer Netherlands, Dordrecht, 2007, pp. 1–23.
- 48 F. M. Bulnes, V. D. Pereyra and J. L. Riccardo, *Phys. Rev. E: Stat. Phys., Plasmas, Fluids, Relat. Interdiscip. Top.*, 1998, **58**, 86–92.
- 49 A. Van der Ven and G. Ceder, *Electrochem. Solid-State Lett.*, 2000, **3**, 301.

- 50 A. Van der Ven, J. C. Thomas, Q. Xu, B. Swoboda and D. Morgan, *Phys. Rev. B: Condens. Matter Mater. Phys.*, 2008, **78**, 104306.
- 51 L. Wang, T. Maxisch and G. Ceder, *Chem. Mater.*, 2007, **19**, 543–552.
- 52 L. J. Miara, W. D. Richards, Y. E. Wang and G. Ceder, *Chem. Mater.*, 2015, **27**, 4040–4047.
- 53 V. D. Parker, *J. Am. Chem. Soc.*, 1976, **98**, 98–103.
- 54 Y. Zhu, X. He and Y. Mo, *J. Mater. Chem. A*, 2016, **4**, 3253–3266.
- 55 P. Huang, L. T. Gao and Z.-S. Guo, *Electrochim. Acta*, 2023, **463**, 142873.
- 56 K. Taghikhani, P. J. Weddle, R. M. Hoffman, J. R. Berger and R. J. Kee, *Electrochim. Acta*, 2023, **460**, 142585.
- 57 J. Tippens, J. C. Miers, A. Afshar, J. A. Lewis, F. J. Q. Cortes, H. Qiao, T. S. Marchese, C. V. Di Leo, C. Saldana and M. T. McDowell, *ACS Energy Lett.*, 2019, **4**, 1475–1483.
- 58 F. Sun, C. Wang, M. Osenberg, K. Dong, S. Zhang, C. Yang, Y. Wang, A. Hilger, J. Zhang, S. Dong, H. Markötter, I. Manke and G. Cui, *Adv. Energy Mater.*, 2022, **12**, 2103714.
- 59 C. Miehe, H. Dal, L. M. Schäzel and A. Raina, *Int. J. Numer. Meth. Eng.*, 2016, **106**, 683–711.
- 60 X. Zhang, A. Krischok and C. Linder, *Comput. Methods Appl. Mech. Eng.*, 2016, **312**, 51–77.
- 61 Z.-T. Sun and S.-H. Bo, *J. Mater. Res.*, 2022, **37**, 3130–3145.
- 62 C. Yuan, X. Gao, Y. Jia, W. Zhang, Q. Wu and J. Xu, *Nano Energy*, 2021, **86**, 106057.
- 63 K. T. Butler, F. Oviedo and P. Canepa, *Machine Learning in Materials Science*, American Chemical Society, 2021.
- 64 S. Zheng, H. Ding, S. Li, D. Chen and F. Pan, *Chinese J. Struct. Chem.*, 2023, **42**, 100120.
- 65 A. Jain, S. P. Ong, G. Hautier, W. Chen, W. D. Richards, S. Dacek, S. Cholia, D. Gunter, D. Skinner, G. Ceder and K. A. Persson, *APL Mater.*, 2013, **1**, 011002.
- 66 S. Curtarolo, W. Setyawan, G. L. W. Hart, M. Jahnatek, R. V. Chepulkii, R. H. Taylor, S. Wang, J. Xue, K. Yang, O. Levy, M. J. Mehl, H. T. Stokes, D. O. Demchenko and D. Morgan, *Comput. Mater. Sci.*, 2012, **58**, 218–226.
- 67 S. Kirklin, J. E. Saal, B. Meredig, A. Thompson, J. W. Doak, M. Aykol, S. Rühl and C. Wolverton, *npj Comput. Mater.*, 2015, **1**, 15010.
- 68 S. Li, Z. Chen, W. Zhang, S. Li and F. Pan, *Nano Energy*, 2022, **102**, 107640.
- 69 A. C. C. Dutra and J. A. Dawson, *J. Phys. Chem. C*, 2023, **127**, 18256–18270.
- 70 M. B. Dixit, A. Verma, W. Zaman, X. Zhong, P. Kenesei, J. S. Park, J. Almer, P. P. Mukherjee and K. B. Hatzell, *ACS Appl. Energy Mater.*, 2020, **3**, 9534–9542.
- 71 A. G. Olabi, A. A. Abdelghafar, B. Soudan, A. H. Alami, C. Semeraro, M. Al Radi, M. Al-Murisi and M. A. Abdelkareem, *Ain Shams Eng. J.*, 2023, 102429, DOI: [10.1016/j.asnj.2023.102429](https://doi.org/10.1016/j.asnj.2023.102429).
- 72 Y. LeCun, Y. Bengio and G. Hinton, *Nature*, 2015, **521**, 436–444.
- 73 C. Cortes and V. Vapnik, *Mach. Learn.*, 1995, **20**, 273–297.
- 74 A. Gallo-Bueno, M. Reynaud, M. Casas-Cabanas and J. Carrasco, *Energy AI*, 2022, **9**, 100159.
- 75 Y. Qiu, X. Zhang, Y. Tian and Z. Zhou, *Chinese J. Struct. Chem.*, 2023, 100118, DOI: [10.1016/j.cjsc.2023.100118](https://doi.org/10.1016/j.cjsc.2023.100118).
- 76 A. Asheri, M. Fathidoost, V. Glavas, S. Rezaei and B.-X. Xu, *Comput. Mater. Sci.*, 2023, **226**, 112186.
- 77 W. Chen, Y. Li, D. Feng, C. Lv, H. Li, S. Zhou, Q. Jiang, J. Yang, Z. Gao, Y. He and J. Luo, *J. Power Sources*, 2023, **561**, 232720.
- 78 K. Yang, L. Zhao, X. An, L. Chen, J. Ma, J. Mi and Y.-B. He, *Angew. Chem., Int. Ed.*, 2023, **62**, e202302586.
- 79 M. Botros and J. Janek, *Science*, 2022, **378**, 1273–1274.
- 80 K. Yazhou and Y. Zhiren, *Ceram. Int.*, 2022, **48**, 5035–5039.
- 81 Z. Fu and J. Ferguson, *J. Am. Ceram. Soc.*, 2022, **105**, 6175–6183.
- 82 D. C. Ginnings and T. E. Phipps, *J. Am. Chem. Soc.*, 1930, **52**, 1340–1345.
- 83 S. Wang, Q. Bai, A. M. Nolan, Y. Liu, S. Gong, Q. Sun and Y. Mo, *Angew. Chem., Int. Ed.*, 2019, **58**, 8039–8043.
- 84 R. Schlem, S. Muy, N. Prinz, A. Banik, Y. Shao-Horn, M. Zobel and W. G. Zeier, *Adv. Energy Mater.*, 2020, **10**, 1903719.
- 85 X. Li, J. Liang, N. Chen, J. Luo, K. R. Adair, C. Wang, M. N. Banis, T.-K. Sham, L. Zhang, S. Zhao, S. Lu, H. Huang, R. Li and X. Sun, *Angew. Chem., Int. Ed.*, 2019, **58**, 16427–16432.
- 86 D. Park, H. Park, Y. Lee, S.-O. Kim, H.-G. Jung, K. Y. Chung, J. H. Shim and S. Yu, *ACS Appl. Mater. Interfaces*, 2020, **12**, 34806–34814.
- 87 S. Y. Kim, K. Kaup, K.-H. Park, A. Assoud, L. Zhou, J. Liu, X. Wu and L. F. Nazar, *ACS Mater. Lett.*, 2021, **3**, 930–938.
- 88 L. Wang, W. Xiao, L. Sun, R. Yang, J. Yu and L. Wang, *J. Rare Earths*, 2023, **42**(1), 155–162.
- 89 S.-T. Ko, T. Lee, J. Qi, D. Zhang, W.-T. Peng, X. Wang, W.-C. Tsai, S. Sun, Z. Wang, W. J. Bowman, S. P. Ong, X. Pan and J. Luo, *Matter*, 2023, **6**, 2395–2418.
- 90 S. R. Yeandel, B. J. Chapman, P. R. Slater and P. Goddard, *J. Phys. Chem. C*, 2018, **122**, 27811–27819.
- 91 S. He, Y. Xu, Y. Chen and X. Ma, *J. Mater. Chem. A*, 2020, **8**, 12594–12602.
- 92 Q. Pang, C. Sun, Y. Yu, K. Zhao, Z. Zhang, P. M. Voyles, G. Chen, Y. Wei and X. Wang, *Adv. Energy Mater.*, 2018, **8**, 1800144.
- 93 T. Yu, J. Liang, L. Luo, L. Wang, F. Zhao, G. Xu, X. Bai, R. Yang, S. Zhao, J. Wang, J. Yu and X. Sun, *Adv. Energy Mater.*, 2021, **11**, 2101915.
- 94 L. Gao, M. Song, R. Zhao, S. Han, J. Zhu, W. Xia, J. Bian, L. Wang, S. Gao, Y. Wang, R. Zou and Y. Zhao, *J. Energy Chem.*, 2023, **77**, 521–528.
- 95 A. Hayashi, H. Muramatsu, T. Ohtomo, S. Hama and M. Tatsumisago, *J. Mater. Chem. A*, 2013, **1**, 6320–6326.
- 96 Y. Wang, X. Lü, C. Zheng, X. Liu, Z. Chen, W. Yang, J. Lin and F. Huang, *Angew. Chem., Int. Ed.*, 2019, **58**, 7673–7677.
- 97 P. Bron, S. Johansson, K. Zick, J. Schmedt auf der Günne, S. Dehnens and B. Roling, *J. Am. Chem. Soc.*, 2013, **135**, 15694–15697.

- 98 S. Nachimuthu, H. J. Cheng, H. J. Lai, Y. H. Cheng, R.-T. Kuo, W. G. Zeier, B. J. Hwang and J. C. Jiang, *Mater. Today Chem.*, 2022, **26**, 101223.
- 99 J. Guan, X. Feng, Q. zeng, Z. Li, Y. Liu, A. Chen, H. Wang, W. Cui, W. Liu and L. Zhang, *Adv. Sci.*, 2023, **10**, 2203916.
- 100 B. Qiu, F. Xu, J. Qiu, M. Yang, G. Zhang, C. He, P. Zhang, H. Mi and J. Ma, *Energy Storage Mater.*, 2023, **60**, 102832.
- 101 D. Guo, D. B. Shinde, W. Shin, E. Abou-Hamad, A.-H. Emwas, Z. Lai and A. Manthiram, *Adv. Mater.*, 2022, **34**, 2201410.
- 102 D. Guo, F. Ming, D. B. Shinde, L. Cao, G. Huang, C. Li, Z. Li, Y. Yuan, M. N. Hedhili, H. N. Alshareef and Z. Lai, *Adv. Funct. Mater.*, 2021, **31**, 2101194.
- 103 C. Niu, W. Luo, C. Dai, C. Yu and Y. Xu, *Angew. Chem., Int. Ed.*, 2021, **60**, 24915–24923.
- 104 B. Dunn, H. Kamath and J.-M. Tarascon, *Science*, 2011, **334**, 928–935.
- 105 J.-F. Wu, E.-Y. Chen, Y. Yu, L. Liu, Y. Wu, W. K. Pang, V. K. Peterson and X. Guo, *ACS Appl. Mater. Interfaces*, 2017, **9**, 1542–1552.
- 106 Y. Inaguma, C. Liquan, M. Itoh, T. Nakamura, T. Uchida, H. Ikuta and M. Wakihara, *Solid State Commun.*, 1993, **86**, 689–693.
- 107 J. Kim, J. Kim, M. Avdeev, H. Yun and S.-J. Kim, *J. Mater. Chem. A*, 2018, **6**, 22478–22482.
- 108 X. Xu, Z. Wen, X. Yang and L. Chen, *Mater. Res. Bull.*, 2008, **43**, 2334–2341.
- 109 H. Yamane, M. Shibata, Y. Shimane, T. Junke, Y. Seino, S. Adams, K. Minami, A. Hayashi and M. Tatsumisago, *Solid State Ionics*, 2007, **178**, 1163–1167.
- 110 N. Kamaya, K. Homma, Y. Yamakawa, M. Hirayama, R. Kanno, M. Yonemura, T. Kamiyama, Y. Kato, S. Hama, K. Kawamoto and A. Mitsui, *Nat. Mater.*, 2011, **10**, 682–686.
- 111 H.-J. Deiseroth, S.-T. Kong, H. Eckert, J. Vannahme, C. Reiner, T. Zaiß and M. Schlosser, *Angew. Chem., Int. Ed.*, 2008, **47**, 755–758.
- 112 Y. Kato, S. Hori, T. Saito, K. Suzuki, M. Hirayama, A. Mitsui, M. Yonemura, H. Iba and R. Kanno, *Nat. Energy*, 2016, **1**, 16030.
- 113 P. Lu, Y. Xia, G. Sun, D. Wu, S. Wu, W. Yan, X. Zhu, J. Lu, Q. Niu, S. Shi, Z. Sha, L. Chen, H. Li and F. Wu, *Nat. Commun.*, 2023, **14**, 4077.
- 114 B. Choi, B. Moon, H. Seo, J. Jeong, H. Lee and W. Seo, *Mater. Des.*, 2000, **21**, 567–570.
- 115 X. Li, J. Liang, J. Luo, M. Norouzi Banis, C. Wang, W. Li, S. Deng, C. Yu, F. Zhao, Y. Hu, T.-K. Sham, L. Zhang, S. Zhao, S. Lu, H. Huang, R. Li, K. R. Adair and X. Sun, *Energy Environ. Sci.*, 2019, **12**, 2665–2671.
- 116 H. D. Lutz, Z. Zhang and A. Pfitzner, *Solid State Ionics*, 1993, **62**, 1–3.
- 117 Y. Seino, T. Ota, K. Takada, A. Hayashi and M. Tatsumisago, *Energy Environ. Sci.*, 2014, **7**, 627–631.
- 118 X. He, Y. Zhu and Y. Mo, *Nat. Commun.*, 2017, **8**, 15893.
- 119 J. Xu, Y. Li, P. Lu, W. Yan, M. Yang, H. Li, L. Chen and F. Wu, *Adv. Energy Mater.*, 2022, **12**, 2102348.
- 120 A. Manthiram, X. Yu and S. Wang, *Nat. Rev. Mater.*, 2017, **2**, 16103.
- 121 T. Asano, A. Sakai, S. Ouchi, M. Sakaida, A. Miyazaki and S. Hasegawa, *Adv. Mater.*, 2018, **30**, 1803075.
- 122 S. Muy, J. C. Bachman, L. Giordano, H.-H. Chang, D. L. Abernathy, D. Bansal, O. Delaire, S. Hori, R. Kanno, F. Maglia, S. Lupart, P. Lamp and Y. Shao-Horn, *Energy Environ. Sci.*, 2018, **11**, 850–859.
- 123 A. D. Sendek, E. R. Antoniuk, E. D. Cubuk, B. Ransom, B. E. Francisco, J. Buettner-Garrett, Y. Cui and E. J. Reed, *ACS Appl. Mater. Interfaces*, 2020, **12**, 37957–37966.
- 124 T. Kimura, A. Inoue, K. Nagao, T. Inaoka, H. Kowada, A. Sakuda, M. Tatsumisago and A. Hayashi, *ACS Appl. Energy Mater.*, 2022, **5**, 1421–1426.
- 125 Y. Ma, J. Wan, X. Xu, A. D. Sendek, S. E. Holmes, B. Ransom, Z. Jiang, P. Zhang, X. Xiao, W. Zhang, R. Xu, F. Liu, Y. Ye, E. Kaeli, E. J. Reed, W. C. Chueh and Y. Cui, *ACS Energy Lett.*, 2023, **8**, 2762–2771.
- 126 T. Krauskopf, S. Muy, S. P. Culver, S. Ohno, O. Delaire, Y. Shao-Horn and W. G. Zeier, *J. Am. Chem. Soc.*, 2018, **140**, 14464–14473.
- 127 Y. Lu, C.-Z. Zhao, H. Yuan, X.-B. Cheng, J.-Q. Huang and Q. Zhang, *Adv. Funct. Mater.*, 2021, **31**, 2009925.
- 128 J. Fang Wu, Z. Zou, B. Pu, L. Ladenstein, S. Lin, W. Xie, S. Li, B. He, Y. Fan, W. K. Pang, H. M. R. Wilkening, X. Guo, C. Xu, T. Zhang, S. Shi and J. Liu, *Adv. Mater.*, 2023, 2303730.
- 129 Y.-C. Yin, J.-T. Yang, J.-D. Luo, G.-X. Lu, Z. Huang, J.-P. Wang, P. Li, F. Li, Y.-C. Wu, T. Tian, Y.-F. Meng, H.-S. Mo, Y.-H. Song, J.-N. Yang, L.-Z. Feng, T. Ma, W. Wen, K. Gong, L.-J. Wang, H.-X. Ju, Y. Xiao, Z. Li, X. Tao and H.-B. Yao, *Nature*, 2023, **616**, 77–83.
- 130 C. Wang, S. Wang, X. Liu, Y. Wu, R. Yu, H. Duan, J. T. Kim, H. Huang, J. Wang, Y. Mo and X. Sun, *Energy Environ. Sci.*, 2023, **16**(11), 5136–5143.
- 131 W. Weppner, P. Hartwig and A. Rabenau, *J. Power Sources*, 1981, **6**, 251–259.
- 132 V. Landgraf, T. Famprakis, J. de Leeuw, L. J. Bannenberg, S. Ganapathy and M. Wagemaker, *ACS Appl. Energy Mater.*, 2023, **6**, 1661–1672.
- 133 Y. Li, S. Daikuhabara, S. Hori, X. Sun, K. Suzuki, M. Hirayama and R. Kanno, *Chem. Mater.*, 2020, **32**, 8860–8867.
- 134 N. Minafra, S. P. Culver, T. Krauskopf, A. Senyshyn and W. G. Zeier, *J. Mater. Chem. A*, 2018, **6**, 645–651.
- 135 Y. Li, S. Song, H. Kim, K. Nomoto, H. Kim, X. Sun, S. Hori, K. Suzuki, N. Matsui, M. Hirayama, T. Mizoguchi, T. Saito, T. Kamiyama and R. Kanno, *Science*, 2023, **381**, 50–53.
- 136 P. Lennartz, B. A. Paren, A. Herzog-Arbeitman, X. C. Chen, J. A. Johnson, M. Winter, Y. Shao-Horn and G. Brunklaus, *Joule*, 2023, **7**, 1471–1495.
- 137 N. Meng, Y. Ye, Z. Yang, H. Li and F. Lian, *Adv. Funct. Mater.*, 2023, 2305072.
- 138 J. Gao, C. Wang, D.-W. Han and D.-M. Shin, *Chem. Sci.*, 2021, **12**, 13248–13272.
- 139 L. Chen, Y. Li, S.-P. Li, L.-Z. Fan, C.-W. Nan and J. B. Goodenough, *Nano Energy*, 2018, **46**, 176–184.

- 140 Z. Li, H.-M. Huang, J.-K. Zhu, J.-F. Wu, H. Yang, L. Wei and X. Guo, *ACS Appl. Mater. Interfaces*, 2019, **11**, 784–791.
- 141 W. Jia, Z. Li, Z. Wu, L. Wang, B. Wu, Y. Wang, Y. Cao and J. Li, *Solid State Ionics*, 2018, **315**, 7–13.
- 142 Z. Wang, L. Shen, S. Deng, P. Cui and X. Yao, *Adv. Mater.*, 2021, **33**, 2100353.
- 143 Q. Kang, Y. Li, Z. Zhuang, D. Wang, C. Zhi, P. Jiang and X. Huang, *J. Energy Chem.*, 2022, **69**, 194–204.
- 144 W. Han, T. Kim, B. Yoo and H.-H. Park, *Sci. Rep.*, 2018, **8**, 4086.
- 145 S. Dai, J. He, X. Chen, J. Cui, H. Zhao, R. Zhang, H. Lei, J. Yin, L. Cai, F. Ye, X. Kong, R. Hu and M. Huang, *Macromolecules*, 2023, **56**, 3660–3667.
- 146 D. Sharon, C. Deng, P. Bennington, M. A. Webb, S. N. Patel, J. J. de Pablo and P. F. Nealey, *Macromolecules*, 2022, **55**, 7212–7221.
- 147 K. Tanaka, Y. Tago, M. Kondo, Y. Watanabe, K. Nishio, T. Hitosugi and M. Moriya, *Nano Lett.*, 2020, **20**, 8200–8204.
- 148 P. Prakash, A. Shylendran, B. Fall, M. J. Zdilla, S. L. Wunder and A. Venkatnathan, *J. Phys. Chem. C*, 2022, **126**, 4744–4750.
- 149 B. Fall, P. Prakash, M. R. Gau, S. L. Wunder, A. Venkatnathan and M. J. Zdilla, *Chem. Mater.*, 2019, **31**, 8850–8863.
- 150 P. Prakash, B. Fall, J. Aguirre, L. A. Sonnenberg, P. R. Chinnam, S. Chereddy, D. A. Dikin, A. Venkatnathan, S. L. Wunder and M. J. Zdilla, *Nat. Mater.*, 2023, **22**, 627–635.
- 151 Z. Hu, F. Xian, Z. Guo, C. Lu, X. Du, X. Cheng, S. Zhang, S. Dong, G. Cui and L. Chen, *Chem. Mater.*, 2020, **32**, 3405–3413.
- 152 A. Wang, S. Geng, Z. Zhao, Z. Hu and J. Luo, *Adv. Funct. Mater.*, 2022, **32**, 2201861.
- 153 H. Chen, D. Adekoya, L. Hencz, J. Ma, S. Chen, C. Yan, H. Zhao, G. Cui and S. Zhang, *Adv. Energy Mater.*, 2020, **10**, 2000049.
- 154 S. Wang, Q. Sun, Q. Zhang, C. Li, C. Xu, Y. Ma, X. Shi, H. Zhang, D. Song and L. Zhang, *Adv. Energy Mater.*, 2023, **13**, 2204036.
- 155 L. Wang, Y. He and H. L. Xin, *J. Electrochem. Soc.*, 2023, **170**(9), 090525.
- 156 L.-Z. Fan, H. He and C.-W. Nan, *Nat. Rev. Mater.*, 2021, **6**, 1003–1019.
- 157 F. Xu, S. Deng, Q. Guo, D. Zhou and X. Yao, *Small Methods*, 2021, **5**, 2100262.
- 158 Q. Sun, S. Wang, Y. Ma, D. Song, H. Zhang, X. Shi, N. Zhang and L. Zhang, *Adv. Mater.*, 2023, **35**, 2300998.
- 159 K. D. Fong, J. Self, K. M. Diederichsen, B. M. Wood, B. D. McCloskey and K. A. Persson, *ACS Cent. Sci.*, 2019, **5**, 1250–1260.
- 160 H. G. Buss, S. Y. Chan, N. A. Lynd and B. D. McCloskey, *ACS Energy Lett.*, 2017, **2**, 481–487.
- 161 P.-F. Cao, B. Li, G. Yang, S. Zhao, J. Townsend, K. Xing, Z. Qiang, K. D. Vogiatzis, A. P. Sokolov, J. Nanda and T. Saito, *Macromolecules*, 2020, **53**, 3591–3601.
- 162 R. Bouchet, S. Maria, R. Meziane, A. Aboulaich, L. Lienafa, J.-P. Bonnet, T. N. T. Phan, D. Bertin, D. Gigmes, D. Devaux, R. Denoyel and M. Armand, *Nat. Mater.*, 2013, **12**, 452–457.
- 163 H.-Y. Zhou, Y. Ou, S.-S. Yan, J. Xie, P. Zhou, L. Wan, Z.-A. Xu, F.-X. Liu, W.-L. Zhang, Y.-C. Xia and K. Liu, *Angew. Chem., Int. Ed.*, 2023, e202306948.
- 164 Y. Ye, X. Zhu, N. Meng and F. Lian, *Adv. Funct. Mater.*, 2023, 2307045.
- 165 P. Ding, L. Wu, Z. Lin, C. Lou, M. Tang, X. Guo, H. Guo, Y. Wang and H. Yu, *J. Am. Chem. Soc.*, 2023, **145**, 1548–1556.
- 166 J. Seo, G.-H. Lee, J. Hur, M.-C. Sung, J.-H. Seo and D.-W. Kim, *Adv. Energy Mater.*, 2021, **11**, 2102583.
- 167 J. Chen, X. Deng, Y. Gao, Y. Zhao, X. Kong, Q. Rong, J. Xiong, D. Yu and S. Ding, *Angew. Chem., Int. Ed.*, 2023, **62**, e202307255.
- 168 D. G. Mackanic, X. Yan, Q. Zhang, N. Matsuhisa, Z. Yu, Y. Jiang, T. Manika, J. Lopez, H. Yan, K. Liu, X. Chen, Y. Cui and Z. Bao, *Nat. Commun.*, 2019, **10**, 5384.
- 169 S. Yan, Z. Wang, F. Liu, H. Zhou and K. Liu, *Adv. Funct. Mater.*, 2023, 2303739.
- 170 J. Bae, Z. Zhu, J. Yan, D.-M. Kim, Y. Ko, A. Jain and B. A. Helms, *Sci. Adv.*, 2023, **9**, eadh9020.
- 171 G. Cai, P. Yan, L. Zhang, H.-C. Zhou and H.-L. Jiang, *Chem. Rev.*, 2021, **121**, 12278–12326.
- 172 Z. Chang, H. Yang, X. Zhu, P. He and H. Zhou, *Nat. Commun.*, 2022, **13**, 1510.
- 173 Y. Ouyang, W. Gong, Q. Zhang, J. Wang, S. Guo, Y. Xiao, D. Li, C. Wang, X. Sun, C. Wang and S. Huang, *Adv. Mater.*, 2023, 2304685.
- 174 X.-X. Wang, D.-H. Guan, C.-L. Miao, D.-C. Kong, L.-J. Zheng and J.-J. Xu, *J. Am. Chem. Soc.*, 2023, **145**, 5718–5729.
- 175 M. J. Baran, M. E. Carrington, S. Sahu, A. Baskin, J. Song, M. A. Baird, K. S. Han, K. T. Mueller, S. J. Teat, S. M. Meckler, C. Fu, D. Prendergast and B. A. Helms, *Nature*, 2021, **592**, 225–231.
- 176 X.-X. Wang, L.-N. Song, L.-J. Zheng, D.-H. Guan, C.-L. Miao, J.-X. Li, J.-Y. Li and J.-J. Xu, *Angew. Chem., Int. Ed.*, 2023, e202308837.
- 177 Y. Li, W. Zhang, Q. Dou, K. W. Wong and K. M. Ng, *J. Mater. Chem. A*, 2019, **7**, 3391–3398.
- 178 S.-J. Tan, X.-X. Zeng, Q. Ma, X.-W. Wu and Y.-G. Guo, *Electrochim. Energy Rev.*, 2018, **1**, 113–138.
- 179 F. Croce, G. B. Appetecchi, L. Persi and B. Scrosati, *Nature*, 1998, **394**, 456–458.
- 180 A. R. Polu and H.-W. Rhee, *J. Ind. Eng. Chem.*, 2016, **37**, 347–353.
- 181 H. M. J. C. Pitawala, M. A. K. L. Dissanayake, V. A. Seneviratne, B. E. Mellander and I. Albinson, *J. Solid State Electrochem.*, 2008, **12**, 783–789.
- 182 Y. Liang, L. Ji, B. Guo, Z. Lin, Y. Yao, Y. Li, M. Alcoutabi, Y. Qiu and X. Zhang, *J. Power Sources*, 2011, **196**, 436–441.
- 183 J. Zhang, N. Zhao, M. Zhang, Y. Li, P. K. Chu, X. Guo, Z. Di, X. Wang and H. Li, *Nano Energy*, 2016, **28**, 447–454.

- 184 Y. Cheng, X. Liu, Y. Guo, G. Dong, X. Hu, H. Zhang, X. Xiao, Q. Liu, L. Xu and L. Mai, *Adv. Mater.*, 2023, 2303226.
- 185 J. Ma, G. Zhong, P. Shi, Y. Wei, K. Li, L. Chen, X. Hao, Q. Li, K. Yang, C. Wang, W. Lv, Q.-H. Yang, Y.-B. He and F. Kang, *Energy Environ. Sci.*, 2022, **15**, 1503–1511.
- 186 C. Hu, Y. Shen, M. Shen, X. Liu, H. Chen, C. Liu, T. Kang, F. Jin, L. Li, J. Li, Y. Li, N. Zhao, X. Guo, W. Lu, B. Hu and L. Chen, *J. Am. Chem. Soc.*, 2020, **142**, 18035–18041.
- 187 K. Yang, L. Chen, J. Ma, C. Lai, Y. Huang, J. Mi, J. Biao, D. Zhang, P. Shi, H. Xia, G. Zhong, F. Kang and Y.-B. He, *Angew. Chem., Int. Ed.*, 2021, **60**, 24668–24675.
- 188 S. Mogurampelly and V. Ganesan, *Macromolecules*, 2015, **48**, 2773–2786.
- 189 H. Kwon, H.-J. Choi, J.-k Jang, J. Lee, J. Jung, W. Lee, Y. Roh, J. Baek, D. J. Shin, J.-H. Lee, N.-S. Choi, Y. S. Meng and H.-T. Kim, *Nat. Commun.*, 2023, **14**, 4047.
- 190 S. Chen, Y. Wu, S. Niu, Z. Wei, Y. Wu and W. Wei, *ACS Appl. Energy Mater.*, 2023, **6**, 1989–2000.
- 191 Z. Lu, L. Peng, Y. Rong, E. Wang, R. Shi, H. Yang, Y. Xu, R. Yang and C. Jin, *Energy Environ. Mater.*, 2023, e12498.
- 192 J. Cuan, Y. Zhou, T. Zhou, S. Ling, K. Rui, Z. Guo, H. Liu and X. Yu, *Adv. Mater.*, 2019, **31**, 1803533.
- 193 Y. Wei, Z. Li, Z. Chen, P. Gao, M. Gao, C. Yan, Z. Wu, Q. Ma, Y. Jiang, X. Yu, X. Zhang, Y. Liu, Y. Yang, M. Gao, W. Sun, Z. Qu, J. Chen and H. Pan, *Energy Environ. Sci.*, 2023, **16**(10), 4679–4692.
- 194 Y. S. Choi, Y.-S. Lee, K. H. Oh and Y. W. Cho, *Phys. Chem. Chem. Phys.*, 2016, **18**, 22540–22547.
- 195 D. Blanchard, A. Nale, D. Sveinbjörnsson, T. M. Eggenhuisen, M. H. W. Verkuijlen, Suwarno, T. Vegge, A. P. M. Kentgens and P. E. de Jongh, *Adv. Funct. Mater.*, 2015, **25**, 184–192.
- 196 Z. Liu, T. Zhang, S. Ju, Y. Ji, Z. Hu, Y. Lv, G. Xia and X. Yu, *ACS Appl. Energy Mater.*, 2022, **5**, 14301–14310.
- 197 Y. Hu, L. Yu, T. Meng, S. Zhou, X. Sui and X. Hu, *Chem. – Asian J.*, 2022, **17**, e202200794.
- 198 M. Watanabe, M. L. Thomas, S. Zhang, K. Ueno, T. Yasuda and K. Dokko, *Chem. Rev.*, 2017, **117**, 7190–7239.
- 199 M. Armand, F. Endres, D. R. MacFarlane, H. Ohno and B. Scrosati, *Nat. Mater.*, 2009, **8**, 621–629.
- 200 X. Chen, B. Put, A. Sagara, K. Gandrud, M. Murata, J. A. Steele, H. Yabe, T. Hantschel, M. Roeffaers, M. Tomiyama, H. Arase, Y. Kaneko, M. Shimada, M. Mees and P. M. Vereecken, *Sci. Adv.*, 2020, **6**, eaav3400.
- 201 L. Yu, Q. Liu, L. Wang, S. Guo, Q. Hu, Y. Li, X. Lan, Z. Liu and X. Hu, *J. Energy Chem.*, 2021, **62**, 408–414.
- 202 K. Deng, S. Zhou, Z. Xu, M. Xiao and Y. Meng, *Chem. Eng. J.*, 2022, **428**, 131224.
- 203 D. Yu, X. Pan, J. E. Bostwick, C. J. Zanelotti, L. Mu, R. H. Colby, F. Lin and L. A. Madsen, *Adv. Energy Mater.*, 2021, **11**, 2003559.
- 204 Y. Zhai, W. Hou, M. Tao, Z. Wang, Z. Chen, Z. Zeng, X. Liang, P. Paoprasert, Y. Yang, N. Hu and S. Song, *Adv. Mater.*, 2022, **34**, 2205560.
- 205 Q. Ruan, M. Yao, S. Luo, W. Zhang, C.-J. Bae, Z. Wei and H. Zhang, *Nano Energy*, 2023, **113**, 108571.
- 206 Y. Zhang, P. Li, L. Qiao, J. Sun, G. Li, Y. Yan, A. Liu, T. Ma and C. Hao, *Electrochim. Acta*, 2022, **416**, 140292.
- 207 X. Chen, L. Liang, W. Hu, H. Liao and Y. Zhang, *J. Power Sources*, 2022, **542**, 231766.
- 208 L. Dong, L. Nie and W. Liu, *Adv. Mater.*, 2020, **32**, 1908494.
- 209 Y. Zheng, W. Zhang, J. Gui, Q. Cao, Y. Wang, Y. Xu, Y. Liu and Y. Liang, *Energy Storage Mater.*, 2023, **61**, 102884.
- 210 L. Xu, S. Tang, Y. Cheng, K. Wang, J. Liang, C. Liu, Y.-C. Cao, F. Wei and L. Mai, *Joule*, 2018, **2**, 1991–2015.
- 211 K. Yan, Z. Lu, H.-W. Lee, F. Xiong, P.-C. Hsu, Y. Li, J. Zhao, S. Chu and Y. Cui, *Nat. Energy*, 2016, **1**, 16010.
- 212 C. Yu, S. Ganapathy, E. R. H. v Eck, H. Wang, S. Basak, Z. Li and M. Wagemaker, *Nat. Commun.*, 2017, **8**, 1086.
- 213 X. Gao, Z. Xing, M. Wang, C. Nie, Z. Shang, Z. Bai, S. X. Dou and N. Wang, *Energy Storage Mater.*, 2023, **60**, 102821.
- 214 R. Chen, Q. Li, X. Yu, L. Chen and H. Li, *Chem. Rev.*, 2020, **120**, 6820–6877.
- 215 X. Rui, D. Ren, X. Liu, X. Wang, K. Wang, Y. Lu, L. Li, P. Wang, G. Zhu, Y. Mao, X. Feng, L. Lu, H. Wang and M. Ouyang, *Energy Environ. Sci.*, 2023, **16**, 3552–3563.
- 216 E. A. Wu, C. S. Kompella, Z. Zhu, J. Z. Lee, S. C. Lee, I.-H. Chu, H. Nguyen, S. P. Ong, A. Banerjee and Y. S. Meng, *ACS Appl. Mater. Interfaces*, 2018, **10**, 10076–10086.
- 217 X.-B. Cheng, R. Zhang, C.-Z. Zhao, F. Wei, J.-G. Zhang and Q. Zhang, *Adv. Sci.*, 2016, **3**, 1500213.
- 218 H. Wan, S. Liu, T. Deng, J. Xu, J. Zhang, X. He, X. Ji, X. Yao and C. Wang, *ACS Energy Lett.*, 2021, **6**, 862–868.
- 219 F. Ren, Z. Liang, W. Zhao, W. Zuo, M. Lin, Y. Wu, X. Yang, Z. Gong and Y. Yang, *Energy Environ. Sci.*, 2023, **16**, 2579–2590.
- 220 Y. Zhu and Y. Mo, *Angew. Chem., Int. Ed.*, 2020, **59**, 17472–17476.
- 221 M. Yang, Y. Liu and Y. Mo, *Nat. Commun.*, 2023, **14**, 2986.
- 222 A. Sharafi, E. Kazyak, A. L. Davis, S. Yu, T. Thompson, D. J. Siegel, N. P. Dasgupta and J. Sakamoto, *Chem. Mater.*, 2017, **29**, 7961–7968.
- 223 J. Nguyen, B. Fleutot and R. Janot, *Solid State Ionics*, 2018, **315**, 26–32.
- 224 Y. Li, X. Chen, A. Dolocan, Z. Cui, S. Xin, L. Xue, H. Xu, K. Park and J. B. Goodenough, *J. Am. Chem. Soc.*, 2018, **140**, 6448–6455.
- 225 G. Ferraresi, M. El Kazzi, L. Czornomaz, C.-L. Tsai, S. Uhlenbruck and C. Villevieille, *ACS Energy Lett.*, 2018, **3**, 1006–1012.
- 226 R. H. Basappa, T. Ito and H. Yamada, *J. Electrochem. Soc.*, 2017, **164**, A666.
- 227 Z. Gao, J. Yang, H. Yuan, H. Fu, Y. Li, Y. Li, T. Ferber, C. Guhl, H. Sun, W. Jaegermann, R. Hausbrand and Y. Huang, *Chem. Mater.*, 2020, **32**, 3970–3979.
- 228 A. C. Thenuwara, E. L. Thompson, T. F. Malkowski, K. D. Parrotte, K. E. Lostracco, S. Narayan, R. T. Rooney, L. A. Seeley, M. R. Borges, B. D. Conway, Z. Song, M. E. Badding and K. G. Gallagher, *ACS Energy Lett.*, 2023, **8**, 4016–4023.

- 229 V. Raj, V. Venturi, V. R. Kankanallu, B. Kuiri, V. Viswanathan and N. P. B. Aetukuri, *Nat. Mater.*, 2022, **21**, 1050–1056.
- 230 S. Tang, G. Chen, F. Ren, H. Wang, W. Yang, C. Zheng, Z. Gong and Y. Yang, *J. Mater. Chem. A*, 2021, **9**, 3576–3583.
- 231 K. Lee, S. Han, J. Lee, S. Lee, J. Kim, Y. Ko, S. Kim, K. Yoon, J.-H. Song, J. H. Noh and K. Kang, *ACS Energy Lett.*, 2022, **7**, 381–389.
- 232 Y. Tian, T. Shi, W. D. Richards, J. Li, J. C. Kim, S.-H. Bo and G. Ceder, *Energy Environ. Sci.*, 2017, **10**, 1150–1166.
- 233 H. Tang, Z. Deng, Z. Lin, Z. Wang, I.-H. Chu, C. Chen, Z. Zhu, C. Zheng and S. P. Ong, *Chem. Mater.*, 2018, **30**, 163–173.
- 234 Y. Wei, Y. Yang, Z. Chen, P. Gao, Q. Ma, M. Gao, C. Yan, Z. Wu, Y. Jiang, J. Chen, X. Yu, Z. Li, X. Zhang, Y. Liu, M. Gao, W. Sun and H. Pan, *Adv. Mater.*, 2023, 2304285.
- 235 K. Wang, Z. Liang, S. Weng, Y. Ding, Y. Su, Y. Wu, H. Zhong, A. Fu, Y. Sun, M. Luo, J. Yan, X. Wang and Y. Yang, *ACS Energy Lett.*, 2023, **8**, 3450–3459.
- 236 G. Zhao, C. Luo and Q. Hua, *J. Mater. Chem. A*, 2023, **11**(37), 20174–20186.
- 237 M. Yang, Y. Yao, M. Chang, F. Tian, W. Xie, X. Zhao, Y. Yu and X. Yao, *Adv. Energy Mater.*, 2023, 2300962.
- 238 X. Fu, H. Duan, L. Zhang, Y. Hu and Y. Deng, *Adv. Funct. Mater.*, 2023, 2308022.
- 239 S. Lee, K.-s Lee, S. Kim, K. Yoon, S. Han, M. H. Lee, Y. Ko, J. H. Noh, W. Kim and K. Kang, *Sci. Adv.*, 2023, **8**, eabq0153.
- 240 Q. Gao, D. Wu, Z. Wang, P. Lu, X. Zhu, T. Ma, M. Yang, L. Chen, H. Li and F. Wu, *Energy Storage Mater.*, 2023, **63**, 103007.
- 241 H. Huo, Y. Chen, N. Zhao, X. Lin, J. Luo, X. Yang, Y. Liu, X. Guo and X. Sun, *Nano Energy*, 2019, **61**, 119–125.
- 242 Y. Wang, S. Song, C. Xu, N. Hu, J. Molenda and L. Lu, *Nano Mater. Sci.*, 2019, **1**, 91–100.
- 243 Z. Cheng, M. Liu, S. Ganapathy, C. Li, Z. Li, X. Zhang, P. He, H. Zhou and M. Wagemaker, *Joule*, 2020, **4**, 1311–1323.
- 244 S. Kaboli, H. Demers, A. Paolella, A. Darwiche, M. Dontigny, D. Clément, A. Guerfi, M. L. Trudeau, J. B. Goodenough and K. Zaghib, *Nano Lett.*, 2020, **20**, 1607–1613.
- 245 Y. Wang, Z. Wang, F. Zheng, J. Sun, J. A. S. Oh, T. Wu, G. Chen, Q. Huang, M. Kotobuki, K. Zeng and L. Lu, *Adv. Sci.*, 2022, **9**, 2105849.
- 246 M. Li, L. Shi, J. Jin, M. Wu and Z. Wen, *Mater. Today Energy*, 2023, **36**, 101361.
- 247 K. Shi, Z. Wan, L. Yang, Y. Zhang, Y. Huang, S. Su, H. Xia, K. Jiang, L. Shen, Y. Hu, S. Zhang, J. Yu, F. Ren, Y.-B. He and F. Kang, *Angew. Chem., Int. Ed.*, 2020, **59**, 11784–11788.
- 248 C. Wang, S. Hwang, M. Jiang, J. Liang, Y. Sun, K. Adair, M. Zheng, S. Mukherjee, X. Li, R. Li, H. Huang, S. Zhao, L. Zhang, S. Lu, J. Wang, C. V. Singh, D. Su and X. Sun, *Adv. Energy Mater.*, 2021, **11**, 2100210.
- 249 H.-Y. Xia, X.-X. Wang, G.-X. Ren, W.-W. Wang, Y.-N. Zhou, Z. Shadike, E. Hu, X.-Q. Yang, J.-Y. Zheng, X.-S. Liu and Z.-W. Fu, *J. Power Sources*, 2021, **514**, 230603.
- 250 K. Borzutzki, K. Dong, J. R. Nair, B. Wolff, F. Hausen, R.-A. Eichel, M. Winter, I. Manke and G. Brunklaus, *Cell Rep. Phys. Sci.*, 2021, **2**, 100496.
- 251 C.-Z. Zhao, Q. Zhao, X. Liu, J. Zheng, S. Stalin, Q. Zhang and L. A. Archer, *Adv. Mater.*, 2020, **32**, 1905629.
- 252 Y. Wang, S. Chen, Z. Li, C. Peng, Y. Li and W. Feng, *Energy Storage Mater.*, 2022, **45**, 474–483.
- 253 J. Luo, Q. Sun, J. Liang, K. Adair, F. Zhao, S. Deng, Y. Zhao, R. Li, H. Huang, R. Yang, S. Zhao, J. Wang and X. Sun, *ACS Energy Lett.*, 2023, **8**, 3676–3684.
- 254 K. Mu, D. Wang, W. Dong, Q. Liu, Z. Song, W. Xu, P. Yao, Y. A. Chen, B. Yang, C. Li, L. Tian, C. Zhu and J. Xu, *Adv. Mater.*, 2023, 2304686.
- 255 X. Zhang, G. Gao, W. Wang, J. Wang, L. Wang and T. Liu, *ACS Appl. Mater. Interfaces*, 2022, **14**, 49811–49819.
- 256 H. Shin, S. J. Choi, S. Choi, B. Y. Jang, J. Jeong, Y.-G. Cho, S.-Y. Lee, H.-K. Song, J. H. Yu and T.-H. Kim, *J. Power Sources*, 2022, **546**, 231926.
- 257 M.-H. Chiou, E. Verweyen, D. Diddens, L. Wichmann, C. Schmidt, K. Neuhaus, A. Choudhary, D. Bedrov, M. Winter and G. Brunklaus, *ACS Appl. Energy Mater.*, 2023, **6**, 4422–4436.
- 258 Y. Li, S. Ma, Y. Zhao, S. Chen, T. Xiao, H. Yin, H. Song, X. Pan, L. Cong and H. Xie, *Energy Environ. Mater.*, 2023, e12648.
- 259 J. C. Barbosa, R. Gonçalves, C. M. Costa, V. de Zea Bermudez, A. Fidalgo-Marijuan, Q. Zhang and S. Lanceros-Méndez, *Mater. Adv.*, 2021, **2**, 3790–3805.
- 260 H. Jamal, F. Khan, S. Hyun, S. W. Min and J. H. Kim, *J. Mater. Chem. A*, 2021, **9**, 4126–4137.
- 261 C. Fu, G. Homann, R. Grissa, D. Rentsch, W. Zhao, T. Gouveia, A. Falgayrat, R. Lin, S. Fantini and C. Battaglia, *Adv. Energy Mater.*, 2022, **12**, 2200412.
- 262 L. Yang, Q. Liu, H. Ma, Q. An, X. Wang, Y. Ding, Z. Mei, X. Sheng, L. Duan, J. Xie and H. Guo, *Energy Storage Mater.*, 2023, **62**, 102954.
- 263 J. C. Barbosa, D. M. Correia, A. Fidalgo-Marijuan, R. Gonçalves, S. Ferdov, V. de Zea Bermudez, S. Lanceros-Mendez and C. M. Costa, *ACS Appl. Mater. Interfaces*, 2023, **15**, 32301–32312.
- 264 S. Kalnaus, N. J. Dudney, A. S. Westover, E. Herbert and S. Hackney, *Science*, 2023, **381**, eabg5998.
- 265 F. Strauss, T. Bartsch, L. de Biasi, A. Y. Kim, J. Janek, P. Hartmann and T. Brezesinski, *ACS Energy Lett.*, 2018, **3**, 992–996.
- 266 D. Y. Oh, Y. J. Nam, K. H. Park, S. H. Jung, K. T. Kim, A. R. Ha and Y. S. Jung, *Adv. Energy Mater.*, 2019, **9**, 1802927.
- 267 T. Shi, Q. Tu, Y. Tian, Y. Xiao, L. J. Miara, O. Kononova and G. Ceder, *Adv. Energy Mater.*, 2020, **10**, 1902881.
- 268 A. Bielefeld, D. A. Weber and J. Janek, *ACS Appl. Mater. Interfaces*, 2020, **12**, 12821–12833.
- 269 A. Bielefeld, D. A. Weber and J. Janek, *J. Phys. Chem. C*, 2019, **123**, 1626–1634.
- 270 A. L. Davis, V. Goel, D. W. Liao, M. N. Main, E. Kazyak, J. Lee, K. Thornton and N. P. Dasgupta, *ACS Energy Lett.*, 2021, **6**, 2993–3003.

- 271 M. K. Jangid, A. L. Davis, D. W. Liao and N. P. Dasgupta, *ACS Energy Lett.*, 2023, **8**, 2522–2531.
- 272 Z. Zou, Y. Li, Z. Lu, D. Wang, Y. Cui, B. Guo, Y. Li, X. Liang, J. Feng, H. Li, C.-W. Nan, M. Armand, L. Chen, K. Xu and S. Shi, *Chem. Rev.*, 2020, **120**, 4169–4221.
- 273 P. Shi, J. Ma, M. Liu, S. Guo, Y. Huang, S. Wang, L. Zhang, L. Chen, K. Yang, X. Liu, Y. Li, X. An, D. Zhang, X. Cheng, Q. Li, W. Lv, G. Zhong, Y.-B. He and F. Kang, *Nat. Nanotechnol.*, 2023, **18**, 602–610.
- 274 Y.-F. Huang, T. Gu, G. Rui, P. Shi, W. Fu, L. Chen, X. Liu, J. Zeng, B. Kang, Z. Yan, F. J. Stadler, L. Zhu, F. Kang and Y.-B. He, *Energy Environ. Sci.*, 2021, **14**, 6021–6029.
- 275 Y. Yuan, L. Chen, Y. Li, X. An, J. Lv, S. Guo, X. Cheng, Y. Zhao, M. Liu, Y.-B. He and F. Kang, *Energy Mater. Devices*, 2023, **1**, 9370004.
- 276 Y.-F. Huang, J.-P. Zeng, S.-F. Li, C. Dai, J.-F. Liu, C. Liu and Y.-B. He, *Adv. Energy Mater.*, 2023, **13**, 2203888.
- 277 Y. Suzuki, K. Kami, K. Watanabe, A. Watanabe, N. Saito, T. Ohnishi, K. Takada, R. Sudo and N. Imanishi, *Solid State Ionics*, 2015, **278**, 172–176.
- 278 R. Chen, C. Zhang, J. Li, Z. Du, F. Guo, W. Zhang, Y. Dai, W. Zong, X. Gao, J. Zhu, Y. Zhao, X. Wang and G. He, *Energy Environ. Sci.*, 2023, **16**, 2540–2549.
- 279 G. Bucci, T. Swamy, Y.-M. Chiang and W. C. Carter, *J. Mater. Chem. A*, 2017, **5**, 19422–19430.
- 280 L.-L. Lu, Y.-Y. Lu, Z.-J. Xiao, T.-W. Zhang, F. Zhou, T. Ma, Y. Ni, H.-B. Yao, S.-H. Yu and Y. Cui, *Adv. Mater.*, 2018, **30**, 1706745.
- 281 T. Wu, Z. Zhao, J. Zhang, C. Zhang, Y. Guo, Y. Cao, S. Pan, Y. Liu, P. Liu, Y. Ge, W. Liu, L. Dong and H. Lu, *Energy Storage Mater.*, 2021, **36**, 265–271.
- 282 R. Guan, S. Liu, C. Wang, Y. Yang, D. Lu and X. Bian, *Chem. Eng. J.*, 2021, **425**, 130177.
- 283 X. Xue, D. Lin and Y. Li, *Small Structures*, 2022, **3**, 2200159.
- 284 Z. Lyu, G. J. H. Lim, R. Guo, Z. Kou, T. Wang, C. Guan, J. Ding, W. Chen and J. Wang, *Adv. Funct. Mater.*, 2019, **29**, 1806658.
- 285 C. Liu, N. Zhao, K. Xu, Y. Li, J. P. Mwizerwa, J. Shen and Z. Chen, *Mater. Today Energy*, 2022, **29**, 101098.
- 286 D. W. McOwen, S. Xu, Y. Gong, Y. Wen, G. L. Godbey, J. E. Gritton, T. R. Hamann, J. Dai, G. T. Hitz, L. Hu and E. D. Wachsman, *Adv. Mater.*, 2018, **30**, 1707132.
- 287 P. Sun, J. Davis, L. Cao, Z. Jiang, J. B. Cook, H. Ning, J. Liu, S. Kim, F. Fan, R. G. Nuzzo and P. V. Braun, *Energy Storage Mater.*, 2019, **17**, 151–156.
- 288 X. Zhang, Z. Hui, S. King, L. Wang, Z. Ju, J. Wu, K. J. Takeuchi, A. C. Marschilok, A. C. West, E. S. Takeuchi and G. Yu, *Nano Lett.*, 2021, **21**, 5896–5904.
- 289 J. Wu, Z. Ju, X. Zhang, K. J. Takeuchi, A. C. Marschilok, E. S. Takeuchi and G. Yu, *Nano Lett.*, 2021, **21**, 9339–9346.
- 290 J. I. Hur, L. C. Smith and B. Dunn, *Joule*, 2018, **2**, 1187–1201.
- 291 B. T. Heligman and A. Manthiram, *ACS Energy Lett.*, 2021, **6**, 2666–2672.
- 292 X. Zhan, M. Li, S. Li, X. Pang, F. Mao, H. Wang, Z. Sun, X. Han, B. Jiang, Y.-B. He, M. Li, Q. Zhang and L. Zhang, *Energy Storage Mater.*, 2023, **61**, 102875.
- 293 S. He, S. Huang, S. Wang, I. Mizota, X. Liu and X. Hou, *Energy Fuels*, 2021, **35**, 944–964.
- 294 D. Cao, T. Ji, A. Singh, S. Bak, Y. Du, X. Xiao, H. Xu, J. Zhu and H. Zhu, *Adv. Energy Mater.*, 2023, **13**, 2203969.
- 295 Y. Liu, C. Wang, S. G. Yoon, S. Y. Han, J. A. Lewis, D. Prakash, E. J. Klein, T. Chen, D. H. Kang, D. Majumdar, R. Gopalaswamy and M. T. McDowell, *Nat. Commun.*, 2023, **14**, 3975.
- 296 L. Geng, D. Xue, J. Yao, Q. Dai, H. Sun, D. Zhu, Z. Rong, R. Fang, X. Zhang, Y. Su, J. Yan, S. J. Harris, S. Ichikawa, L. Zhang, Y. Tang, S. Zhang and J. Huang, *Energy Environ. Sci.*, 2023, **16**, 2658–2668.
- 297 C. Wang, S. Hwang, M. Jiang, J. Liang, Y. Sun, K. Adair, M. Zheng, S. Mukherjee, X. Li and R. Li, *Adv. Energy Mater.*, 2021, **11**, 2100210.
- 298 J. Zhao, C. Zhao, J. Zhu, X. Liu, J. Yao, B. Wang, Q. Dai, Z. Wang, J. Chen, P. Jia, Y. Li, S. J. Harris, Y. Yang, Y. Tang, L. Zhang, F. Ding and J. Huang, *Nano Lett.*, 2022, **22**, 411–418.
- 299 Y. Guo, X. Qu, Z. Hu, J. Zhu, W. Niu and X. Liu, *J. Mater. Chem. A*, 2021, **9**, 13597–13607.
- 300 Y. Ma, J. Wan, Y. Yang, Y. Ye, X. Xiao, D. T. Boyle, W. Burke, Z. Huang, H. Chen, Y. Cui, Z. Yu, S. T. Oyakhire and Y. Cui, *Adv. Energy Mater.*, 2022, **12**, 2103720.
- 301 S. Liu, W. Liu, D. Ba, Y. Zhao, Y. Ye, Y. Li and J. Liu, *Adv. Mater.*, 2023, **35**, 2110423.
- 302 F. Han, A. S. Westover, J. Yue, X. Fan, F. Wang, M. Chi, D. N. Leonard, N. J. Dudney, H. Wang and C. Wang, *Nat. Energy*, 2019, **4**, 187–196.
- 303 J. Wang, L. Chen, H. Li and F. Wu, *Energy Environ. Mater.*, 2023, e12613.
- 304 L. Porz, T. Swamy, B. W. Sheldon, D. Rettenwander, T. Frömling, H. L. Thaman, S. Berendts, R. Uecker, W. C. Carter and Y.-M. Chiang, *Adv. Energy Mater.*, 2017, **7**, 1701003.
- 305 W. Manalastas, J. Rikarte, R. J. Chater, R. Brugge, A. Aguadero, L. Buannic, A. Llordés, F. Aguesse and J. Kilner, *J. Power Sources*, 2019, **412**, 287–293.
- 306 J. Biao, B. Han, Y. Cao, Q. Li, G. Zhong, J. Ma, L. Chen, K. Yang, J. Mi, Y. Deng, M. Liu, W. Lv, F. Kang and Y.-B. He, *Adv. Mater.*, 2023, **35**, 2208951.
- 307 M. Klinsmann, F. E. Hildebrand, M. Ganser and R. M. McMeeking, *J. Power Sources*, 2019, **442**, 227226.
- 308 L. Barroso-Luque, Q. Tu and G. Ceder, *J. Electrochem. Soc.*, 2020, **167**, 020534.
- 309 Z. Ning, G. Li, D. L. R. Melvin, Y. Chen, J. Bu, D. Spencer-Jolly, J. Liu, B. Hu, X. Gao, J. Perera, C. Gong, S. D. Pu, S. Zhang, B. Liu, G. O. Hartley, A. J. Bodey, R. I. Todd, P. S. Grant, D. E. J. Armstrong, T. J. Marrow, C. W. Monroe and P. G. Bruce, *Nature*, 2023, **618**, 287–293.
- 310 Q. Tu, T. Shi, S. Chakravarthy and G. Ceder, *Matter*, 2021, **4**, 3248–3268.

- 311 Y. Liu, X. Xu, X. Jiao, O. O. Kapitanova, Z. Song and S. Xiong, *Adv. Mater.*, 2023, **35**, 2301152.
- 312 Y. Ren, K. Zhang, Y. Zhou and Y. Cao, *ACS Appl. Mater. Interfaces*, 2022, **14**, 30658–30671.
- 313 T. Krauskopf, H. Hartmann, W. G. Zeier and J. Janek, *ACS Appl. Mater. Interfaces*, 2019, **11**, 14463–14477.
- 314 S.-Y. Ham, H. Yang, O. Nunez-cuacuas, D. H. S. Tan, Y.-T. Chen, G. Deysher, A. Cronk, P. Ridley, J.-M. Doux, E. A. Wu, J. Jang and Y. S. Meng, *Energy Storage Mater.*, 2023, **55**, 455–462.
- 315 S. Luo, Z. Wang, X. Li, X. Liu, H. Wang, W. Ma, L. Zhang, L. Zhu and X. Zhang, *Nat. Commun.*, 2021, **12**, 6968.
- 316 Y. Huang, B. Shao and F. Han, *J. Mater. Chem. A*, 2022, **10**, 12350–12358.
- 317 L. Zhao, W. Li, C. Wu, Q. Ai, L. Guo, Z. Chen, J. Zheng, M. Anderson, H. Guo, J. Lou, Y. Liang, Z. Fan, J. Zhu and Y. Yao, *Adv. Energy Mater.*, 2023, 2300679.
- 318 W. Yan, Z. Mu, Z. Wang, Y. Huang, D. Wu, P. Lu, J. Lu, J. Xu, Y. Wu, T. Ma, M. Yang, X. Zhu, Y. Xia, S. Shi, L. Chen, H. Li and F. Wu, *Nat. Energy*, 2023, **8**, 800–813.
- 319 J. Peng, D. Wu, Z. Jiang, P. Lu, Z. Wang, T. Ma, M. Yang, H. Li, L. Chen and F. Wu, *ACS Nano*, 2023, **17**, 12706–12722.
- 320 B. Liu, L. Zhang, S. Xu, D. W. McOwen, Y. Gong, C. Yang, G. R. Pastel, H. Xie, K. Fu, J. Dai, C. Chen, E. D. Wachsman and L. Hu, *Energy Storage Mater.*, 2018, **14**, 376–382.
- 321 Z. Zheng, B. Chen, N. Fritz, Y. Gurumukhi, J. Cook, M. N. Ates, N. Miljkovic, P. V. Braun and P. Wang, *J. Energy Storage*, 2020, **30**, 101502.
- 322 Y. Liu, D. Lin, Z. Liang, J. Zhao, K. Yan and Y. Cui, *Nat. Commun.*, 2016, **7**, 10992.
- 323 G. V. Alexander, C. Shi, J. O'Neill and E. D. Wachsman, *Nat. Mater.*, 2023, **22**, 1136–1143.
- 324 K. Fu, Y. Gong, G. T. Hitz, D. W. McOwen, Y. Li, S. Xu, Y. Wen, L. Zhang, C. Wang, G. Pastel, J. Dai, B. Liu, H. Xie, Y. Yao, E. D. Wachsman and L. Hu, *Energy Environ. Sci.*, 2017, **10**, 1568–1575.
- 325 S.-J. Zhang, J.-H. You, J.-D. Chen, Y.-Y. Hu, C.-W. Wang, Q. Liu, Y.-Y. Li, Y. Zhou, J.-T. Li, J. Świątowska, L. Huang and S.-G. Sun, *ACS Appl. Mater. Interfaces*, 2019, **11**, 47939–47947.
- 326 J. Noh, W. Chen, P. Wu, Y. Huang, J. Tan, H.-C. Zhou and C. Yu, *Adv. Funct. Mater.*, 2021, **31**, 2104899.
- 327 J. Lee, H. Park, J. Hwang, J. Noh and C. Yu, *ACS Nano*, 2023, **17**(16), 16020–16035.
- 328 P. Barai, T. Fuchs, E. Trevisanello, H. K. Kim, F. H. Richter, J. Janek and V. Srinivasan, *ACS Appl. Energy Mater.*, 2023, **6**, 2160–2177.
- 329 K. Fu, Y. Gong, B. Liu, Y. Zhu, S. Xu, Y. Yao, W. Luo, C. Wang, S. D. Lacey, J. Dai, Y. Chen, Y. Mo, E. Wachsman and L. Hu, *Sci. Adv.*, 2017, **3**, e1601659.
- 330 V. V. Gusev, D. Adamson, A. Deligkas, D. Antypov, C. M. Collins, P. Krysta, I. Potapov, G. R. Darling, M. S. Dyer, P. Spirakis and M. J. Rosseinsky, *Nature*, 2023, **619**, 68–72.
- 331 S. Pereznieta, R. Jaafreh, J.-g Kim and K. Hamad, *Mater. Lett.*, 2023, **349**, 134848.
- 332 S. Pereznieta, R. Jaafreh, J.-g Kim and K. Hamad, *Mater. Lett.*, 2023, **337**, 133926.
- 333 A. K. Mishra, S. Rajput, M. Karamta and I. Mukhopadhyay, *ACS Omega*, 2023, **8**, 16419–16427.
- 334 P. Friederich, F. Häse, J. Proppe and A. Aspuru-Guzik, *Nat. Mater.*, 2021, **20**, 750–761.
- 335 I. S. Novikov, K. Gubaev, E. V. Podryabinkin and A. V. Shapeev, *Mach. Learn.: Sci. Technol.*, 2021, **2**, 025002.
- 336 J. Wang, A. A. Panchal and P. Canepa, *Mater. Futures*, 2023, **2**, 015101.
- 337 Z. Xu, H. Duan, Z. Dou, M. Zheng, Y. Lin, Y. Xia, H. Zhao and Y. Xia, *npj Comput. Mater.*, 2023, **9**, 105.
- 338 Z. Zhang and L. F. Nazar, *Nat. Rev. Mater.*, 2022, **7**, 389–405.
- 339 Y. Sun, B. Ouyang, Y. Wang, Y. Zhang, S. Sun, Z. Cai, V. Lacivita, Y. Guo and G. Ceder, *Matter*, 2022, **5**, 4379–4395.
- 340 D. Yan, A. D. Smith and C.-C. Chen, *Nat. Comput. Sci.*, 2023, **3**, 572–574.
- 341 S. Muy, J. Voss, R. Schlem, R. Koerver, S. J. Sedlmaier, F. Maglia, P. Lamp, W. G. Zeier and Y. Shao-Horn, *iScience*, 2019, **16**, 270–282.
- 342 Z. Wan, X. Chen, Z. Zhou, X. Zhong, X. Luo and D. Xu, *J. Energy Chem.*, 2023, **88**, 28–38.
- 343 J. Sharma, A. Pareek, K. Kumar and K. Pareek, *Energy Storage*, 2023, e503.
- 344 H. Li, C. Liu, A. Saini, Y. Wang, H. Jiang, T. Yang, L. Chen, C. Pan and H. Shen, *J. Power Sources*, 2019, **438**, 226974.
- 345 J. Park, D. Kim, W. A. Appiah, J. Song, K. T. Bae, K. T. Lee, J. Oh, J. Y. Kim, Y.-G. Lee, M.-H. Ryou and Y. M. Lee, *Energy Storage Mater.*, 2019, **19**, 124–129.
- 346 A. Neumann, S. Randau, K. Becker-Steinberger, T. Danner, S. Hein, Z. Ning, J. Marrow, F. H. Richter, J. Janek and A. Latz, *ACS Appl. Mater. Interfaces*, 2020, **12**, 9277–9291.
- 347 J. Park, K. T. Kim, D. Y. Oh, D. Jin, D. Kim, Y. S. Jung and Y. M. Lee, *Adv. Energy Mater.*, 2020, **10**, 2001563.